DEPARTMENT OF PHYSICS AND ASTRONOMY

CP-VIOLATION IN THE INERT DOUBLET MODEL: DARK MATTER AND BARYOGENESIS

Master thesis in Physics
submitted by

MARÍA ISABEL DIAS ASTROS

born in Maracay, Venezuela

Heidelberg, March 10, 2022

CP-VIOLATION IN THE INERT DOUBLET MODEL DARK MATTER AND BARYOGENESIS

This Master thesis has been carried out by

MARÍA ISABEL DIAS ASTROS

at the

Max Planck Institute for Nuclear Physics

under the supervision of

Dr. FLORIAN GOERTZ

Dedicated to my mother, who was brave enough
to start a new better life. I am very proud of you.

ABSTRACT

The Inert Doublet Model (IDM) has been widely studied as a possible theory explaining Dark Matter (DM) and in the context of the Electroweak Phase Transition (EWPhT), as a first step towards accommodating the three Sakharov conditions allowing for baryogenesis. With this aim in mind, in this work the IDM is extended with higher-dimensional CP-violating operators which are added in three distinct sectors of the theory, specifically, in the scalar potential, in the Yukawa Lagrangian, and in the gauge sector. In each case, DM phenomenology is extensively studied and the corresponding parameter spaces are shown in detail, taking into account theoretical and the latest experimental constraints. In particular, for DM masses over 500 GeV further higher-dimensional derivative operators were also included and it is shown that a new parameter space becomes available even for non-(quasi)degenerate scalar masses. Similarly, in one of the extensions and for low DM masses it is argued that the Baryon Asymmetry of the Universe (BAU) can be explained by considering the chiral anomaly during the first step of a two-step phase transition in the Universe. Possible benchmark points are, likewise, analysed. We conclude that the IDM as an effective theory could, in principle, serve as a model where both DM and baryogenesis are accounted for.

ZUSAMMENFASSUNG

Das Inert Doublet-Model (IDM) wurde umfassend als mögliche Theorie zur Erklärung der Dunklen Materie (DM) und im Kontext des elektroschwachen Phasenübergangs (EWPhT) untersucht, als erster Schritt zur Erfüllung der drei Sakharov Bedingungen für Baryogenese. Mit diesem Ziel vor Augen, wird in dieser Arbeit das IDM um höherdimensionale CP-verletzende Operatoren erweitert, die in drei verschiedenen Sektoren der Theorie hinzugefügt werden, nämlich im Skalarpotential, in der Yukawa-Lagrangedichte und im Eichsektor. In jedem Fall wird

die DM-Phänomenologie intensiv untersucht und die entsprechenden Parameterräume werden unter Berücksichtigung theoretischer und neuester experimenteller Einschränkungen detailliert angegeben. Insbesondere werden für DM-Massen über 500 GeV weitere höherdimensionale Ableitungsoperatoren einbezogen, und es wird gezeigt, dass ein neuer Parameterraum sogar für nicht (quasi-)entartete Skalarmassen verfügbar ist. In ähnlicher Weise wird in einer der Erweiterungen für niedrige DM-Massen argumentiert, dass die Baryonen-Asymmetrie des Universums (BAU) durch die chirale Anomalie während des ersten Schritts eines zweistufigen Phasenübergangs im Universum erklärt werden kann. Mögliche Referenzwerte der Parameter werden ebenfalls analysiert. Wir kommen zu dem Schluss, dass das IDM als effektive Theorie im Prinzip als Modell dienen könnte, in dem sowohl DM als auch Baryogenese realisierbar sind.

ACKNOWLEDGMENTS

First I would like to thank my supervisor Dr. Florian Goertz, who gave me the opportunity to work in a fascinating subject and surrounded with an incredible research group. Without your guide this project would have not been possible. I am also grateful to the Max Planck Institute for Nuclear Physics for welcoming me. It was a great experience to work in Prof. Dr. Dr. h.c. Manfred Lindner's division.

Besides, I would also like to thank Dr. Andrei Angelescu for many fruitful discussions and to Sven Fabian who, from the beginning, taught me so much. It was a pleasure working with you both.

Additionally, I thank my family and boyfriend, the pillars I can always rely on. Last but not least, many thanks to my friends in Heidelberg: Mireia Tolosa, Laura Batini, Janning Meinert, Álvaro Lozano and Álvaro Pastor. You have become my family in Germany. Special thanks to Mireia, Janning and Álvaro Lozano for taking the time to proofread my work.

CONTENTS

LIST OF FIGURES

LIST OF TABLES

ACRONYMS

SM Standard Model of Particle Physics
GR General Relativity
DM Dark Matter
QCD Quantum Chromodynamics
BBN Big Bang Nucleosynthesis
CMB Cosmic Microwave Background
MACHOs Massive Compact Halo Objects
CKM Cabibbo–Kobayashi–Maskawa
WIMPs Weakly Interacting Massive Particles
EW Electroweak
BAU Baryon Asymmetry of the Universe
CDM Cold Dark Matter
EWBG Electroweak Baryogenesis
IDM Inert Doublet Model
VEV Vacuum Expectation Value
EDMs Electric Dipole Moments
SSB Spontaneous Symmetry Breaking
EWPhT Electroweak Phase Transition
BSM Beyond The Standard Model
QFT Quantum Field Theory
EFT Effective Field Theory
PhT Phase Transition
EWBG Electroweak Baryogenesis
IDM Inert Doublet Model

1 INTRODUCTION

In 2012 the discovery of the Higgs boson at CERN became a landmark event in the history of physics; it was the year when the last piece of the puzzle was finally found. The Standard Model of Particle Physics (SM) was now complete and, since then, it has proven to be a remarkable precise theory of the quantum world, with several experiments measuring its predictions to a great degree of accuracy. Nonetheless, the SM is not the last word as it fails to explain several phenomena that, as today, remain as open questions.

Among the greatest mysteries not explained by the SM, for instance, we could name the origin of the predominance of matter over antimatter (also referred to as the Baryon Asymmetry of the Universe (BAU)) and the nature of the so called Dark Matter (DM) which comprises approximately 26% of the universe. Both phenomena, widely supported by experiments, are far from being completely understood. Many theories, however, have been proposed in order to solve these questions. One of these theories is the Inert Doublet Model (IDM), an extension of the SM where an additional inert Electroweak (EW) doublet is added. The new doublet does not couple to fermions by means of an extra $\mathbb{Z}_2$ symmetry, under which all the SM fields are even, but the inert doublet is odd. This allows for the lightest $\mathbb{Z}_2$-odd particle to be a suitable candidate for DM and the possible parameter space and its implications are thoroughly discussed, for example, in [15, 19, 39, 42, 70]. On the other hand, it has also been studied that the IDM can accommodate a strong first order phase transition [42, 49, 50], being one of the three Sakharov conditions which must be fulfilled in any model where the BAU is produced via a dynamical mechanism usually referred to as baryogenesis. Nonetheless, the IDM is still lacking of an important ingredient in order to explain the BAU, *i.e.* CP violation. With this purpose in mind, there already exist some extensions of the IDM that include CP violation (see *e.g.* [53, 65]) but, most of them, rely on the introduction of new scalars or additional doublets. In this thesis, however, we study differ-

ent extensions of the IDM via higher dimensional CP-violating operators, which are analysed in the context of their impact in the DM relic abundance and their contributions to the generation of the BAU. Using higher dimensional operators is the simplest and most general "model independent" way in which one can extend the theory, yet it has not been done so far. In this work, particularly, CP-violating operators are added in distinct sectors of the theory: directly in the scalar potential, in the Yukawa Lagrangian and in the gauge sector. Furthermore, for each extension DM physics is analysed in detail and possible ways to account for baryogenesis are discussed, all by taking into account current experimental and theoretical constraints.

The work is organized as follows: the first part is dedicated to a purely theoretical background. Chapters [2] and [3] are dedicated to presenting the current paradigms in physics for describing the largest and the smallest of scales, *i.e.* the standard cosmological ΛCDM model and the SM, along with their respective shortcomings. Subsequently, chapters [4] and [5] are dedicated to the discussion of the main issues addressed in this work: DM and baryogenesis. The second part of the thesis, on the other hand, is devoted to the analysis of the IDM and its extensions. First, the vanilla IDM is explained in detail in chapter [6] in the light of DM abundance and the nature of the phase transition. Later on, in chapters [7], [8] and [9] CP violating extensions of the IDM are presented together with an in-depth analysis of the DM physics and possible mechanisms to generate the BAU. Finally, chapter [10] briefly summarizes the results and discusses possible sources for further studies.

As a final remark, for the rest of this work natural units are used, *i.e.* $\hbar = c = k_B = 1$ and, unless stated differently, Einstein's summation rule for repeated indices is applied. Similarly, the metric signature is $(+---)$.

Part I

THEORETICAL BACKGROUND

2

COSMOLOGY: THE BIG PICTURE

I have no special talents
I am only passionately
curious.

— Albert Einstein, Physicist

Since Albert Einstein's publication of General Relativity (GR) in 1915, our understanding of the universe and the laws of physics governing it have profoundly changed. As soon as we got a hold of Einstein's equations we were able to explain and describe the history of the universe down to when it was only approximately 10^{-12} seconds old, meaning that, for the first time, humanity was able to retell almost all of the 13.8 billion years of cosmic history.

GR is essentially encoded in Einstein's field equations, a set of non-linear differential equations describing how energy and momentum influence spacetime and how the curvature of spacetime manifests itself as gravity. This was a dramatic change in views, from gravity as a force in the Newtonian sense, to **gravity as a feature of geometry**. Including the cosmological constant Λ, Einstein's equations read [27, 64]

$$R_{\mu\nu} - \frac{1}{2}\mathcal{R}g_{\mu\nu} = 8\pi G T_{\mu\nu} + \Lambda g_{\mu\nu} \,, \tag{2.0.1}$$

with $R_{\mu\nu}$ the Riemann tensor, $\mathcal{R}$ the Ricci scalar, $g_{\mu\nu}$ the metric of spacetime, G the universal constant of gravitation and $T_{\mu\nu}$ the corresponding energy-momentum tensor. One must keep in mind that the original equations did not contain the cosmological constant, which was added retrospectively by Einstein himself in an attempt to find static and homogeneous solutions [26]. However, even though now it is known that static solutions cannot describe reality, later observations showed that the cosmological constant plays an important role in the dynamics of our universe. Solving Einstein's Eqs. (2.0.1) is a highly non-trivial task and, in fact, just a few exact solutions have been found so far, solutions which heavily rely on symmetries. So,

how do we get about finding solutions to Eqs. (2.0.1)?

As a first step, we start by choosing the energy-momentum tensor of a perfect fluid, characterized by its energy density ρ and the isotropic pressure p in its rest frame. Using that U_μ is the fluid four-velocity, the energy-momentum tensor can be written as [14, 27]

$$T_{\mu\nu} = (\rho + p)U_\mu U_\nu - p g_{\mu\nu} \, . \tag{2.0.2}$$

Conservation of energy-momentum, written in tensor form as $\nabla_\mu T^\mu{}_\nu = 0$, leads then to the continuity equation

$$\dot{\rho} + 3\frac{\dot{a}}{a}(\rho + p) = 0 \, . \tag{2.0.3}$$

As a second step, we can make the assumption of the **Cosmological Principle** which is the statement that, when averaging over large scales, the universe looks exactly the same at every point. Mathematically, this statement means that the universe is homogeneous and isotropic in space, but not necessarily in time [101]. The reason why time is not included in the cosmological principle is that, thanks to Hubble and his experimental work, since 1929 we know for a fact that the universe is expanding (specifically accelerating). Such expanding spacetime is usually described by the Robertson-Walker metric given, in comoving coordinates, by [64]

$$ds^2 = dt^2 - a^2(t)\left[\frac{dr^2}{1-kr^2} + r^2(d\theta^2 + \sin^2\theta d\varphi^2)\right] \, , \tag{2.0.4}$$

where $a(t)$ is the dimensionless scale factor and $k \in \{-1, 0, 1\}$ determines the curvature of the universe, *i.e.* for $k = 1$ the universe is closed, for $k = -1$ the universe is open, and for $k = 0$ the universe is flat. It is the scale factor that dictates how each slice of space looks like at any given time t.

Then, if one takes the Robertson-Walker metric in Eq. (2.0.4) together with the energy-momentum tensor of a perfect fluid

in Eq. (2.0.2), one finds the well-known Friedmann equations, which describe how the scale factor evolves with time [14, 27]

$$H^2 \stackrel{\text{def}}{=} \left(\frac{\dot{a}}{a}\right)^2 = \frac{8\pi G}{3}\rho + \frac{\Lambda}{3} - \frac{k}{a^2} \,, \tag{2.0.5}$$

$$\frac{\ddot{a}}{a} = -\frac{4\pi G}{3}(\rho + 3p) + \frac{\Lambda}{3} \,, \tag{2.0.6}$$

where we have introduced the Hubble parameter H. Metrics of the form in Eq. (2.0.4) satisfying Eqs. (2.0.5- 2.0.6) describe the so called **Friedmann-Lemaître-Robertson-Walker universes** [101].

2.1 COSMIC INVENTORY

From the Friedmann equations, we must understand ρ and p as the sum of all possible contributions to the energy density and the pressure in the universe, respectively. In our universe, these contributions will come in the form of matter, radiation and vacuum energy (the cosmological constant) [14]. Each component will evolve differently as the universe expands depending on its equation of state, given by the continuity Eq. (2.0.3). Fortunately, we usually have simple equations of state in the form

$$p_i = w_i \rho_i \,. \tag{2.1.1}$$

with w_i a proportionality constant. Plugging Eq. (2.1.1) into Eq. (2.0.3), one obtains that the energy density of the individual components evolves as a power law in the scale factor [26]

$$\rho_i \propto a^{-3(1+w_i)} \,. \tag{2.1.2}$$

COMPONENT	w_i	EVOLUTION
Matter	0	$\rho_m \propto a^{-3}$
Radiation	$\frac{1}{3}$	$\rho_r \propto a^{-4}$
Cosmological constant	-1	$\rho_\Lambda \propto a^{0}$

Table 2.1.1: Evolution of the energy density for the different components that make up the universe.

In table [2.1.1] a summary of the particular values of w_i for each component and its corresponding evolution with respect to a is presented.

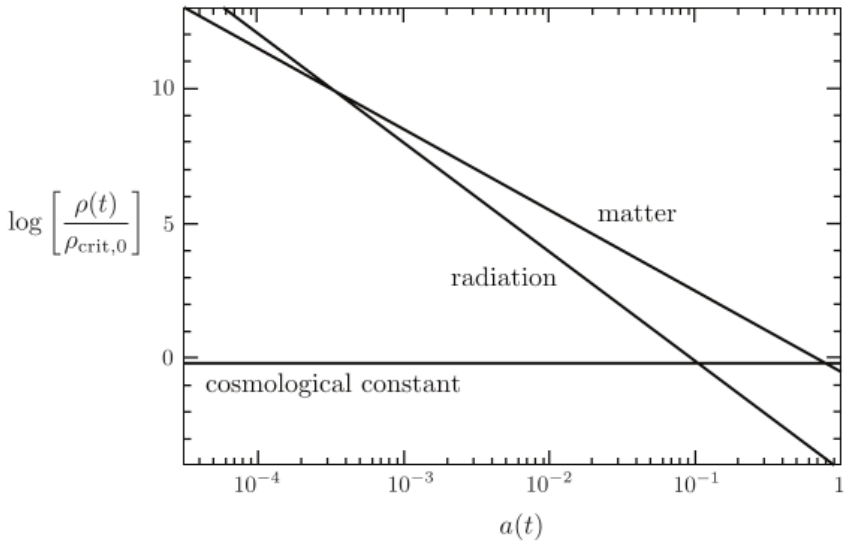

Figure 2.1.1: Evolution of the energy density for the individual components. Taken from Ref.[14].

2.2 COSMOLOGICAL PARAMETERS

Given our lack of understanding of the nature of the cosmological constant, it is also customary in cosmology to refer to the mysterious 70% of the energy budget of the universe as ***dark energy.*** *In fact, the terms "cosmological constant", "vacuum energy" and "dark energy" are essentially interchangeable.*

It is customary in cosmology to define, for each of the contributions to the energy budget of the universe, a density parameter given by [101]

$$\Omega_i \overset{\text{def}}{=} \frac{\rho_i}{\rho_{crit}} = \left(\frac{8\pi G}{3H^2}\right)\rho_i \,, \tag{2.2.1}$$

where the subscript i specifies the component (matter, radiation or dark energy) and the critical density ρ_{crit} is the value of the energy density when the spatial geometry of the universe is flat, *i.e.* $k = 0$. It is also conventional to use the subscript 0 to denote the value of the quantities at present time, that is, at $t = t_0$. For example, the value of the Hubble parameter today, measured using Type IA supernovae is [92]

$$H_0 = (74.0 \pm 1.4)\ \mathrm{km\,s^{-1}Mpc^{-1}} \,, \tag{2.2.2}$$

in contrast with the Cosmic Microwave Background (CMB) measurement of [1], given by

$$H_0 = (67.4 \pm 0.5)\,\mathrm{km\,s^{-1}Mpc^{-1}}\,. \tag{2.2.3}$$

The $\sim 3\sigma$ discrepancies between the two measurements of the Hubble parameter supposes a tension. The key question here is whether the Hubble tension is the result of systematic errors or if it indicates something more fundamental.

Using a conservative value of $H_0 = 70\,\mathrm{km\,s^{-1}Mpc^{-1}}$ one finds that the critical density of our universe today is of the order [101]

$$\rho_{crit,0} = 8.5 \times 10^{-10}\mathrm{kg\,m^{-1}s^{-2}}\,. \tag{2.2.4}$$

On the other hand, by defining an effective energy density for curvature

$$\Omega_k = -\frac{k}{(aH)^2}\,, \tag{2.2.5}$$

the first Friedman equation (2.0.5) can be recast as [14]

$$\left(\frac{H}{H_0}\right)^2 = \Omega_{r,0}\left(\frac{a_0}{a}\right)^4 + \Omega_{m,0}\left(\frac{a_0}{a}\right)^3 + \Omega_{k,0}\left(\frac{a_0}{a}\right)^2 + \Omega_\Lambda\,. \tag{2.2.6}$$

Note that the convention is to normalize the scale factor such that $a_0 = 1$. The goal of observational cosmology is to find the values appearing in Eq. (2.2.6).

2.3 ΛCDM

After many years of observation, the best current consensus among the scientific community is that our universe is filled with matter, radiation and dark energy (we also add the contribution from curvature for completeness) in the following proportions [101]

$$\Omega_m = 0.31\,, \quad \Omega_r = 5.38 \times 10^{-5}\,, \quad \Omega_\Lambda = 0.69\,, \quad |\Omega_k| < 0.01\,. \tag{2.3.1}$$

This means that we live in a fairly flat universe composed of approximately 70% of the – so far unknown – dark energy and only around 30% of matter. Even more worrisome is the fact that, from the 30% of matter making up the universe only about 5% corresponds to baryonic matter and about 26% corresponds to DM, leaving us with a huge misunderstanding of

about 95% of our universe.

The numbers given in Eq. (2.3.1) are often called the ΛCDM model, where Λ stands for the cosmological constant and CDM stands for Cold Dark Matter.

2.4 THERMAL HISTORY OF THE UNIVERSE

To understand the universe as it is today we must play the movie in reverse [101]. As we go back in time, the universe becomes hotter and the energy density increases. Indeed, for the first 300.000 years, the universe consisted of a hot plasma in which the photons were in thermal equilibrium with matter. When hydrogen atoms began to form during recombination, the universe finally became transparent, liberating the photons we find today in the CMB. Further back in time, neutrons and protons came together to form light nuclei in what is known as the Big Bang Nucleosynthesis (BBN). For even hotter temperatures and preceding the QCD phase transition, these protons and neutrons were melted into the so called quark-gluon plasma. Even earlier yet, the Electroweak Phase Transition (EWPhT) took place, giving mass to all particles. Before this time we know very little, except for selected events we think must occur, such as inflation.

Tab. [2.4.1] briefly summarizes the most important events in our understanding of cosmic history. For now we turn ourselves into the study of equilibrium and non-equilibrium dynamics which will allow us to understand the thermal evolution of the universe and to which the following sections are dedicated.

2.4.1 *Equilibrium*

A system of particles is said to be in **thermodynamic equilibrium** when the constituents exchange energy, momentum and particles efficiently. When this happens, the state reached is one of maximum entropy described by the Fermi-Dirac or Bose-Einstein distribution functions [14]

$$f(p) = \frac{1}{e^{(E(p)-\mu)/T} \pm 1}\,, \tag{2.4.1}$$

EVENT	t	T
Inflation	10^{-36} s (?)	Unknown
Baryogenesis	Unknown	Unknown
Electroweak Phase Transition	10^{-12} s	10^{22} K
QCD Phase Transition	10^{-6} s	10^{16} K
DM Freeze Out	Unknown	Unknown
Neutrino Decoupling	1 s	10^{10} K
e^+e^- Annihilation	6 s	$5 \cdot 10^9$ K
Nucleosynthesis	3 min	10^9 K
Matter-Radiation Equality	50.000 years	8700 K
Recombination	300.000 years	3600 K
Last Scattering	350.000 years	3100 K
Matter-Λ Equality	10^{10} years	3.8 K
Today	$1.4 \cdot 10^{10}$ years	2.7 K

Table 2.4.1: Important events in the thermal history of the universe [101].

where the $+$ sign is for fermions, the $-$ sign is for bosons, T is the temperature and μ is the chemical potential. Assuming that the chemical potential is zero, the number density of particles is then given by

$$n^{eq}(p) = \frac{g}{(2\pi)^3} \int d^3p f(p) \,, \tag{2.4.2}$$

with g being the number of internal degrees of freedom. Although solving the integral in Eq. (2.4.2) is not easily done analytically, one can clearly distinguish between two extremal cases. In the relativistic limit $(T \gg m)$ one gets [64]

$$n^{eq} = \frac{\zeta(3)}{\pi^2} g T^3 \begin{cases} 1 & \text{Bosons} \\ \frac{3}{4} & \text{Fermions,} \end{cases} \tag{2.4.3}$$

with the Riemann ζ-function. While in the non-relativistic limit $(T \ll m)$ the number density is given by

$$n^{eq} = g\left(\frac{mT}{2\pi}\right)^{3/2} e^{-m/T} \,. \tag{2.4.4}$$

This a key result. At low temperatures and in equilibrium the number density of particles is **Boltzmann suppressed**.

2.4.2 *Beyond Equilibrium*

If equilibrium had persisted until today, effectively the number density of every massive particle would be exponentially suppressed as given by Eq. (2.4.4), rendering a universe made out of only photons [14]. Therefore it is important that we understand the **out of equilibrium** conditions leading to the **freeze out** of massive particles.

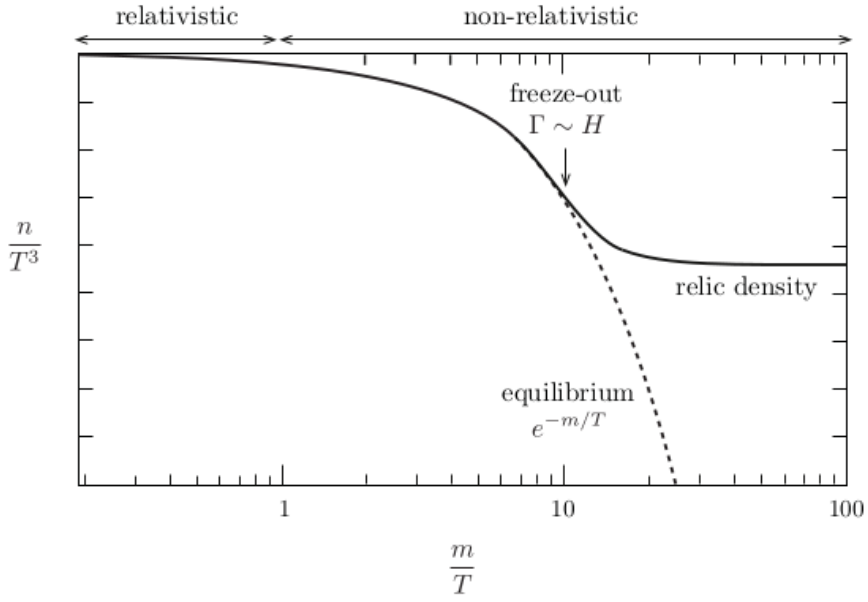

Figure 2.4.1: Particle freeze out. For high temperatures, the number density agrees with the equilibrium value. For low temperatures, the particles freeze out and keep a number density that is much greater than the Boltzmann suppressed equilibrium value. Taken from Ref.[14].

The key ingredient here is the comparison between the rate of interactions Γ of particle species, with the rate of expansion of the universe, H. When $\Gamma \gg H$, local thermal equilibrium

is reached before the expansion of the universe becomes too dominant. As the temperature decreases and $\Gamma \sim H$, the particles decouple from the thermal bath and they retain a number density that is much greater than the equilibrium value (see Fig.[2.4.1]). This number density is usually known as a **relic density** and the entire mechanism is known as the freeze out.

2.4.2.1 *The Boltzmann Equation*

Evolution beyond thermal equilibrium is described by the **Boltzmann equation** given by [14, 64]

$$\frac{dn_i}{dt} + 3\frac{\dot{a}}{a}n_i = C_i[n_j] \,, \tag{2.4.5}$$

where the left-hand side reflects the fact that the number density dilutes with the expanding universe , *i.e.* $n_i \sim a^{-3}$, and the right-hand side contains a collision term that depends on the specific interactions under consideration.

As an example, we consider the following process [14]

$$1 + 2 \rightleftharpoons 3 + 4 \,, \tag{2.4.6}$$

meaning that particle number 1 can annihilate with particle number 2 to produce particles 3 and 4 and vice-versa. For now we are only interested in tracking the number density of particle 1. Then, the Boltzmann equation reads

$$\frac{1}{a^3}\frac{d(n_1 a^3)}{dt} = -\alpha n_1 n_2 + \beta n_3 n_4 \,. \tag{2.4.7}$$

The right-hand side of Eq. (2.4.7) takes into account that the rate of change of n_1 must be given by the difference between the rates for producing and eliminating the species. The coefficient α is simply the **thermally averaged cross section** $\langle \sigma v \rangle$. Similarly the β coefficient can be related to α given that the collision term in Eq. (2.4.5) must vanish in equilibrium

$$\beta = \left(\frac{n_1 n_2}{n_3 n_4}\right)_{eq} \alpha \,. \tag{2.4.8}$$

Replacing the number density by the number of particles in a comoving volume, *i.e.* $N_i \stackrel{\text{def}}{=} n_i/s$, where s is the entropy density

of the universe, one can finally write the Boltzmann equation as [14]

$$\frac{d \ln N_1}{d \ln a} = -\frac{\Gamma_1}{H} \left[1 - \left(\frac{N_1 N_2}{N_3 N_4} \right)_{eq} \frac{N_3 N_4}{N_1 N_2} \right] , \tag{2.4.9}$$

with $\Gamma_1 = n_2 \langle \sigma v \rangle$. Solutions to the Boltzmann equation are usually found numerically.

3

THE STANDARD MODEL: THE SMALL PICTURE

Those who are not shocked when they first come across quantum theory cannot possibly have understood it.

— Niels Bohr, Physicist

Just as GR constitutes the present paradigm for physics at very large scales, the Standard Model of particle physics (SM) is the present framework to describe the physics of the quantum world. The history behind the SM is full of brilliant ideas, daring experiments and countless efforts [105] which have resulted in an extremely powerful theory capable of describing and predicting phenomena in a wide range of energies [24].

In fact, there are four fundamental forces in nature: weak, strong, electromagnetic and gravity. Nonetheless, gravity is not contemplated within the SM.

In short, the SM is a **Quantum Field Theory (QFT)** of elementary particles and their interactions, governed by three fundamental forces. It combines the Glashow-Weinberg-Salam EW theory with Quantum Chromodynamics (QCD). It can be characterized as a gauge theory with an overall gauge group of $SU(3)_c \times SU(2)_L \times U(1)_Y$ so that each field transforms in a particular irreducible representation of the group (see Tab. [3.0.1]). The particle content is divided in two main categories: fermions (matter particles) with half-integer spin, and bosons with integer spin. In the fermionic sector there is a total of 15 Weyl spinors grouped in 3 different generations. Since the SM is a **chiral theory**, one must distinguish between the left-handed $SU(2)$ doublets and the right-handed singlets. These are given by [98]

$$
\begin{aligned}
L^i &= \begin{pmatrix} \nu_e \\ e \end{pmatrix}_L , \begin{pmatrix} \nu_\mu \\ \mu \end{pmatrix}_L , \begin{pmatrix} \nu_\tau \\ \tau \end{pmatrix}_L , \\
Q^i &= \begin{pmatrix} u \\ d \end{pmatrix}_L , \begin{pmatrix} c \\ s \end{pmatrix}_L , \begin{pmatrix} t \\ b \end{pmatrix}_L , \\
e_R^i &= \{e_R, \mu_R, \tau_R\}, \qquad u_R^i = \{u_R, c_R, t_R\} , \\
d_R^i &= \{d_R, s_R, b_R\} .
\end{aligned}
\tag{3.0.1}
$$

Furthermore, in the SM we have an additional complex $SU(2)$ doublet, known as the **Higgs doublet** (Φ), which spontaneously breaks the EW symmetry, *i.e.* $SU(2)_L \times U(1)_Y \to U(1)_{EM}$, and plays a crucial role in giving mass to the particles in the model. The Lagrangian contains all gauge invariant terms up to dimension four, rendering the theory as renormalizable [54]. In its simplest form, the Lagrangian can be written as [68]

$$\mathcal{L}_{SM} = \mathcal{L}_H + \mathcal{L}_G + \mathcal{L}_F + \mathcal{L}_Y \ , \tag{3.0.2}$$

where we take into account the contributions coming from the Higgs sector, the gauge sector, the fermion sector and the Yukawa sector, respectively. Each term is, at the same time, given by

$$\begin{aligned}
\mathcal{L}_H &= \left|D_\mu \Phi\right|^2 - \mu^2 \left|\Phi\right|^2 - \lambda \left|\Phi\right|^4 \ , \\
\mathcal{L}_G &= -\frac{1}{2} Tr\left(G_{\mu\nu} G^{\mu\nu}\right) - \frac{1}{2} Tr\left(W_{\mu\nu} W^{\mu\nu}\right) - \frac{1}{4} B_{\mu\nu} B^{\mu\nu} \ , \\
\mathcal{L}_F &= i\bar{Q}^i \not{D} Q^i + i\bar{u}^i_R \not{D} u^i_R + i\bar{d}^i_R \not{D} d^i_R + i\bar{L}^i \not{D} L^i + i\bar{e}^i_R \not{D} e^i_R \ , \\
\mathcal{L}_Y &= -y^{ij}_d \bar{Q}^i \Phi \, d^j_R - y^{ij}_u Q^i \tilde{\Phi} \, u^j_R - y^{ij}_e L^i \Phi \, e^j_R + h.c. \ ,
\end{aligned} \tag{3.0.3}$$

where

$$\begin{aligned}
G_{\mu\nu} &= \partial_\mu G_\nu - \partial_\nu G_\mu + i g_S [G_\mu, G_\nu] \ , \\
W_{\mu\nu} &= \partial_\mu W_\nu - \partial_\nu W_\mu + i g [W_\mu, W_\nu] \ , \\
B_{\mu\nu} &= \partial_\mu B_\nu - \partial_\nu B_\mu \ ,
\end{aligned} \tag{3.0.4}$$

are the field strength tensors for $SU(3)_c$, $SU(2)_L$ and $U(1)_Y$, respectively. The covariant derivative $\not{D} = \gamma^\mu D_\mu$ is defined as follows

$$D_\mu = \partial_\mu - \frac{i}{2} g_S \lambda^a G^a_\mu - \frac{i}{2} g \sigma^i W^i_\mu - i g' Y B_\mu \ , \tag{3.0.5}$$

with $a = 1, \ldots, 8$, $i = 1, 2, 3$, λ^a are Gell-Mann matrices, σ^i are Pauli matrices and g_S, g and g' are the correspoding coupling constants for $SU(3)_c$, $SU(2)_L$ and $U(1)_Y$, respectively. For the Yukawa Lagrangian we have also defined

$$\tilde{\Phi} = i\sigma^2 \Phi^* \ , \tag{3.0.6}$$

with the second Pauli matrix σ^2.

FIELD	$SU(3)_c$	$SU(2)_L$	$U(1)_Y$
Q^i	3	2	$\frac{1}{6}$
L^i	1	2	$-\frac{1}{2}$
u_R^i	3	1	$\frac{2}{3}$
d_R^i	3	1	$-\frac{1}{3}$
e_R^i	1	1	-1

Table 3.0.1: SM fermion fields and their corresponding representations.

3.1 THE HIGGS MECHANISM

One of the last puzzles to be solved in the SM was how to include masses for the gauge bosons in the theory, in particular for the Z and the $W^{\pm}$ which were discovered at CERN in 1983 [105]. Given that an explicit mass term violates the gauge symmetry of the Lagrangian and spoils the renormalizability of the theory [74], another mechanism has to be used, a tool known as the **Higgs mechanism** [40, 55–57].

The Higgs mechanism relies on the idea of **Spontaneous Symmetry Breaking (SSB)**. In fact, SSB is one of the most important concepts in QFT having different consequences depending on the type of symmetry being broken. Unlike an explicit breaking of a symmetry, an spontaneous breaking means that the Lagrangian remains invariant under the symmetry while the ground state does not [98]. According to **Goldstone's theorem**, for each broken generator of the symmetry we will have a corresponding Goldstone boson [86]. When the broken symmetry is a global one, the generated bosons will be massless, whereas if the symmetry is local (gauged), the massless Goldstone's modes will combine with the longitudinal modes of the gauge bosons, conserving the number of degrees of freedom. In the SM the $SU(2)_L \times U(1)_Y$ electroweak symmetry is broken down to $U(1)_{EM}$ by the Vacuum Expectation Value (VEV) of the Higgs doublet. Its potential, given by

$$V(\Phi) = \mu^2 |\Phi|^2 + \lambda |\Phi|^4 \ , \tag{3.1.1}$$

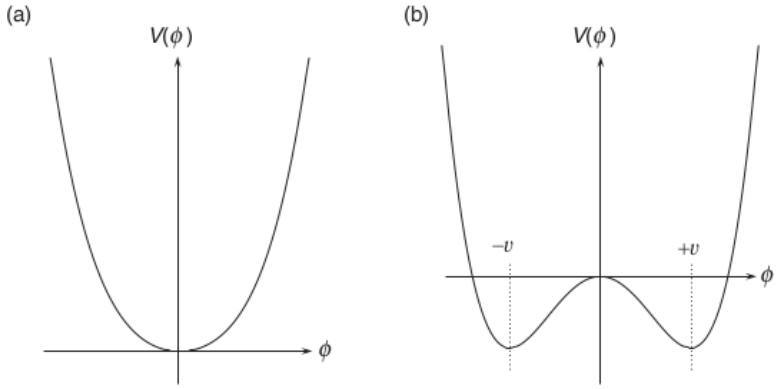

Figure 3.1.1: Sketch of the one-dimensional potential in Eq. (3.1.1). **Left panel**: in the $\mu^2 > 0$ case, the potential has a unique minimum at $\Phi = 0$. **Right panel**: when $\mu^2 < 0$, the potential has a degenerate minima. Taken from Ref. [100].

has a minimum at $\frac{v}{\sqrt{2}} = \sqrt{-\frac{\mu^2}{2\lambda}}$ when $\mu^2 < 0$, such that we can write

$$\langle \Phi \rangle = \frac{1}{\sqrt{2}} \begin{pmatrix} 0 \\ v \end{pmatrix} . \tag{3.1.2}$$

The gauge bosons will therefore acquire mass terms from the square of the covariant derivative of the Higgs [36, 73, 86, 98],

$$D_\mu \Phi = \left(\partial_\mu - i g \sigma^i W_\mu^i - i \frac{g'}{2} B_\mu \right) \Phi , \tag{3.1.3}$$

with the relevant terms being

$$|D_\mu \Phi|^2 \supset \frac{g^2 v^2}{8} \left[\left(W_\mu^1 \right)^2 + \left(W_\mu^2 \right)^2 + \left(\frac{g'}{g} B_\mu - W_\mu^3 \right)^2 \right] . \tag{3.1.4}$$

According to Eq. (3.1.4), we get three massive and one massless vector boson, specified by

$$W_\mu^\pm = \frac{1}{\sqrt{2}} \left(W_\mu^1 \mp i W_\mu^2 \right) \quad \text{with} \quad m_W = \frac{v}{2} g , \tag{3.1.5}$$

respectively, and

$$\begin{pmatrix} Z_\mu \\ A_\mu \end{pmatrix} = \begin{pmatrix} \cos\theta_W & -\sin\theta_W \\ \sin\theta_W & \cos\theta_W \end{pmatrix} \begin{pmatrix} W_\mu^3 \\ B_\mu \end{pmatrix} \quad \text{with} \quad m_Z = \frac{m_W}{\cos\theta_W} ,$$

(3.1.6)

where we have defined the weak mixing (Weinberg) angle as

$$\tan\theta_W = \frac{g'}{g} \,. \tag{3.1.7}$$

In 2012, more than 40 years after the postulate of the EW theory, the first detection of the Higgs boson by ATLAS and CMS at CERN [13] at long last allowed us to complete the SM puzzle.

3.2 WHAT CANNOT BE EXPLAINED?

Even though the SM is a very successful theory, we know it is not the last word. In fact, there are many experimental observations that cannot be explained within the theory and many other aspects that, while contemplated within the SM, are not offered satisfactory explanations. Among the most important and unanswered questions, we have the following:

- **The Hierarchy Problem**: This problem consists in the hierarchy between the Planck scale and the EW scale [68]. Particularly, why is the mass of the Higgs boson so small, *i.e.* $m_h = 125\,\text{GeV}$, in comparison to the Planck mass $m_{PL} \sim 10^{18}\,\text{GeV}$? In fact, we expect loop corrections to the mass of the Higgs (the most important coming from the top quark) of the order [76]

  $$\delta\mathcal{L}_{mass} \sim \frac{6y_t^2}{(4\pi)^2}\Lambda^2|\Phi|^2 \,, \tag{3.2.1}$$

  where Λ is a cutoff for the loop momentum and usually taken to be of the order of the Planck scale. Nonetheless, to keep the corrections below the EW scale one needs to take $\Lambda \lesssim 500\,\text{GeV}$. This means that, either some new physics will kick in at this energy scale, or we must accept that there is some fine-tuning taking place in our theory.

- **The Strong CP Problem**: The strong CP problem is concerned with the smallness of the strong CP phase discussed in more detail in Sec. [4.2.1]. It is indeed an unsolved mystery why weak CP violation is nearly maximal, while strong CP violation is so small [98].

To be fair, the hierarchy problem is not a problem of the SM itself. It is related to new energy thresholds. If we suppose the SM is valid only up to ~ 500 GeV the hierarchy problem does not even exist. It is only if we assume the cutoff of the theory to be bigger, for example to lie in the Planck scale where we expect quantum gravity to kick in, that we need to worry about the "lightness" of the Higgs.

- **Dark Matter**: There is overwhelming experimental evidence for the existence of DM. However, up to date, we still do not know the true nature of this mysterious form of matter that makes up for approximately 80% of the matter in our universe. The subject of DM is discussed in more detail in Chapter [4].

- **Dark Energy**: As discussed in Sec. [2.3], approximately 70% of our universe is made out of dark energy. Also known as the cosmological constant, this term appears as an addition to the Einstein's Lagrangian allowing us to find accelerated expanding solutions to Einstein's equations. Its addition is rather natural. Since all energy and momentum in the universe must gravitate, a constant energy density will have a physical impact in GR, unlike other branches of physics where only changes in energy between states are measurable [27]. The most natural choice for explaining this dark component in the universe is that of the vacuum energy which is actually predicted by the SM. However, the predicted value for the energy density of the vacuum is of the order $\rho_\Lambda^{SM} \sim \left(10^{18}\,\text{GeV}\right)^4$, while the observed value is only about $\rho_\Lambda^{obs} \lesssim \left(10^{-12}\,\text{GeV}\right)^4$ [26]. Thus, we are left with a ratio of $\rho_\Lambda^{SM}/\rho_\Lambda^{obs} \sim 10^{120}$ which is by far a worrisome number [14].

- **Neutrino Masses**: In the SM neutrinos are massless. We can see from Eq. (3.0.3) that no mass term is included for neutrinos. Nevertheless, experimental observations of neutrino oscillations show that they indeed have a small but non-zero mass [100]. It is still an open question in physics how this mass is generated.

- **Baryon Asymmetry**: Why is the Universe made of matter and not of antimatter? Assuming this asymmetry was not an initial condition of the Big Bang (a rather strange and fine-tuned condition which supposes tensions with inflation as well), we still lack of a complete model that can explain how baryons came to dominate the Universe in a ratio of just 1 extra baryon for every billion of baryon-antibaryon pairs [101]. The problem of baryogenesis will be discussed in detail in Chapter [5].

3.3 BSM: EFFECTIVE FIELD THEORY

Now that we know that the SM does not have the final word, we ask ourselves: what lies Beyond The Standard Model (BSM)? This has remained as an open question for a long time and the answer is probably complicated but, at least, we can be certain that our new theory must approach the SM at some limit. Other than that, we could in principle write down any Lagrangian we like. However, if we assume the new physics is really heavy, then we can abide by some rules going by the name of Effective Field Theory (EFT) with which we can study BSM physics in a general way (for a dedicated study of EFT see, e.g. [48, 75, 87, 95, 106]).

In a QFT in 4 dimensions, for example, we can classify operators according to their mass dimension d: for $d < 4$ we say the operator is relevant, for $d = 4$ we call it marginal and for $d > 4$ we call it irrelevant. The latter name does not mean these operators are not interesting, but rather that their impact at low energies is negligible [76, 87]. Note that we can make this classification of operators for theories in arbitrary dimensions.

The recipe is very simple. One just needs to construct all possible local operators involving the fields of the theory (and respecting the symmetries) and put them into the Lagrangian. The rules for constructing an EFT are not that different from the rules for constructing any QFT, the only distinction being that we stop insisting in renormalizability, because we accept that our theory comes with an energy cutoff Λ beyond which it will break down [52]. For example, we could consider the SM as an

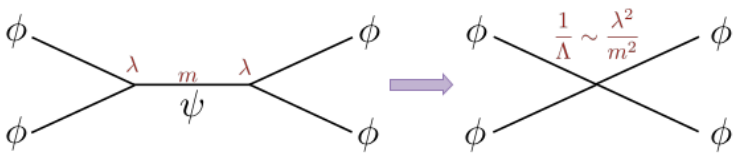

Figure 3.3.1: Generation of operators with higher mass dimensions by integrating fields out. Taken from Ref. [76].

EFT for energies well below the EW scale $\sim 10^2$ GeV. At these energies, we can never produce a W, Z or h boson on shell, so we can simply integrate them out of the theory (see Fig. [3.3.1]). This is exactly what happens, for instance, in the 4-Fermi theory for weak interactions.

An important point now is that, since we do not know how the complete theory looks like, the coefficients of our operators (usually referred to as "Wilson coefficients") are in principle arbitrary. However, we can estimate their sizes because we expect our expansion in operators to break down at energies

$\sim \Lambda$. Therefore, the natural size for our coefficients is of $\mathcal{O}(1)$ in units of the cutoff [52]. This can be better understood via dimensional analysis. We know that the mass dimension of our Lagrangian (for a theory in 4 dimensions) must be $[\mathcal{L}] = 4$, such that our action be dimensionless. Scattering amplitudes will, therefore, scale as $(E/\Lambda)^n$ for any operator where $n = d - 4$ and d is the mass dimension for the particular operator under consideration. This means that operators of lower mass dimension will become most relevant at lower energies, while operators with higher mass dimension will become important only at very high energies. We can see then that, when the energy starts to approach the cutoff, the perturbative expansion will not converge; when this happens, we are forced to specify the full theory, where the new physics will certainly involve new fields and particles [76].

On the other hand, at this point one might be worried that, in principle, there would be an infinite amount of operators with a respective infinite amount of coefficients and this would make it impossible to make any predictions with an EFT. Nonetheless, once we truncate the theory at a given order in the operators expansion, we make sure the numbers of coefficients is finite, thus recovering the predicting power [23, 62]. Therefore, the advantage of effective field theories is clear: we do not need to worry trying to understand the underlying and certainly complicated physics that waits beyond the cutoff. But, even without doing so, we still have a powerful tool that will help us make predictions that can be measured in our available range of energies.

4

DARK MATTER

As mentioned in Sec. [2.3], approximately 26% of our universe is made out of a mysterious form of matter called **dark matter**. We know very little about it, except perhaps for a few facts [89, 90, 107]:

- It seems to be **cold**, meaning that it is non-relativistic and it has not been relativistic for a long time.
- It is **dark**, *i.e.* it must have a tiny electric charge, if it has any at all.
- It must be a **stable** particle, such that its lifetime must be long compared to cosmological timescales.
- Its mass can be anywhere in between 10^{-22} eV and $5\,M_\odot \sim 10^{66}$ eV covering an impressive range of $\sim$ 90 orders of magnitude.

However, besides these tiny pieces of information we are almost completely clueless.

4.1 EVIDENCE FOR DARK MATTER

4.1.1 *Galaxy Clusters*

The problem of dark matter historically first came to be known as the problem of **missing matter** [16]. As early as in 1933, the swiss astronomer Fritz Zwicky used the virial theorem to estimate the mass of the Coma Cluster. He found out that the galaxies in the cluster were moving too fast to be explained by the measured mass in the cluster [18]. In its simplest form, the virial theorem states that for any potentially bounded system (such as a gravitational one), the time average of the total kinetic energy is related to the time average of the potential energy as [101]

$$\overline{T} = -\frac{1}{2}\overline{V}\,. \tag{4.1.1}$$

Making some simple assumptions, such as considering that the cluster consists of N galaxies with mass m, and that the system is "self-averaging" (*i.e.* averages over time are equivalent to averages over many galaxies), one can finally write

$$M_{tot} \equiv Nm = \frac{2\left\langle v^2 \right\rangle}{G\left\langle \frac{1}{r} \right\rangle} \,, \tag{4.1.2}$$

where $\langle 1/r \rangle$ is the averaged inverse distance between the galaxies and $\left\langle v^2 \right\rangle$ is their averaged square velocity. Using the data taken by Hubble and Humason, Zwicky estimated the virial mass of the Coma Cluster to be around $4.5 \times 10^{13} M_{\odot}$. Comparing this estimate to the mass measured by the luminosity of the cluster, Zwicky found that **the virial mass was greater than the luminosity mass by a factor of around 500** [89].

He then postulated the existence of additional mass in the form of "**Dunkel Materie**" providing the necessary gravitational pull to speed up the galaxies [44].

4.1.2 *Galaxy Rotation Curves*

Galaxy rotation curves play an important role in the experimental evidence for dark matter. These curves are essentially velocity profiles of the stars and gas in a given galaxy as a function of their distance to the galactic center [18]. As a rough estimate, assuming spherical symmetry, the centrifugal force of a star orbiting the galaxy at a distance r must be given by [101]

$$\frac{v^2}{r} = \frac{GM(r)}{r^2} \,, \tag{4.1.3}$$

where $M(r)$ is the mass enclosed inside a sphere of radius r. Thereby, it is expected that the rotational speed as we move away from the center changes as

$$v(r) \sim \sqrt{\frac{GM(r)}{r}} \,. \tag{4.1.4}$$

This means that measuring the speed profile of a galaxy gives us an indirect value of its mass [89]. Far away from the galactic center one should expect the rotational speed to decrease as $v(r) \sim \sqrt{1/r}$. Nonetheless, this is not the case. Already in the

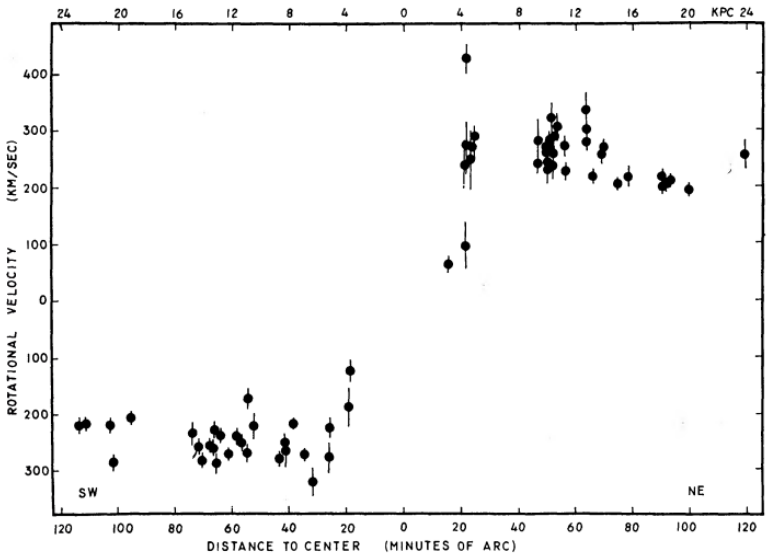

Figure 4.1.1: Rotational velocities for 67 emission regions in Andromeda as a function of the distance from the galactic center. Taken from Ref.[96].

1970's Vera Rubin and Kent Ford, performing an spectroscopic study of Andromeda, found that the velocities for objects far away from the galactic center remained constant, *i.e.* **the rotation curve became flat** [44] as shown in Fig. [4.1.1]. To explain the data, it is assumed that galaxies must have enormous **dark halos** made of DM.

4.1.3 *Gravitational Lensing*

One of the most famous predictions of General Relativity is the bending or deflection of light when passing near heavy objects curving the fabric of spacetime. As a consequence, the image we receive here on Earth may appear distorted or repeated [44]. Through gravitational lensing one can accurately determine the mass of the massive object sourcing the deflection. Generally, **the masses measured by gravitational lensing greatly exceed the visible matter**.

4.1.4 *Big Bang Nucleosynthesis*

The Big Bang Nucleosynthesis is an extremely accurate and powerful theory describing the formation of light elements in early stages of the universe [101]. It is the case that the rela-

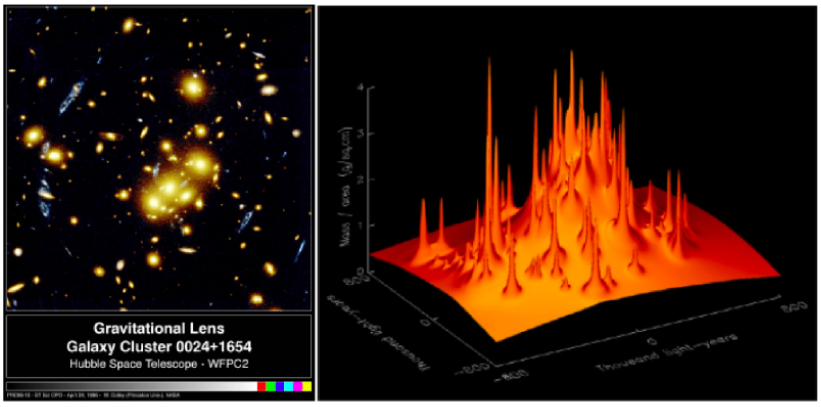

Figure 4.1.2: Gravitational lensing. **Left panel**: Cluster of galaxies lenses the blue background galaxy into several images. **Right panel**: A computer reconstruction of the lens shows a smooth background, not accounted by the luminous matter. Taken from Ref. [44].

tive abundances of light elements depend heavily on the total amount of baryonic matter. The predictions of the relative abundances are 0.25 for helium, 10^{-5} for deuterium and 10^{-10} for lithium [44]. All these numbers are compatible with baryonic matter making up only 5% of the universe.

4.1.5 *Cosmic Microwave Background*

The CMB is thermal radiation filling out our entire universe. It comes from the early stages of cosmic history, when the photons finally decoupled from the hot plasma at a redshift of about 1100 [101]. This makes the CMB a powerful tool to probe cosmological parameters, such as the energy density of the universe and the baryonic fraction [89]. In fact, the power spectrum of the CMB (the heights and positions of its peaks) is in agreement with the cosmological parameters given in Eq. (2.3.1) and, therefore, with the corresponding abundance of DM.

4.1.6 *Structure Formation*

The CMB also shows that our universe is approximately isotropic and homogeneous, with tiny fluctuations of the order of 10^{-5}. These small fluctuations evolved to form the structures we see

nowadays, such as clusters, galaxies and stars [101].

However, **structure formation could not have been possible with baryonic matter alone**. We know that visible matter was coupled to photons until approximately 300.000 years after the Big Bang, leaving insufficient time to reproduce the universe as we see it today [89]. By contrast, **dark matter is expected to decouple much earlier** allowing for its density perturbations to grow and to form gravitational wells into which baryonic matter can subsequently fall.

4.2 CANDIDATES FOR DARK MATTER

Given the overwhelming experimental support and the scientific consensus on the existence of dark matter, the next natural question comes into mind: **what is the nature of dark matter?**

The bad news is that we do not really know the answer to this question. The good news is that, currently, there are many efforts being made by theoretical and experimental physicists in order to shed some light into the darkness. For example, twenty years ago it was still reasonable to believe that dark matter could consist of **Massive Compact Halo Objects (MACHOs)**, *i.e.* faint starts like neutron stars or brown dwarfs [44]. However, thanks to the experimental evidence provided by the CMB and BBN, we now know that **DM is made out of non-baryonic material**. Here we list the most popular candidates.

4.2.1 *Axionic Dark Matter*

Axions first arose in the Peccei-Quinn solution to the strong CP problem. In the SM there are two sources for CP violation, one coming from the phase of the CKM matrix, and one coming from the **strong CP phase**. The latter emerges from a CP violating term in the QCD Lagrangian [76]

$$\mathcal{L}_{QCD} \supset \bar{\theta}\frac{g_S^2}{32\pi^2}\varepsilon^{\mu\nu\alpha\beta}G^a_{\mu\nu}G^a_{\alpha\beta}\,, \tag{4.2.1}$$

where $G_{\mu\nu}$ is the gluon field strength tensor and $\varepsilon^{\mu\nu\alpha\beta}$ is the Levi-Civita tensor. Present measurements of the neutron elec-

tric dipole moment set an upper bound for $\bar{\theta}$ of the order of [98]

$$\bar{\theta} < 10^{-10} \, . \tag{4.2.2}$$

Why is $\bar{\theta}$ so small? This is known as the strong CP problem. The Peccei-Quinn proposal to solve this problem consisted in adding a new and anomalous spontaneously broken $U(1)_{PQ}$ symmetry, thus introducing a new Nambu-Goldstone boson: the **axion** (a). The axion couples in the following way [82]

$$\mathcal{L}_{QCD} \supset \left(\bar{\theta} + \frac{a}{f_a}\right) \frac{g_S^2}{32\pi^2} \varepsilon^{\mu\nu\alpha\beta} G^a_{\mu\nu} G^a_{\alpha\beta} \, , \tag{4.2.3}$$

where f_a is the axion decay constant. Its potential is approximately given by

$$V \sim \left[1 - \cos\left(\bar{\theta} + \frac{a}{f_a}\right)\right] \, , \tag{4.2.4}$$

such that it is minimized for $\langle a \rangle = -\bar{\theta} f_a$, giving a natural resolution to the strong CP problem. As a bonus we also get a new particle as a suitable candidate for DM. Axions are weakly interacting and are very light, with an expected mass of the order of $m_a \lesssim 10^{-3}$eV [18].

4.2.2 *WIMP's*

As the name suggests, Weakly Interacting Massive Particles (WIMPs) are heavy elementary particles interacting weakly. Since the 1980's, WIMPs have gained enormous popularity as natural candidates for DM [18]. To understand why, let us make a rough estimate of the WIMPs abundance in our universe. Suppose our new elementary particle is called the X-particle. Its mass can be somewhere between a few GeV to a few TeV, so we know it will decouple from the thermal bath in the radiation dominated era. At that time, the Hubble parameter is given by [82]

$$H = g_*^{1/2} \frac{T^2}{M_{PL}} \left(\frac{\pi^2}{90}\right)^{1/2} \sim g_*^{1/2} \frac{T^2}{M_{PL}} \, , \tag{4.2.5}$$

where g_* is the number of relativistic degrees of freedom and M_{PL} is the Planck mass. Correspondingly, the annihilation rate of the WIMP will be given by

$$\Gamma = \langle \sigma v \rangle \, n_X \, , \tag{4.2.6}$$

with n_X being the number density of X and $\langle \sigma v \rangle$ its thermally averaged annihilation cross section. When $\Gamma \sim H$, the annihilation effectively stops, **freezing out** the number density to the value

$$n_X(T_f) \simeq g_*^{1/2} \frac{T_f^2}{M_{PL} \langle \sigma v \rangle} \, , \tag{4.2.7}$$

at the freeze out temperature T_f. The abundance can then be computed using the entropy density at T_f given by $s \sim g_* T_f^3$, the present entropy density s_0 and the critical density as [14, 82]

$$\Omega_X = m_X \frac{n_X}{s} \frac{s_0}{\rho_{crit,0}} \sim \frac{m_X g_*^{-1/2}}{\langle \sigma v \rangle \, M_{PL} T_f} \frac{s_0}{\rho_{crit,0}} \, . \tag{4.2.8}$$

To obtain the correct observed abundance of $\Omega_X h^2 \sim 0.12$ we need an average cross section of the order of

$$\langle \sigma v \rangle \sim 10^{-19} \text{GeV}^{-2} \sim 1 \text{pb} \, . \tag{4.2.9}$$

Surprisingly, this is a typical weak interaction cross section. Therefore, for an arbitrary particle X with SM gauge couplings and a mass of ranging from a few GeV to a few TeV, the resulting relic abundance turns out to be pretty close to the observed value. This coincidence is known as the **WIMP miracle** [16].

4.3 THERMAL PRODUCTION OF WIMP DARK MATTER

For now let us focus in WIMP DM and discuss its production and evolution during the cosmic history. With this purpose in mind, let us suppose our dark matter candidate is the X particle discussed in Sec. [4.2.2]. Let us also suppose that X and its antiparticle $\bar{X}$ can annihilate into two light (essentially massless) particles l and $\bar{l}$ [14]. The l particles are heavily coupled to the thermal bath such that, throughout, they maintain their equi-

librium abundances $n_l = n_l^{eq}$. Under the additional assumption that $n_X = n_{\bar{X}}$ one can write the Boltzmann equation (2.4.7) as

$$\frac{dN_X}{dt} = -s \langle \sigma v \rangle \left[N_X^2 - \left(N_X^{eq} \right)^2 \right] . \tag{4.3.1}$$

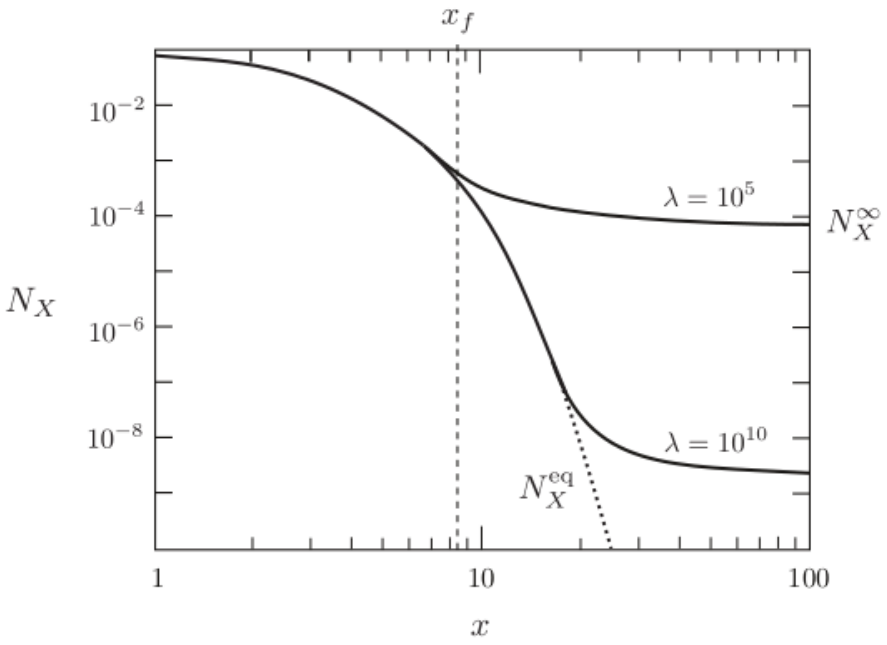

Figure 4.3.1: Dark matter abundance as a function of temperature. Taken from Ref.[14].

Since all interesting dynamics will take place when $m_X \sim T$ we define the quantity $x \equiv m_X / T$. Taking a radiation-dominated universe at the time of freeze out we can convert Eq. (4.3.1) into the so called **Riccati Equation** [14]

$$\frac{dN_X}{dt} = -\frac{\lambda}{x^2} \left[N_X^2 - \left(N_X^{eq} \right)^2 \right] , \tag{4.3.2}$$

with g_{*S} being the number of relativistic degrees on freedom in entropy,

$$\lambda \equiv \frac{2\pi^2}{45} g_{*S} \frac{m_X^3 \langle \sigma v \rangle}{H(m_X)} , \tag{4.3.3}$$

where $H(m_X)$ is the Hubble parameter at $T = m_X$. Eq. (4.3.2) has no analytical solutions so numerical results are depicted in Fig. [4.3.1]. These show that DM freeze out occurs at around $x_f \sim 10$.

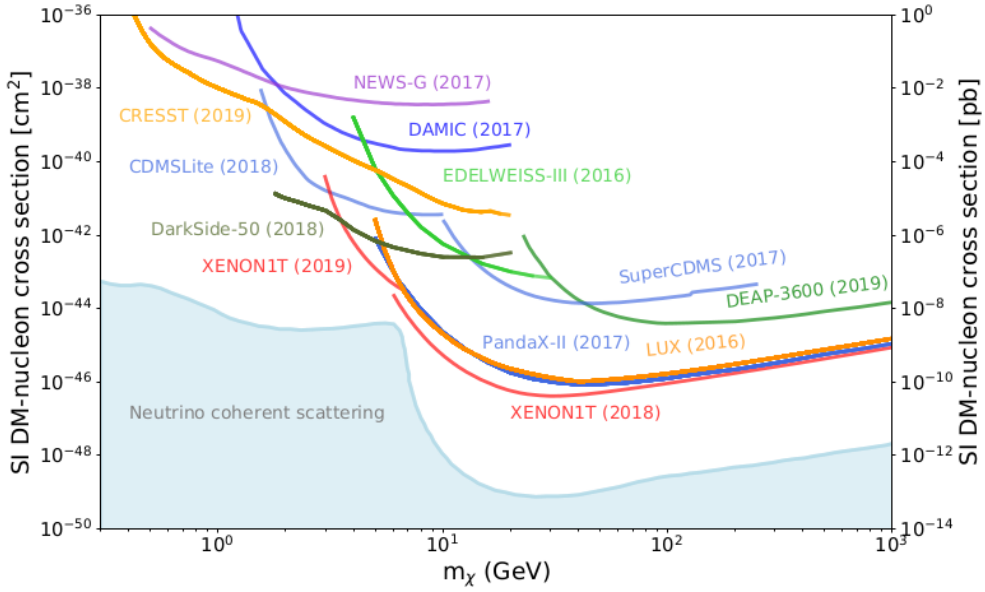

Figure 4.3.2: Upper limits on the spin-independent DM-nucleon cross section as a function of the DM mass. Taken from Ref.[107].

4.4 SEARCHES FOR DARK MATTER

Currently there is a lot of effort being made to detect dark matter directly or indirectly, including several experiments around the world. Direct detection experiments aim to observe scattering events of galactic DM particles with nucleons or electrons in the material of the detector in the form of ionisation, scintillation or lattice vibrations. These events are very rare and the signals are expected to be very small [107].

In Fig. [4.3.2] the best constraints on the spin-independent DM-nucleon cross section for different experiments are shown. It can be seen that the most stringent constraints come from the XENON1T collaboration [3, 4].

5

BARYOGENESIS

The idea of antimatter as we know it today was first proposed by Dirac in 1928 as a negative energy solution to his equation [72]. Two years later, the positron (the anti-partner of the electron) was discovered and the scientific community started wondering about the nature and the reason for the predominance of matter over antimatter.

It is reasonable, for example, to expect equal amounts of matter and antimatter when the universe came to be at first. However, this preconception is problematic because matter and antimatter usually annihilate with each other in processes like $e^- + e^+ \rightarrow \gamma + \gamma$. So, if the universe indeed started in a symmetric state, today we would expect it to be filled with only radiation [14].

Nonetheless, we know this is not the case. After all, the universe is filled with galaxies, stars and so on. In fact, observations show that **antimatter is very rare**. Out of everyday experience we know the Earth is made out of matter, with slightly amounts of antimatter being found only in the physics laboratories. From experience we also know the moon, the Sun and the Solar System must all be made out of matter. Moreover, cosmic rays coming from our galaxy further exhibit this asymmetry with antiprotons showing up in a ratio of only 10^{-4} compared to protons [64]. This is consistent with the idea of secondary production of antiprotons by ray collisions with the interstellar medium. It seems, then, that wherever we set eyes on we find this asymmetry: everything appears to be made out of baryons alone.

Even if we postulate the existence of big matter- and antimatter-dominated regions of the universe separated by large distances, we would expect to see a great flux of gamma rays coming from the boundaries between regions, but we have not seen any so far. Therefore, we have good reasons to believe in the asymme-

try [104].

This asymmetry usually goes by the name of the BAU. The main pieces of evidence for the BAU come from BBN and the CMB anisotropies [14] from which we obtain the baryon-to-photon number as the quantity measuring the amount of asymmetry. Presently its value is [107]

$$\eta = 6.14(19) \times 10^{-10} \,, \tag{5.0.1}$$

where η is defined as the ratio between the number density of baryons and the number density of photons, *i.e.* n_B/n_γ. Since the number density of photons is not a conserved quantity it is also customary to use the ratio n_B/s, with $s_0 = 7.04\, n_{\gamma_0}$ the entropy density of the universe today [81]. Considering that the number density of baryons is also defined as

$$n_B = n_b - n_{\bar{b}} \,, \tag{5.0.2}$$

with n_b and $n_{\bar{b}}$ the number densities of baryons and antibaryons, respectively, η is a clear indicator of the BAU.

There are two possible explanations for the BAU. One is to accept the asymmetry as an initial condition of our universe. However, this means accepting an extremely fined-tuned number of only **one extra baryon for every billion baryon-antibaryon pairs** [101]. It also means having tensions with inflation, because even this small number is way to big for inflationary models where all initial conditions are effectively washed out [99]. The other possibility, on the other hand, is to assume that we started with a symmetric universe but, some dynamical mechanism known as **Baryogenesis** created the asymmetry we see today. In 1967 Andrei Sakharov established 3 basic conditions that must be fulfilled in any model of baryogenesis [97] and that we present in detail in the next section.

5.1 SAKHAROV CONDITIONS

5.1.1 *Baryon Number Violation*

We begin with the most intuitive and obvious condition. If we start with a symmetric universe with $B = 0$, then we need some

baryon number violating processes in order to evolve to a universe with $B \neq 0$, where the baryon number B is defined as

$$B = \frac{n_q - n_{\bar{q}}}{3} \,, \tag{5.1.1}$$

for n_q and $n_{\bar{q}}$ being the number of quarks and anti-quarks, respectively.

As a caveat, baryon number violating interactions in any model will be constrained by the proton lifetime ($\tau_p \sim 10^{32}$ years [93]).

5.1.2 *C and CP Violation*

The violation of charge conjugation (C) and charge conjugation plus parity symmetry (CP) may appear as a less obvious condition. However, C and CP violation are essential to ensure that particles and antiparticles behave differently under certain processes, providing us with a mechanism under which particles are favoured over antiparticles.

For the purpose of illustration let us consider a theory in which we have a heavy boson X and its antiparticle $\bar{X}$, both of which decay in baryon number violating processes [28]

$$\begin{aligned} X &\to qq \quad \text{with} \quad \Delta B_X = \frac{2}{3} \quad \text{and} \\ \bar{X} &\to \bar{q}\bar{q} \quad \text{with} \quad \Delta B_{\bar{X}} = -\frac{2}{3}. \end{aligned} \tag{5.1.2}$$

We then denote by r and $\bar{r}$ the corresponding branching ratios

$$r = \frac{\Gamma(X \to qq)}{\Gamma_X} \quad \text{and} \quad \bar{r} = \frac{\Gamma(\bar{X} \to \bar{q}\bar{q})}{\Gamma_{\bar{X}}} \,, \tag{5.1.3}$$

with $\Gamma_{X,\bar{X}}$ the total decay rate. Because of CPT invariance we also know that $\Gamma_X = \Gamma_{\bar{X}}$. It follows that the net baryon number produced in the decays will be given by

$$\epsilon = \Delta B_X + \Delta B_{\bar{X}} = \frac{2}{3}\,(r - \bar{r}) \,, \tag{5.1.4}$$

where

$$r - \bar{r} = \frac{\Gamma(X \to qq) - \Gamma(\bar{X} \to \bar{q}\bar{q})}{\Gamma_X} \,. \tag{5.1.5}$$

Therefore, if we suppose our theory is invariant under charge conjugation [104], *i.e.* $X \to \bar{X}$ and $q \to \bar{q}$, then we immediately see that $\Gamma(X \to qq) = \Gamma(\bar{X} \to \bar{q}\bar{q})$, giving a vanishing contribution to the baryon number in Eq. (5.1.4). In the same way, rewriting the decay rates to explicitly show the contributions from left-handed and right-handed particles

$$\Gamma(X \to qq) = \Gamma(X \to q_L q_L) + \Gamma(X \to q_R q_R) \,, \tag{5.1.6}$$

we can recast Eq. (5.1.5) as

$$r - \bar{r} = \frac{\Gamma(X \to q_L q_L) + \Gamma(X \to q_R q_R) - \Gamma(\bar{X} \to \bar{q}_L \bar{q}_L) - \Gamma(\bar{X} \to \bar{q}_R \bar{q}_R)}{\Gamma_X} \,. \tag{5.1.7}$$

From here we see that if our theory is invariant under CP, such that

$$\begin{aligned} &\Gamma(X \to q_L q_L) = \Gamma(\bar{X} \to \bar{q}_R \bar{q}_R) \quad \text{and} \\ &\Gamma(X \to q_R q_R) = \Gamma(\bar{X} \to \bar{q}_L \bar{q}_L) \,, \end{aligned} \tag{5.1.8}$$

we obtain again $r - \bar{r} = 0$ and, consequently, no net baryon number can be produced.

5.1.3 *Departure from Thermal Equilibrium*

Finally, we arrive at the last and least intuitive condition for baryogenesis. However, if all the particles in the universe had remained in thermal equilibrium, CPT invariance would have prevented the appearance of any asymmetry. In order to see this, let us consider a certain species X that is in thermal equilibrium at $T \ll m_X$ such that, according to Eq. (2.4.4), its number density will be given by

$$n_X = g_X \left(\frac{m_X T}{2\pi}\right)^{3/2} e^{\frac{-m_X + \mu_X}{T}} \,, \tag{5.1.9}$$

where μ_X is the chemical potential and g_X is the number of degrees of freedom [93]. When in equilibrium the chemical potential must be conserved, *i.e.* in a process $1 + 2 \leftrightarrow 3 + 4$ we must have [14]

$$\mu_1 + \mu_2 = \mu_3 + \mu_4 \, . \tag{5.1.10}$$

Therefore, due to the matter-antimatter annihilation process $X + \bar{X} \to 2\gamma$, we can conclude that $\mu_X = -\mu_{\bar{X}}$. It follows that baryon number will get a contribution of the form

$$B \propto n_x - n_{\bar{X}} = 2g_X \left(\frac{m_X T}{2\pi}\right)^{3/2} e^{-m_X/T} \sinh\left(\frac{\mu_X}{T}\right) \, . \tag{5.1.11}$$

When X undergoes B violating processes (as required by the first Sakharov condition) such as $X + X \to \bar{X} + \bar{X}$, then $\mu_X = 0$ and, from Eq. (5.1.11), we get $B = 0$. Thus, no net asymmetry can be developed when in equilibrium.

5.2 ELECTROWEAK BARYOGENESIS

As surprising as it may be, in the SM we have all the necessary ingredients, as given in the last section, to explain the baryon asymmetry within the model. In this section, however, we will explain in detail how each of the Sakharov conditions are manifested in the SM and why they fail to explain the observed BAU, thus calling for BSM theories.

5.2.1 *Baryon Number Violation in the SM*

We know for a fact that in the SM baryon number and lepton number (L) are conserved at tree level and at any order in perturbation theory. They are **accidental symmetries** [28] with corresponding conserved currents

$$\begin{aligned} J^\mu_B &= \sum_q \frac{1}{3} \bar{q} \gamma^\mu q \\ J^\mu_L &= \sum_l \bar{l} \gamma^\mu l + \bar{\nu}_l \gamma^\mu \nu_l \, . \end{aligned} \tag{5.2.1}$$

At classical level we must have $\partial_\mu J^\mu_B = \partial_\mu J^\mu_L = 0$, which results in a conservation law for B and L [104].

However, the conservation is spoiled by quantum corrections through the chiral anomaly [91]. Already in 1976 't Hooft [58] realized that non-perturbative effects can give rise to processes in which $B + L$ is not conserved.

In order to see how this violation comes about, let us consider the following generating function in Euclidean space [98]

$$\exp[-\mathcal{Z}] = \int \mathcal{D}\Psi\mathcal{D}\bar{\Psi}\, \exp[-S] \tag{5.2.2}$$

for a Dirac field Ψ. Let us now consider a general phase transformation for the Dirac field in the following way

$$\Psi(x) \to e^{i(a+b\gamma_5)\theta(x)}\Psi(x)\ . \tag{5.2.3}$$

with $\theta(x)$ a spacetime-dependent phase. For $a = \frac{1}{3}$ and $b = 0$, Eq. (5.2.3) reduces to a rotation of baryon number, while we get a rotation of lepton number when $a = 1$ and $b = 0$. Under the general transformation in Eq. (5.2.3) the action changes as [47, 93]

$$\delta S_0 = -\int d^4x \left[\bar{\Psi} m \left(e^{2ib\gamma_5\theta(x)} - 1\right)\Psi + \bar{\Psi}\gamma^\mu(a + b\gamma_5)\Psi\partial_\mu\theta(x)\right]\ . \tag{5.2.4}$$

Moreover, since the measure in Eq. (5.2.2) is not invariant under the transformation in Eq. (5.2.3), we will get an extra term which can be written as an extra contribution to the action

$$\delta S_1 = i\int d^4x\, \theta(x)\left[\frac{(a-b)}{8\pi^2} TrF^{(L)\mu\nu}\tilde{F}^{(L)}_{\mu\nu} - \frac{(a+b)}{8\pi^2} TrF^{(R)\mu\nu}\tilde{F}^{(R)}_{\mu\nu}\right]\ , \tag{5.2.5}$$

where $F^{(L)}_{\mu\nu}$ and $F^{(R)}_{\mu\nu}$ are the field strength tensors coupled to the left-handed and right-handed fields respectively, and $\tilde{F}$ is the dual field strength tensor defined as

$$\tilde{F}_{\mu\nu} = \frac{1}{2}\varepsilon_{\mu\nu\sigma\rho}F^{\sigma\rho}\ . \tag{5.2.6}$$

Integrating Eq. (5.2.4) by parts and demanding that the generating function is invariant under baryon and lepton number transformations, we obtain that the derivatives of the baryonic and leptonic currents do not vanish but, rather remarkably, they are given by

$$\partial_\mu J^\mu_B = \partial_\mu J^\mu_L = i\frac{N_F}{32\pi^2}\left(-g^2 W^{a\mu\nu}\tilde{W}^a_{\mu\nu} + g'^2 B^{\mu\nu}\tilde{B}_{\mu\nu}\right) , \quad (5.2.7)$$

with N_F the number of generations, $W_{\mu\nu}$ and $B_{\mu\nu}$ the field strength tensors for $SU(2)_L$ and $U(1)_Y$ respectively, and corresponding coupling constants g and g'. From Eq. (5.2.7) we immediately see that, since $\partial_\mu(J^\mu_B - J^\mu_L) = 0$, the combination $B - L$ will be a conserved quantity [28]. However $B + L$ is not conserved. In fact, we can rewrite the right-hand side of Eq. (5.2.7) as four divergences [91]

$$\partial_\mu J^\mu_B = i\frac{N_F}{32\pi^2}\left(-g^2\partial_\mu K^\mu + g'^2\partial_\mu k^\mu\right) , \quad (5.2.8)$$

where

$$\begin{aligned} k^\mu &= \varepsilon^{\mu\nu\alpha\beta}B_{\nu\alpha}B_\beta \quad \text{and} \\ K^\mu &= \varepsilon^{\mu\nu\alpha\beta}\left(W^a_{\nu\alpha}W^a_\beta - \frac{g}{3}\varepsilon_{abc}W^a_\nu W^b_\alpha W^c_\beta\right) . \end{aligned} \quad (5.2.9)$$

Now, total derivatives are usually unobservable because they can be integrated by parts and they drop from the integrals. This is true, for instance, for the abelian fields in k^μ since they vanish quickly enough at infinity and their integral vanishes. However, due to the topological properties of $SU(2)$ this is not true for the fields in K^μ which will pick contributions at infinity that cannot be dropped. This means the the current non-conservation becomes observable only for non-abelian groups. Indeed, given that baryon number can be obtained from the baryonic current as [93]

$$B = i\int d^3x J^0_B , \quad (5.2.10)$$

baryon number violation will be given by

$$\Delta B = B(t_f) - B(t_i) = N_F\Delta N_{CS} = 3\Delta N_{CS} , \quad (5.2.11)$$

where N_{CS} is known as the **Chern-Simons number** and it is defined as

$$N_{CS} = \frac{g^2}{32\pi^2}\int d^3x\,\varepsilon^{ijk}\left(W^a_{ij}W^a_k - \frac{g}{3}\varepsilon_{abc}W^a_i W^b_j W^c_k\right)\ . \quad (5.2.12)$$

The key point here is that the fields W^a_μ can be gauged away locally, but not globally by a gauge transformation. In fact, under a gauge transformation U the fields transform as

$$W_i \to UW_iU^{-1} + \frac{i}{g}(\partial_i U)U^{-1}, \quad (5.2.13)$$

and the corresponding change in N_{CS} is [47]

$$\delta N_{CS} = \frac{1}{24\pi^2}\int d^3x\varepsilon^{ijk}\ Tr\left[(\partial_i U)U^{-1}(\partial_j U)U^{-1}(\partial_k U)U^{-1}\right]\ . \quad (5.2.14)$$

Evaluating δN_{CS} is easily done by remembering that the most general 2×2 unitary matrix can be written as $U = a\mathbb{1} + ib_j\sigma^j$, where $a^2 + |\mathbf{b}|^2 = 1$ and σ^j are the Pauli matrices. For example we can take the maps [93]

$$\begin{aligned} U^{(0)}(x) &= \mathbb{1} \\ U^{(1)}(x) &= \frac{x_0 + i\vec{x}\cdot\vec{\sigma}}{r} \quad \text{with} \quad r = \left(x_0^2 + |\vec{x}|^2\right)^{1/2}, \\ U^{(n)}(x) &= \left[U^{(1)}\right]^n\ , \end{aligned} \quad (5.2.15)$$

for which it is straightforward to check that $\delta N_{CS}\left(U^{(0)}\right) = 0$, $\delta N_{CS}\left(U^{(1)}\right) = 1$ and $\delta N_{CS}\left(U^{(n)}\right) = n$. Thus, it is clear that we can have two different types of gauge transformations, the ones which do not change N_{CS} and the ones that change N_{CS} by n, the **winding number**. Now, let us suppose that we wish to compute ΔB when we go from an initial to a final configuration of gauge fields. For that purpose we can consider vacuum field strength tensors, *i.e.* configurations for which $W_{\mu\nu} = 0$. The corresponding fields are, therefore, pure gauge fields [91, 93]

$$W_{vac} = \frac{i}{g}(\nabla U)U^{-1}, \quad (5.2.16)$$

where we choose the temporal gauge $W_0 = 0$. Note that all the configurations W_{vac} may be regarded as describing a ground state. As said before, we can have two different classes of gauge transformations for which one can keep $W_{\mu\nu} = 0$:

1. continuous transformations of the fields, *i.e.* $U^{(0)}$ or any transformation related to $U^{(0)}$ by

$$U(x) = U^{(0)}(x)\left(1 + i\epsilon^a(x)\sigma^a\right), \tag{5.2.17}$$

   with $\epsilon^a(x) \to 0$ when $|\vec{x}| \to \infty$;

2. transforming the fields via $U^{(n)}$ which leads to another ground state with different Chern-Simons number.

Accordingly, this tells us that the vacuum structure of $SU(2)$ consists of an infinite amount of degenerate vacua separated by potential barriers and which differ from each other by units of topological charge given by N_{CS} (see Fig. [5.2.1]). Therefore, every time a transition between different vacua occurs, a net change in baryon number arise as given by Eq. (5.2.11).

In a semi-classical approximation, for instance, one can compute the probability of tunneling between neighbouring vacua which is given by the **instanton configurations** [28]. In fact, at zero temperature, the probability of starting at a state $|\Psi, B\rangle$ with baryon number B and tunneling through the barrier to a state $|\Psi, B \pm 3\rangle$ is given by [104]

$$\langle \Psi, B \pm 3 | \Psi, B \rangle \propto e^{-S_{inst}} = e^{-4\pi/\alpha_W} \sim 10^{-164}\,, \tag{5.2.18}$$

where S_{inst} is the action corresponding to the instanton configuration, and $\alpha_W = \frac{g^2}{4\pi}$ is the weak coupling constant.

The number in Eq. (5.2.18) is so small, that it explains why we have not seen any B-violating processes in experiments. At zero temperature, B-violation is basically nonexistent.

5.2.1.1 *Sphalerons*

Even though we can forget about B violation taking place at zero temperature, not everything is lost. In 1985 Kuzmin, Rubakov and Shaposhnikov [66] already pointed out that at finite temperature the picture can be quite different. They realized that,

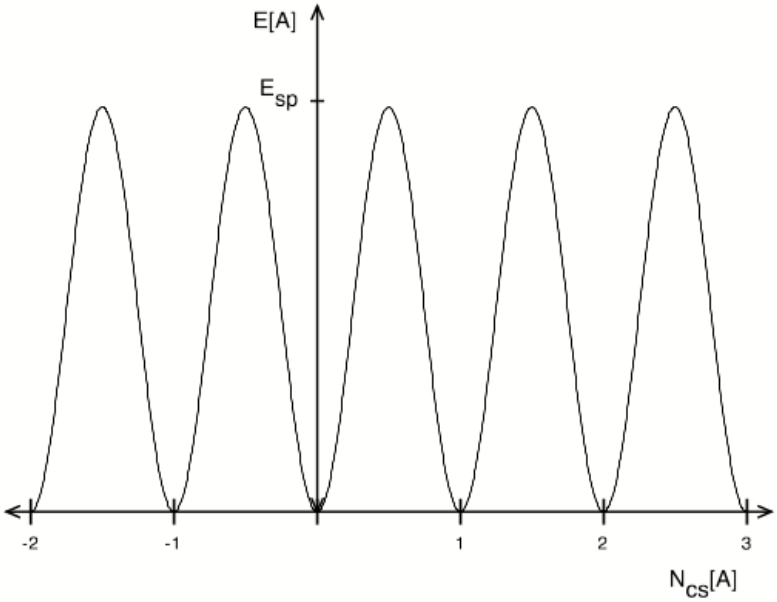

Figure 5.2.1: Energy dependence of the gauge configurations as a function of the winding number N_{CS}. Taken from Ref.[28].

in the presence of a thermal bath, transitions between different vacua can occur, not by tunneling, but by going ("jumping") over the barrier [104]. These field configurations known as **sphalerons** (Greek for "ready to fall") are saddle point solutions to the equations of motion. The rate of baryon number violation per unit volume was computed by Arnold and McLerran [8] and it is given by [104]

$$\frac{\Gamma_{sph}}{V} = c \left(\frac{E_{sph}}{T}\right)^3 [m_W(T)]^4 \, e^{-E_{sph}/T} \,, \tag{5.2.19}$$

where c is a constant and $m_W(T)$ is the temperature-dependent mass of the W boson, written in terms of the temperature-dependent Higgs VEV $\langle\Phi\rangle$ as

$$m_W(T) = \frac{g}{2} \langle\Phi(T)\rangle \,. \tag{5.2.20}$$

The sphaleron energy computed in Ref.[79] is given by

$$E_{sph}(T) = \frac{2m_W(T)}{\alpha_W} B\left(\frac{m_h}{m_W}\right) \,, \tag{5.2.21}$$

The B parameter in Eq. (5.2.21) may appear ill defined for $m_W \to 0$. However, its value in this case is simply $B(\infty) = 2.72$.

where, for the SM, B appearing in Eq. (5.2.21) is a parameter ranging from 1.56 to 2.72 [104]. We can now distinguish between two cases. For temperatures above the EWPhT ($T \sim 100\,\text{GeV}$), *i.e.* in the symmetric phase where the Higgs is still in the symmetric vacuum, the W boson is massless such that $E_{sph} = 0$. This means that the energy barriers between different vacua disappear and the exponential factor in Eq. (5.2.19) drops out. In this case, the computation for the transition rate requires a careful treatment of high-temperature effects which is a very involved task. However, one can estimate the result using dimensional analysis, from which one expects the rate to scale as [91]

$$\frac{\Gamma_{sph}}{V} \sim \kappa(\alpha_W T)^4 \,, \tag{5.2.22}$$

with $0.1 \lesssim \kappa \lesssim 1.0$. A more precise value is obtained on the lattice [77, 78], resulting in a extra damping factor of α_W

$$\frac{\Gamma_{sph}}{V} = \kappa' \alpha_W (\alpha_W T)^4 \,, \tag{5.2.23}$$

where $\kappa' = 29 \pm 6$ [81]. This is a key result. Sphaleron processes are unsuppressed in the unbroken phase, where transitions between different vacua will result in a change in baryon number. In the broken phase, however, the sphalerons are exponentially suppressed meaning that any asymmetry produced before the phase transition will, in principle, be preserved for $T \ll T_{EW}$.

5.2.2 *Sources of CP Violation*

As mentioned in Sec. [5.1.2], both C and CP must be violated in order to generate a baryon asymmetry. Good news is that the theory of electroweak interactions naturally satisfy both conditions. As it happens, C is maximally violated in the weak interactions, given that only left-handed particles and right-handed antiparticles couple to $SU(2)_L$. On the other hand, CP violation has been observed in rare processes involving hadrons, such as the neutral Kaon system [102]. To understand where this comes from, let us consider the charged current Lagrangian in the weak basis which is given by

$$\mathcal{L}_W^{weak} = \frac{g}{\sqrt{2}} \left(\bar{u}_L \gamma^\mu d_L W_\mu^+ + \bar{d}_L \gamma^\mu u_L W_\mu^- \right) \,, \tag{5.2.24}$$

where $u_L = (u, c, t)_L$ and $d_L = (d, s, b)_L$ [28]. We can then perform a chiral rotation on the left-handed quarks, such that masses are diagonalized via unitary transformations $U^{u,d}_{L,R}$ in the following way

$$\begin{aligned} diag(m_u, m_c, m_t) &= U^u_L M^u U^u_R \\ diag(m_d, m_s, m_b) &= U^d_L M^d U^d_R \, . \end{aligned} \tag{5.2.25}$$

The charged current in the mass basis is, therefore [83, 98],

$$\mathcal{L}^{mass}_W = \frac{g}{\sqrt{2}} \left(\bar{u}'_L V \gamma^\mu d'_L W^+_\mu + \bar{d}'_L V^\dagger \gamma^\mu u'_L W^-_\mu \right) \, , \tag{5.2.26}$$

where the prime indicates the rotated fields, *i.e.* $u'_L = U^u_L u_L$, $d'_L = U^d_L d_L$ and $V = U^u_L (U^d_L)^\dagger$ is the Cabibbo–Kobayashi–Maskawa (CKM) matrix. After a CP transformation $\mathcal{L}^{mass}_W$ changes as

$$\mathcal{L}^{mass}_W \xrightarrow{CP} \frac{g}{\sqrt{2}} \left(\bar{u}'_L (V^\dagger)^T \gamma^\mu d'_L W^+_\mu + \bar{d}'_L (V)^T \gamma^\mu u'_L W^-_\mu \right) \, . \tag{5.2.27}$$

This implies that the SM Lagrangian is invariant under CP (for more details on CP violation see Appendix [B]) if and only if $V = V^*$, *i.e.* the CKM matrix is real. In general, a 3×3 unitary matrix can be parametrized by 9 degrees of freedom divided into 3 angles and 6 phases. However, 5 out of the 6 phases can be absorbed into redefinitions of the quark fields, leaving us with 3 angles and one physical phase as the only source of weak CP violation in the SM. In fact, in 1985 Jarlskog [61] found that CP violation in the quark sector originates in a single CP-odd invariant called the **Jarlskog invariant** that depends on the product of the difference between quark masses [67, 84]

$$\begin{aligned} J_{SM} = (m_t^2 - m_c^2) \cdot (m_c^2 - m_u^2) \cdot (m_t^2 - m_u^2) \cdot (m_b^2 - m_s^2) \cdot \\ (m_b^2 - m_d^2) \cdot (m_s^2 - m_d^2) \cdot \Im(V_{ud} V_{cs} V^*_{us} V^*_{cd}) \, . \end{aligned} \tag{5.2.28}$$

Turning back to the problem of baryogenesis, we wonder if the CP violation encoded in the Jarlskog invariant is sufficient to generate the baryon asymmetry we see today. As it happens, the role played by CP violation in baryogenesis turns out to be highly non-trivial and it will be discussed in more detail in next sections. Nonetheless, we are still able to do a naive estimate of its influence. The first thing we need to note is that the

sphaleron processes described in Sec. [5.2.1.1] can create both, a positive and a negative baryon number, resulting in no net change for B. The job for CP violation, however, is to provide us with a fixed direction for the sphaleron processes to occur [102]. Consequently, given the baryon number violation rate Γ_{sph} in Eq. (5.2.22), we can write [28, 43, 47, 93]

$$\eta \sim \frac{\Gamma_{sph}}{sT}\delta_{CP} = \frac{\alpha_W^4 T^3}{s}\delta_{CP} \sim 10^{-8}\delta_{CP} \,, \tag{5.2.29}$$

where s is the entropy density of the universe, and δ_{CP} is a dimensionless suppression factor due to CP violation. As a rough estimate for δ_{CP}, since all the CP violation in the SM must be proportional to J_{SM}, and the Jarlskog invariant has mass dimension 12, the dimensionless quantity will be given by [29]

$$\delta_{CP} = \frac{J_{SM}}{(T_{EW})^{12}} \,, \tag{5.2.30}$$

with the EW temperature of the order $\sim 100\,\text{GeV}$. Hence, for the SM we obtain $\delta_{CP} \sim 10^{-20}$ which, at the same time, implies a baryon-to-photon ratio of the order $\eta \sim 10^{-28}$, such that it is not possible to account for the observed value of $\eta \sim 10^{-10}$.

Another possible source for CP violation within the SM comes from the strong CP phase discussed in Sec.(4.2.1). However, due to electric dipole moments constraints, its effect is even smaller that the one coming from weak CP violation, ruling out the possibility of its influence in baryogenesis.

5.2.3 *The Out of Equilibrium Scenario*

We finally get to the last Sakharov condition. The out of equilibrium scenario we need for baryogenesis is given in standard cosmology by the expansion of the universe itself, as discussed in Sec. [2.4.2]. In this section we will review how this condition is translated into a successful theory of baryogenesis and how it is related to the EWPhT.

5.2.3.1 *The Wash-Out of $B + L$*

A natural question to ask at this point is at what temperature sphalerons were in thermal equilibrium with the hot plasma. In order to answer this, we need to compare the corresponding rate with that of the expansion of the universe. For temperatures above the EWPhT, with the sphaleron rate given by Eq. (5.2.22), B violating processes are in thermal equilibrium when $\Gamma_{sph} \gtrsim H$ [93, 104]. Using that the comoving volume

scales as $V \sim T^{-3}$ and using the Hubble parameter for a radiation dominated universe we find that

$$\frac{(\alpha_W T)^4}{T^3} \gtrsim g_*^{1/2} \frac{T^2}{M_{PL}} \rightarrow T \lesssim 10^{12}\,\text{GeV} \,. \tag{5.2.31}$$

This is a very interesting result. For temperatures above $\sim 10^{13}$ GeV sphalerons are out of thermal equilibrium. Below this temperature, where sphalerons are in equilibrium, any asymmetry created before will then be washed out when sufficient time has passed. However, once we reach the electroweak temperature, the rate of the sphalerons becomes exponentially suppressed, as in Eq. (5.2.19), quickly dropping below H again [29]. The situation is depicted in Fig. [5.2.2]. This opens up the possibility for the asymmetry to be created during the EWPhT; a process known as **Electroweak Baryogenesis (EWBG)**. An important remark here is that we need the sphalerons to turn off quickly after the phase transition has taken place, otherwise our asymmetry created during the EWPhT will also be washed out. This condition translates into a bound of the sphaleron energy at the critical temperature T_c [91]

$$\frac{E_{sph}(T_c)}{T_c} \gtrsim 37 \,, \tag{5.2.32}$$

which, at the same time, can be translated into a condition for the Higgs VEV

$$\xi \overset{def}{=} \frac{\langle \Phi(T_c) \rangle}{T_c} \gtrsim 1.0 \,. \tag{5.2.33}$$

As we will see in next section, Eq. (5.2.33) imposes some direct constraints on the nature of the EWPhT.

5.2.3.2 *Electroweak Phase Transition*

As we have seen in previous sections the electroweak phase transition plays a starring role in EWBG. This Phase Transition (PhT) occurs because at finite temperature the VEV of the Higgs does not correspond to the minimum of the effective potential at zero temperature, but rather to the minimum of the effective potential at finite temperature (for more details about effective potentials at zero and finite temperatures see Appendix [A]). Then, as it happens, even when the minimum at $T = 0$ occurs

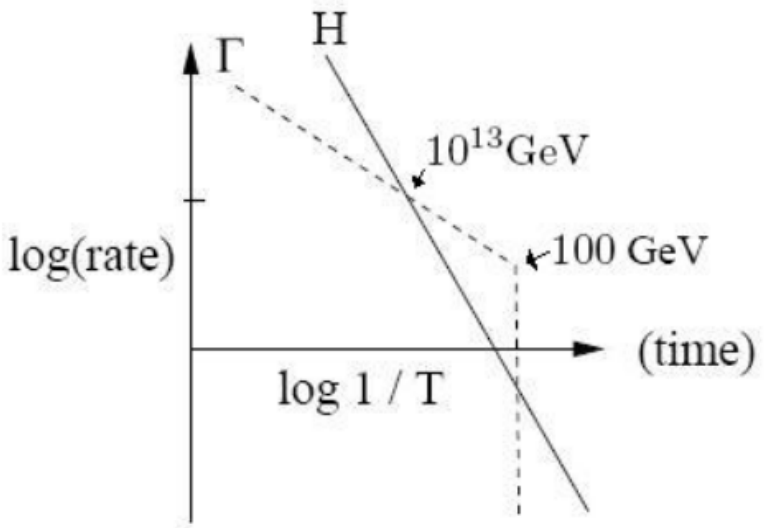

Figure 5.2.2: The log of the spaleron rate Γ and the Hubble rate H as a function of $1/T$. Taken from Ref.[104].

at $\langle\Phi\rangle \neq 0$, the minimum at higher temperatures may occur at $\langle\Phi\rangle = 0$, a process known as **symmetry restoration** [91]. The phase transition from $\langle\Phi\rangle = 0$ to $\langle\Phi\rangle \neq 0$ can be either first or second order. We say there is a first order PhT when a thermodynamic quantity changes discontinuously, meaning that when the transition happens we have two coexisting thermodynamic states in equilibrium with each other. In a second order phase transition, on the other hand, the change happens in a continuous way. We refer to the quantity that is changing as the **order parameter** [102]. In the context of the EWPhT the transition is characterized by the evolution of the Higgs potential as a function of temperature and the order parameter is the VEV of the Higgs itself.

If we were to have a continuous transition, we would have a smooth crossover as depicted in Fig. [5.2.3], so that the field can slowly roll down to the new global minimum.

In contrast, in a first order phase transition, the extremum at $\langle\Phi\rangle = 0$ becomes separated from a second local minimum by

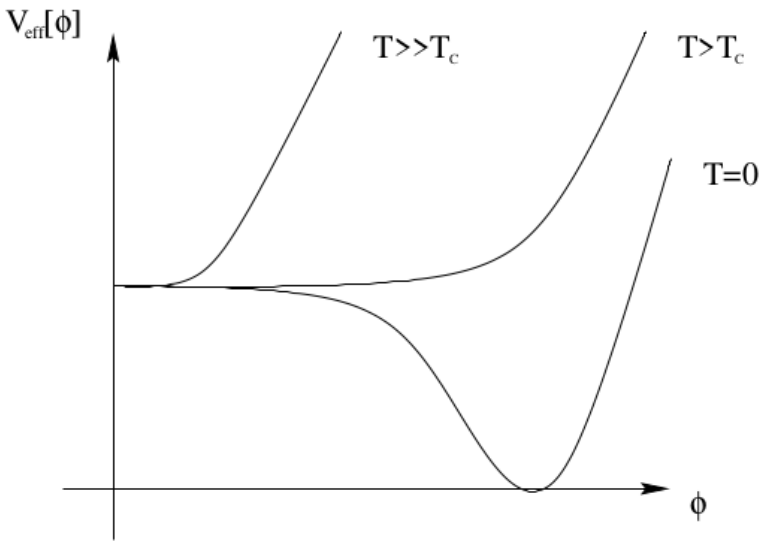

Figure 5.2.3: The evolution of the effective potential in a second order phase transition. Taken from Ref.[102].

a potential barrier. To see how this works we can work with a potential of the form [80, 91]

$$V(\Phi, T) = D(T^2 - T_0^2)\Phi^2 - ET\Phi^3 + \frac{\lambda(T)}{4}\Phi^4 \,, \qquad (5.2.34)$$

where D, E and T_0 are independent coefficients and $\lambda(T)$ is a slowly varying function of temperature. In the limit $E = 0$ the phase transition is second order [80]. In the $E \neq 0$ case, the situation changes. For high temperatures the only minimum occurs for $\langle\Phi\rangle = 0$ but, for a certain temperature T_1, another local minimum appears at

$$\langle\Phi(T_1)\rangle = \frac{3ET_1}{2\lambda(T_1)} \,. \qquad (5.2.35)$$

Subsequently a barrier between both minima (generated by the cubic term in the potential) starts to develop until they become degenerate at the critical temperature T_c as depicted in Fig. [5.2.4]. At later times, for $T_0 < T_c$, the minimum away from the origin becomes the global one.

Nonetheless, the PhT can start already at T_c by quantum tunneling. The transition is to be understood as the formation of bubbles of broken phase in a sea of symmetric phase. The bub-

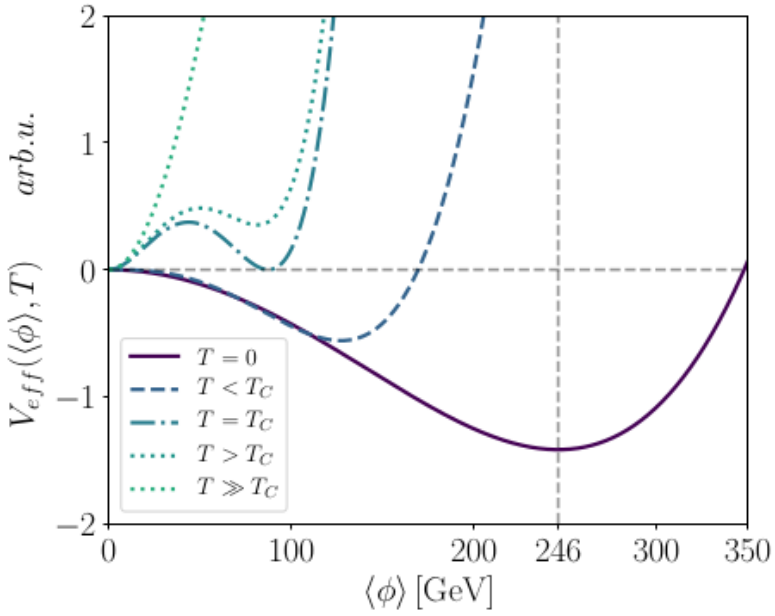

Figure 5.2.4: The evolution of the effective potential in a first order phase transition. Taken from Ref.[81].

bles then spread throughout the universe converting the false vacuum into true one. At the beginning, these bubbles are not big enough and they collapse under surface tension. However, at the nucleation temperature, critical bubbles, *i.e.* bubbles big enough to grow and nucleate, will expand and fill the entire space [102]. In the particular case of the SM the parameters of the potential in Eq. (5.2.34) are given by [91, 93]

$$
\begin{aligned}
D &= \frac{2m_W^2 + m_Z^2 + 2m_t^2}{8v^2} \\
E &= \frac{2m_W^3 + m_Z^3}{4\pi v^3} \\
T_0 &= \frac{m_h^2 - 8Bv^2}{4D} \\
B &= \frac{3}{64\pi^2 v^4}(2m_W^4 + m_z^4 + 4m_t^4) \\
\lambda(T) &= \lambda - \frac{3}{16\pi^2 v^4}\left[2m_W^4 \log\left(\frac{m_W^2}{A_B T^2}\right) + m_Z^4 \log\left(\frac{m_Z^2}{A_B T^2}\right)\right. \\
&\quad \left. - 4m_t^4 \log\left(\frac{m_t^2}{A_F T^2}\right)\right] ,
\end{aligned}
\tag{5.2.36}
$$

where m_t is the mass of the top quark, $A_B = 16$ and

$$A_F = 16\pi^2 e^{(3/2-2\gamma_E)}, \tag{5.2.37}$$

with $\gamma_E \approx 0.5722$ the Euler-Mascheroni constant. At the critical temperature we have that

$$\langle\Phi(T_c)\rangle = \frac{2ET_c}{\lambda(T_c)} \to \frac{\langle\Phi(T_c)\rangle}{T_c} = \frac{2E}{\lambda(T_c)}\,, \tag{5.2.38}$$

so we immediately see that the wash-out condition in Eq. (5.2.33) requires the EWPhT to be of first order. More specifically, it needs to be a **sufficiently strong first order phase transition**. Meanwhile, using that the mass of the Higgs is $m_h^2 = 2\lambda v^2$ we can write

$$\frac{\langle\Phi(T_c)\rangle}{T_c} \sim \frac{4Ev^2}{m_h^2}\,, \tag{5.2.39}$$

such that wash-out condition is converted into a condition for the Higgs mass, *i.e.*

$$m_h \lesssim \sqrt{\frac{4E}{1.3}} \sim 42\,\text{GeV}\,. \tag{5.2.40}$$

As for today, the mass of the Higgs is $m_h = 125.25\,\text{GeV}$ [107], meaning that the EWPhT alone, within the SM, is not strong enough to produce the observed BAU.

5.2.4 *The Baryon Asymmetry during EW Baryogenesis*

Even though EWBG in the SM is ruled out, there is still the possibility to add some extensions in the model in such a way that we get the correct amount of CP violation and a strong enough first order phase transition. So the whole idea of producing the BAU during the EWPhT remains attractive, especially because of its testability [47]. Therefore, in this section we give an outline of how all the ingredients in Sakharov conditions are combined in order to produce the baryon asymmetry.

As discussed in previous sections, the departure from thermal equilibrium scenario will be provided by the strong enough first order EWPhT. At T_c both vacua are degenerate and tunneling becomes possible. At the nucleation temperature, bubbles

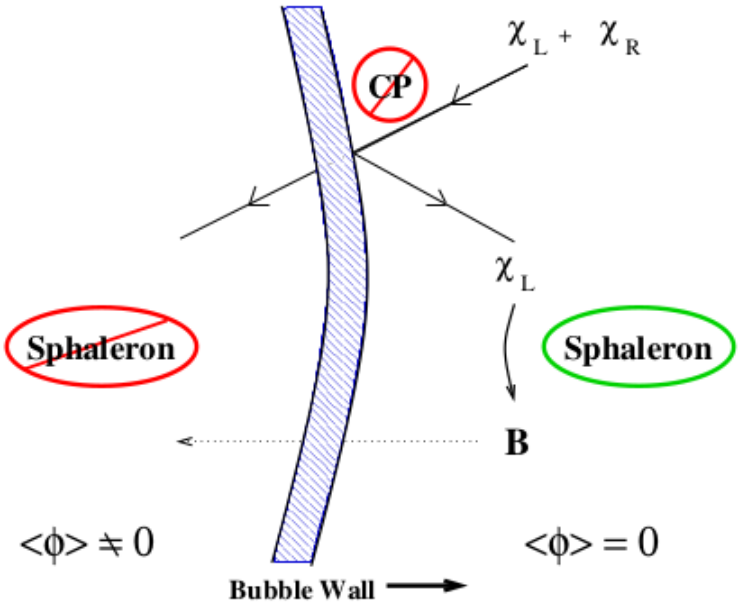

Figure 5.2.5: Baryon number production in front of the bubble wall. Taken from Ref.[80].

of broken phase can grow and fill the universe. The BAU is created then in 3 steps [81]:

- The particles in the plasma scatter with the bubble wall. In this step, CP violation generates an asymmetry of left-handed fermions in front of the bubble wall.
- The excess of left-handed particles then bias the weak sphaleron processes in the unbroken phase to produce more baryons than antibaryons as depicted in Fig. [5.2.5].
- The asymmetry is then swallowed by the expanding bubble. Since in the broken phase the sphaleron processes are exponentially suppressed, the BAU is thus conserved.

Quantitatively we can compute the BAU in the following way [22]. At some point the bubble is large enough as to be approximated with a planar wall of width L_w and expanding with velocity v_w. The direction perpendicular to the wall is z and we set the comoving origin in the middle of the bubble wall. The region of positive z corresponds to the region of symmetric phase, while negative z corresponds to the broken phase (see

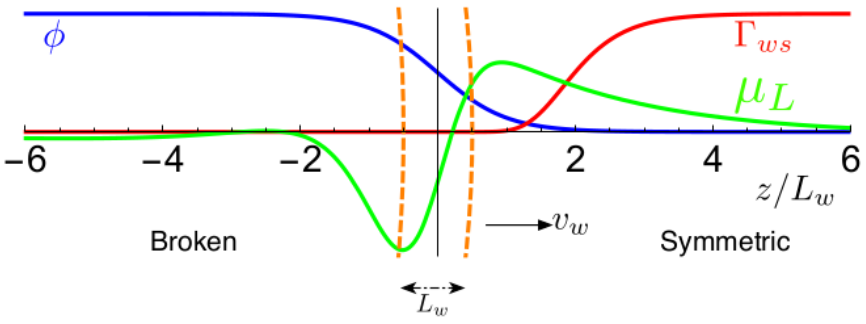

Figure 5.2.6: A cut through the bubble wall. The blue line corresponds to the profile of the Higgs VEV. The red line corresponds to the sphaleron rate which is only important in the symmetric phase. The green line is the profile of the left-handed chemical potential. All curves are in arbitrary units. Taken from Ref.[22].

Fig. [5.2.6]). Baryon number is then obtained by solving the diffusion equation

$$\partial_z n_B = \frac{3}{2} v_w^{-1} \Gamma_{sph} (N_c \mu_L T^2 - A n_B) \,, \tag{5.2.41}$$

where Γ_{sph} is the weak sphaleron rate, N_c is the number of colors and in the SM, $A = 15/2$. Similarly, the left-handed chemical potential is given by

$$\mu_L = \frac{\mu_{tL} + \mu_{bL} + \mu_{cL} + \mu_{sL} + \mu_{uL} + \mu_{dL}}{2} \,. \tag{5.2.42}$$

The first term in Eq. (5.2.41) acts like a source, *i.e.* the excess of left-handed quarks is being converted into a net baryon number. The second term, on the other hand, accounts for the wash out, the fact that sphalerons will relax any asymmetry to zero if they are given enough time to do so. Finally, we can invert Eq. (5.2.41) to obtain

$$\eta = \frac{n_B(-\infty)}{s} = \frac{135 N_c}{4\pi^2 v_w g_* T} \int_{-\infty}^{\infty} dz \Gamma_{sph} \mu_L e^{-\frac{3}{2} A \frac{1}{v_w} \int_{-\infty}^{z} dz_0 \Gamma_{sph}} \,, \tag{5.2.43}$$

with g_* the number of relativistic degrees of freedom. In general, Eq. (5.2.43) is solved numerically.

Part II

THE INERT DOUBLET MODEL AND ITS EXTENSIONS

6

THE VANILLA INERT DOUBLET MODEL

The IDM [19, 70] is a model in which we extend the Higgs sector of the SM adding an additional EW doublet - charged under $SU(2)_L \times U(1)_Y$ as $(\mathbf{2}, 1/2)$ [39] - on top of the traditional Higgs doublet H_1. After electroweak symmetry breaking 3 degrees of freedom become the longitudinal components of the EW gauge bosons, whereas the remaining 5 degrees of freedom correspond to the SM-like Higgs and four new inert scalars. By denoting the second doublet with H_2 we can expand in the following way[42]

$$H_1 = \begin{pmatrix} \phi^+ \\ \frac{1}{\sqrt{2}}(h + i\phi) \end{pmatrix} , \qquad H_2 = \begin{pmatrix} H^+ \\ \frac{1}{\sqrt{2}}(H + iA) \end{pmatrix} , \quad (6.0.1)$$

where h is the SM Higgs boson, ϕ and $\phi^\pm$ are the Goldstone bosons, $H^\pm$ are new charged scalars, and H and A are neutral CP-even and CP-odd scalars, respectively. The new Higgs couples only to the gauge sector which is guaranteed by imposing a $\mathbb{Z}_2$ symmetry under which all the SM fields are even and H_2 is odd, preventing the lightest $\mathbb{Z}_2$-odd particle from decaying and making it a suitable candidate for DM. The $\mathbb{Z}_2$ symmetry is, in fact, the defining feature of the IDM and what makes it different from a general two-Higgs-doublet model. Without loss of generality for the following analysis we will choose H as the DM particle. The scalar Lagrangian is thus given by [15]

$$\mathcal{L} = \left|D_\mu H_1\right|^2 + \left|D_\mu H_2\right|^2 - V(H_1, H_2) , \quad (6.0.2)$$

with the covariant derivative defined as in Eq. (3.1.3) and the tree-level potential

$$V(H_1, H_2) = \mu_1^2 \left|H_1\right|^2 + \mu_2^2 \left|H_2\right|^2 + \lambda_1 \left|H_1\right|^4 + \lambda_2 \left|H_2\right|^4 + \lambda_3 \left|H_1\right|^2 \left|H_2\right|^2 + \lambda_4 \left|H_1^\dagger H_2\right|^2 + \frac{1}{2}\left[\lambda_5 \left(H_1^\dagger H_2\right)^2 + h.c.\right] , \quad (6.0.3)$$

where all the parameters are chosen to be real. The masses for the scalars are

$$\begin{aligned} m_h^2 &= 2\lambda_1 v^2 \,, \\ m_H^2 &= \mu_2^2 + \lambda_{345}\frac{v^2}{2} \,, \\ m_A^2 &= \mu_2^2 + \overline{\lambda}_{345}\frac{v^2}{2} \,, \\ m_{H^\pm}^2 &= \mu_2^2 + \lambda_3\frac{v^2}{2} \,, \end{aligned} \tag{6.0.4}$$

with $v \approx 246\,\text{GeV}$ the Higgs VEV and where we have used the following short-hand notations for the couplings

$$\lambda_{345} = \lambda_3 + \lambda_4 + \lambda_5, \qquad \overline{\lambda}_{345} = \lambda_3 + \lambda_4 - \lambda_5 = \lambda_{345} - 2\lambda_5 \,. \tag{6.0.5}$$

In this way, one can rewrite the quartic couplings in terms of the masses as

$$\begin{aligned} \lambda_3 &= \lambda_{345} + 2\frac{m_{H^\pm}^2 - m_H^2}{v^2} \,, \\ \lambda_4 &= \frac{m_A^2 + m_H^2 - 2m_{H^\pm}^2}{v^2} \,, \\ \lambda_5 &= \frac{m_H^2 - m_A^2}{v^2} < 0 \,. \end{aligned} \tag{6.0.6}$$

Note that, in principle, we have 7 degrees of freedom in the potential in Eq. (6.0.3) but, because the Higgs mass and its VEV are fixed by experimental data, we are left with a total of 5 free parameters [60]. A typical choice is to work with the physical set of parameters including the masses, *i.e.* $\{\lambda_2, \lambda_{345}, m_H, m_{H^\pm}, m_A\}$.

Also, since the second doublet does not couple to fermions, one cannot define an unambiguously CP-property for the scalars of the dark sector [60]. In fact, A could have been chosen as the DM particle in which case all the discussion in this chapter remains valid up to replacing

$$\lambda_5 \to -\lambda_5, \qquad \lambda_{345} \to \overline{\lambda}_{345} \,. \tag{6.0.7}$$

At this point, it is worthwhile mentioning that, as λ_2 only appears in self-couplings in the inert sector, it does not play

any important role in DM physics (at tree-level) [39] as can be seen from Tab. [6.2.1]. We must also note that, since all the couplings in the IDM are real, the IDM alone can not provide with new sources of CP violation as required by baryogenesis. Therefore, CP-violating extensions of the IDM are introduced and discussed in detail in the following chapters. As a final remark, because the IDM is an specific example of a 2HDM (two Higgs doublet model) we expect it to have a rich vacuum structure; one that evolves at high temperatures and opens up the possibility that the early universe, while cooling down, went trough a sequence of phase transitions [15]. The topic of phase transitions in the IDM will be discussed in more detail later on.

In the following section we will introduce the most important theoretical and experimental constraints on the model.

6.1 THEORETICAL AND EXPERIMENTAL CONSTRAINTS

6.1.1 *Vacuum Stability and Perturbativity*

The first constraint to be applied in the model comes from the requirement of the stability of the Higgs potential at tree level, *i.e.* the potential must be bounded from below [60, 69]. Thus, vacuum stability requires that

$$\lambda_1 > 0\,, \quad \lambda_2 > 0\,, \quad \lambda_3 > -2\sqrt{\lambda_1\lambda_2}\,, \quad \lambda_3+\lambda_4-|\lambda_5| > -2\sqrt{\lambda_1\lambda_2}\,, \tag{6.1.1}$$

and we can avoid a charge breaking vacuum when

$$\lambda_4 - |\lambda_5| < 0\,. \tag{6.1.2}$$

In addition, we also need the quartic couplings to have values such that perturbative calculations can be trusted [15]. This is

achieved when the combinations of couplings satisfy $|c_i| < 8\pi$ where

$$\begin{aligned}
c_{1,2} &= \lambda_3 \pm \lambda_4 \,, \\
c_{3,4} &= -3\lambda_1 - 3\lambda_2 \pm \sqrt{9(\lambda_1 - \lambda_2)^2 + (2\lambda_3 + \lambda_4)^2} \,, \\
c_{5,6} &= \lambda_3 \pm \lambda_5 \,, \\
c_{7,8} &= -\lambda_1 - \lambda_2 \pm \sqrt{(\lambda_1 - \lambda_2)^2 + \lambda_4^2} \,, \\
c_{9,10} &= \lambda_3 + 2\lambda_4 \pm 3\lambda_5 \,, \\
c_{11,12} &= -\lambda_1 - \lambda_2 \pm \sqrt{(\lambda_1 - \lambda_2)^2 + \lambda_5^2} \,.
\end{aligned} \tag{6.1.3}$$

6.1.2 *Electroweak Precision Data*

6.1.2.1 *Gauge Bosons Decay Widths*

From the precise measurements of the decay widths of the EW gauge bosons at LEP, the mass spectra of the model must be constrained as well [39, 42]

$$\begin{aligned}
m_H + m_{H^\pm} &> m_{W^\pm} \,, \qquad m_A + m_{H^\pm} > m_{W^\pm} \\
m_H + m_A &> m_Z \,, \qquad 2m_{H^\pm} > m_Z \,,
\end{aligned} \tag{6.1.4}$$

such that the decays of the $W^\pm$ or the Z into states of the additional doublet are kinematically excluded. Furthermore, from the LEP-II data we must exclude a region defined by the intersection of the conditions [71]

$$m_H > 80\,\text{GeV} \quad \cup \quad m_A > 100\,\text{GeV} \quad \cup \quad m_A - m_H < 8\,\text{GeV} \,, \tag{6.1.5}$$

in addition to the more general requirement [88]

$$m_{H^\pm} > 70\,\text{GeV} \,, \tag{6.1.6}$$

coming from searches for charged Higgs pair production.

6.1.2.2 *Oblique Parameters*

The EW precision measurements also provide strong constraints on any physics beyond the SM [39]. Even if the new physics scale is significantly higher than the EW scale, new physics ef-

fects from virtual particles in loops are expected to contribute through vacuum polarization corrections to the EW precision observables [10]. These observables, also known as the oblique parameters are usually denoted by T, S and U. Assuming that U vanishes these are defined as

$$S = \frac{1}{72\pi(x_2^2 - x_1^2)^3}\left\{x_2^6 f_a(x_2) - x_1^6 f_a(x_1) + 9x_1^2 x_2^2\left[x_2^2 f_b(x_2) - x_1^2 f_b(x_1)\right]\right\}, \tag{6.1.7}$$

where

$$x_1 = \frac{m_H}{m_{H^\pm}}, \qquad x_2 = \frac{m_A}{m_{H^\pm}}, \tag{6.1.8}$$

and

$$\begin{aligned} T &= \frac{1}{32\pi^2\alpha v^2}\left[f_c\left(m_{H^\pm}^2, m_A^2\right) + f_c\left(m_{H^\pm}^2, m_H^2\right) - f_c\left(m_A^2, m_H^2\right)\right] \\ &\simeq \frac{1}{24\pi^2\alpha v^2}\left(m_{H^\pm} - m_H\right)\left(m_{H^\pm} - m_A\right), \end{aligned} \tag{6.1.9}$$

with $\alpha \approx 1/127$ the electromagnetic coupling constant at the Z boson mass scale and the functions f_a, f_b and f_c defined as

$$\begin{aligned} f_a(x) &= -5 + 12\ln(x), \\ f_b(x) &= 3 - 4\ln(x), \\ f_c(x,y) &= \begin{cases} \frac{x+y}{2} - \frac{xy}{x-y}\ln\left(\frac{x}{y}\right) & \text{if} \quad x \neq y \\ 0 & \text{if} \quad x = y. \end{cases} \end{aligned} \tag{6.1.10}$$

As today, the best fit yields [107]

$$T = 0.05 \pm 0.06, \qquad S = 0.00 \pm 0.07. \tag{6.1.11}$$

As seen from Eq. (6.1.9), the T parameter is rather sensible to the mass splitting between $H^\pm$ and A. This means that large splittings which lead to large corrections to the T variable are not allowed by the EW precision data constraints.

6.1.3 *Invisible Higgs Decays*

The final constraint comes from the absence of exotic Higgs decays which imply an upper limit in the branching ratio [107]

$$Br(h \to inv) = \frac{\Gamma(h \to inv)}{\Gamma(h \to inv) + \Gamma(h \to SM)} < 19\% \,, \quad (6.1.12)$$

where the decay width is given by

$$\Gamma(h \to inv) = \frac{(\lambda_{345} m_W)^2}{8\pi g^2 m_h} \sqrt{1 - 4\left(\frac{m_H}{m_h}\right)^2} \,, \quad (6.1.13)$$

and the measured decay width has a value of [107]

$$\Gamma(h \to SM) = 3.2\,\text{MeV}^{+2.8}_{-2.2} \,. \quad (6.1.14)$$

All the previous constraints will be implemented in the following analysis.

6.2 DARK MATTER IN THE IDM

Having laid down the basics of the model, we now turn to DM physics. As specified in the previous section we choose H as the dark matter candidate while the masses of the rest of the inert scalars are assumed to be degenerate, *i.e.* $m_{H^\pm} = m_A$. The corresponding relic abundance was computed by using the software micrOMEGAs 5.0.8 which calculates the matrix elements using CalcHEP (keeping in mind that the program only takes tree-level processes into account) and solves the respective Boltzmann equation [108]. In this section - and in the rest of this work - we use the latest fit for the DM relic density which is [107]

$$\Omega h^2 = 0.1200(12) \,, \qquad h = 0.674(5) \,. \quad (6.2.1)$$

The DM relic abundance will be determined by the interplay of the different annihilation and co-annihilation processes. Annihilations of two dark matter particles will take place through different channels (as shown in figures [6.2.1] and [6.2.2]) including four-point interactions with EW gauge bosons and the Higgs, $h-$mediated s-channels, as well as t- and u-channels me-

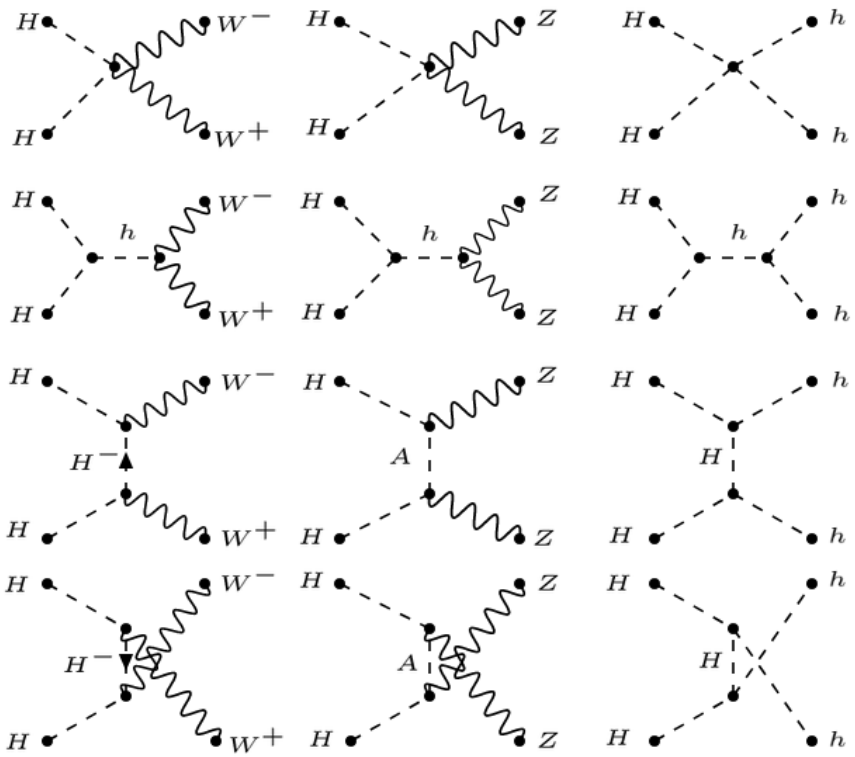

Figure 6.2.1: Tree-level DM annihilation processes with SM bosons in the final state.

diated by non-SM particles. On the other hand, co-annihilation processes (annihilations between H and other $\mathbb{Z}_2$-odd states) will become important for small mass splittings in the dark scalar sector, since this allows for a considerable abundance of $H^{\pm}$ and/or A around freeze out.

We must also point out that the upper limit in Eq. (6.2.1) is taken very strictly in order to avoid overabundant DM. On the contrary, we allow for underabundant DM, in which case it can be argued that other sources or mechanisms (other than freeze-out) could come into play to fill the gap in the relic density. In the following subsections we will show the interesting parameter spaces for the low and the high DM mass regimes. For more detail discussions on inert dark matter see, for example, [15, 19, 39, 42, 70].

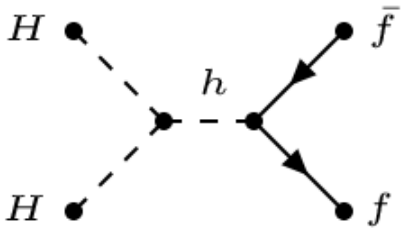

Figure 6.2.2: Tree-level DM annihilation process with SM fermions in the final state.

VERTEX	COUPLING	VERTEX	COUPLING
hhh	$6\lambda_1 v$	hhH^+H^-	λ_3
$hhhh$	$6\lambda_1$	$HHHH$	$6\lambda_2$
hHH	$\lambda_{345} v$	$AAAA$	$6\lambda_2$
$hhHH$	λ_{345}	$H^+H^-H^+H^-$	$4\lambda_2$
hAA	$\overline{\lambda}_{345} v$	$HHAA$	$2\lambda_2$
$hhAA$	$\overline{\lambda}_{345}$	HHH^+H^-	$2\lambda_2$
hH^+H^-	$\lambda_3 v$	AAH^+H^-	$2\lambda_2$

Table 6.2.1: Couplings in the scalar sector of the IDM. Factors of $-i$ are omitted. Taken from [60].

6.2.1 *The Low Mass Regime*

We begin by discussing the low mass regime which consists of DM masses around 50 GeV and 75 GeV. The resulting parameter spaces fulfilling all the constraints are shown in Fig. [6.2.3] for different mass splittings $\Delta m = m_{A,H^\pm} - m_H$. Only regions where one obtains at least 60% of the measured relic density are shown. The black lines represent the XENON1T limits [3, 4], meaning that all the space lying outside the lines is excluded by the experimental constraints. Since the value of λ_2 is irrelevant for DM physics at tree level, we fix its value to 0.4 for the rest of the analysis. One can identify three different regions:

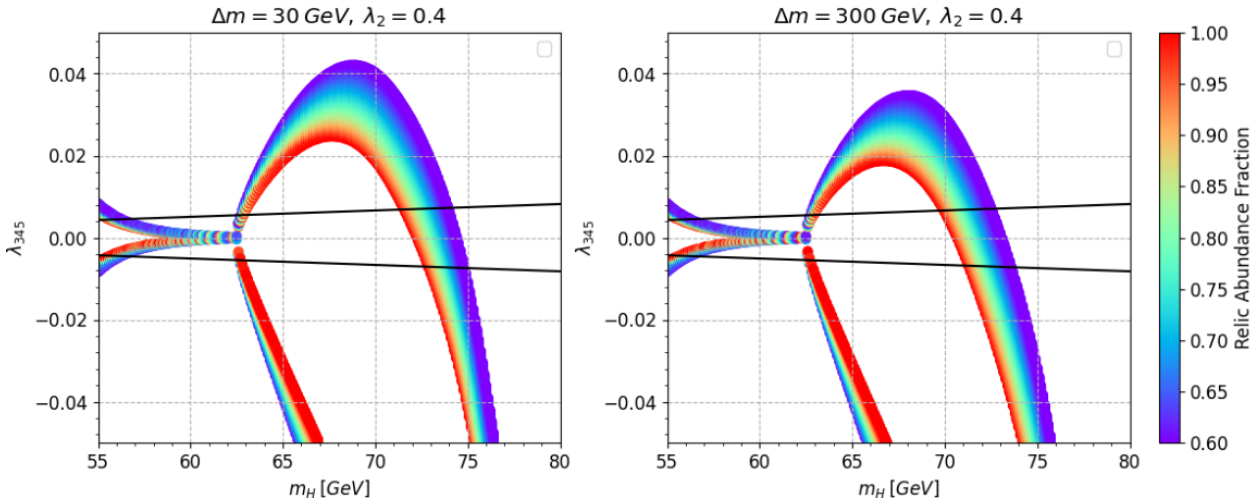

Figure 6.2.3: The relic abundance normalized to $\Omega h^2 = 0.12$ in the $\lambda_{345} - m_H$ plane for different mass splittings $\Delta m = m_{A,H^\pm} - m_H$ in the low mass regime. **Left panel:** $\Delta m = 30$ GeV. **Right panel:** $\Delta m = 300$ GeV. Only points fulfilling $0.6 \cdot 0.1200 \leq \Omega h^2 \leq 0.1200 + 3 \cdot 0.0012$ are shown. The black lines represent the XENON1T limits.

- **The funnel region:** for $m_H < m_h/2$ the dominant annihilation process occurs through the pair production of the heaviest kinematically accessible fermion, that is, the bottom quark. Therefore, the predominant $h-$mediated channel is $HH \to h \to b\bar{b}$ for which the matrix element goes like

$$|\mathcal{M}|^2 \propto \frac{(\lambda_{345} m_b)^2}{(s - m_h^2)^2 + (m_h \Gamma_h)^2}\ , \tag{6.2.2}$$

  where m_b and m_h are the masses of the bottom quark and the SM Higgs, s is the center of mass energy and Γ_h is the total decay width of the Higgs. Note that this matrix element is proportional to the hHH interaction strength governed by λ_{345} as given in table [6.2.1]. Then, the symmetric behaviour of the relic abundance with respect to the portal coupling in this region becomes clear. If we decrease the DM mass below ~ 55 GeV, the absolute value of λ_{345} needs to increase in order to produce the correct relic abundance. However, as we can see from Fig. [6.2.3] large values of the portal coupling are excluded by the XENON1T bounds.

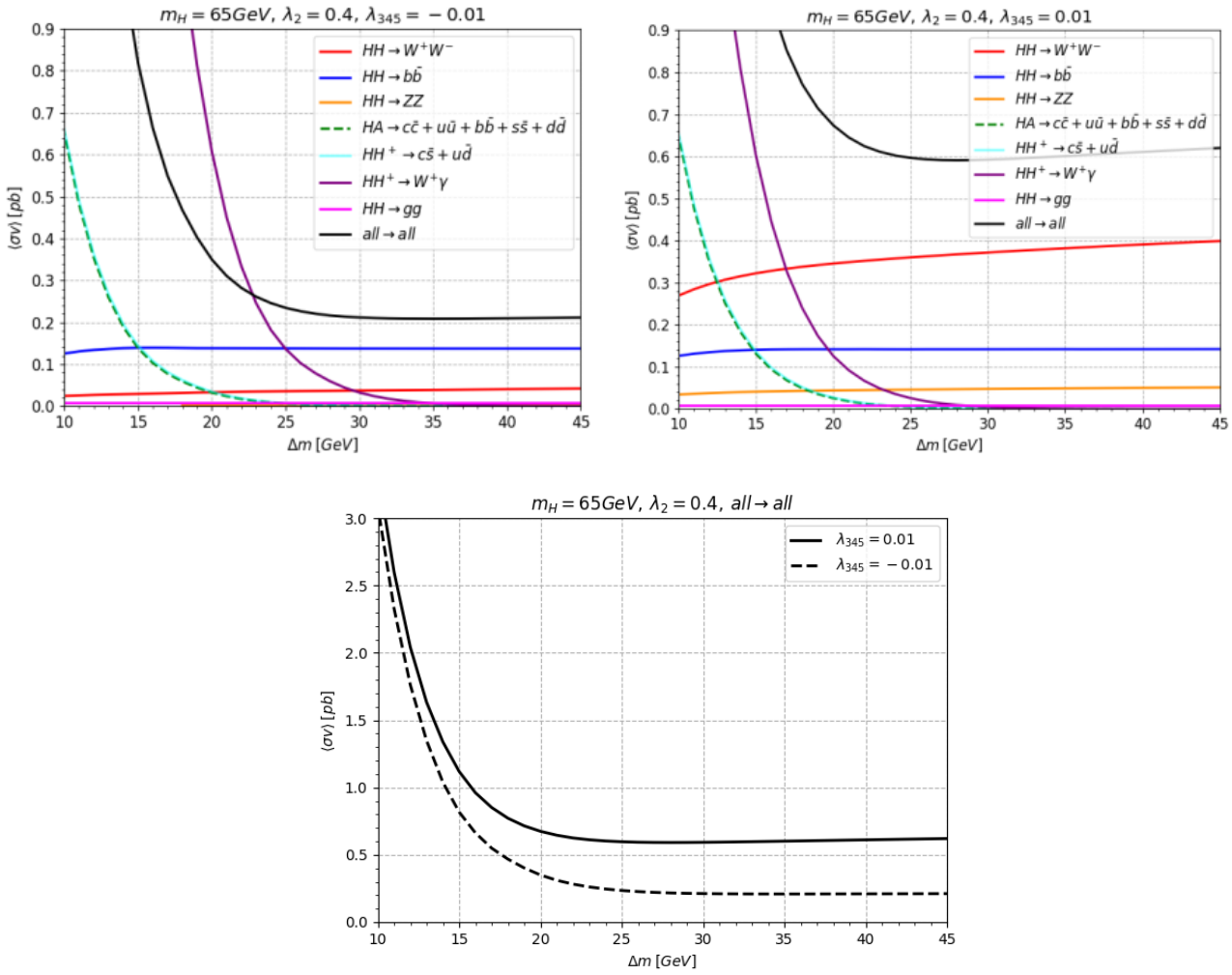

Figure 6.2.4: The evolution of the thermally averaged cross section with respect to the mass splitting for the most important annihilation and co-annihilation channels in the low mass regime. **Left upper panel:** for negative quartic coupling. **Right upper panel:** for positive quartic coupling. **Lower panel:** comparison of the total cross sections for different values of the portal coupling.

- **The resonant region:** when we increase the DM mass and we approach the resonant region $m_H \sim m_h/2$ the relic abundance decreases due to an enhancement of the annihilation cross section via an on-shell Higgs boson exchange in the s-channel. This means that only really small portal couplings allow for the correct relic density for these particular DM masses.

- **The tail region:** above the resonant region, for $m_H > m_h/2$ the pair production of gauge bosons in the final state becomes important (this is true even for zero λ_{345} in which case the contribution comes from four-point interactions), such that the sizes of the portal coupling giving the correct abundance are pushed to larger negative values. For DM masses larger than ~ 75 GeV the annihilation cross section to gauge bosons is so large that the DM becomes underabundant for any combination of parameters.

At this point we notice that, by imposing the theoretical and the experimental constraints from Sec. [6.1], the surviving parameter space lies in the region for which $|\lambda_{345}| \lesssim 0.01$. These results can be cross-checked by looking at the behaviour of the thermally averaged cross section with respect to the mass splitting as shown in Fig. [6.2.4] where the DM mass is fixed to 65 GeV. We see that the total cross section is enhanced by co-annihilation processes for small mass splittings. At around $\Delta m \sim 30$ GeV, the relevance of the co-annihilation processes becomes negligible and only the annihilation processes contribute to the total cross section. It is also clear that for negative values of the portal coupling the $HH \to VV$ channel (with V a gauge boson) is slightly suppressed due to a destructive interference between the four-point interaction and the $h-$mediated channel.

6.2.2 *The High Mass Regime*

Even though from Fig. [6.2.3] one can see that no sizable relic can be attained for $m_H \gtrsim\sim 75$ GeV, another part of parameter space is opened at approximately $m_H \gtrsim 500$ GeV for small mass splittings of the order $\Delta m \lesssim 10$ GeV. This behaviour is explained by realizing that the annihilation of two DM particles into longitudinal gauge bosons W and Z (which are the dominant processes here) scale as λ_3 and $\overline{\lambda}_{345}$, respectively. It is then evident that these couplings can be both made sufficiently small for small Δm (given that λ_{345} is not too large) as seen in Eqs. (6.0.5) and (6.0.6). As a consequence, we get a suppressed annihilation cross section which in turns result in a sizable relic. We also have less severe XENON1T bounds as shown in Fig. [6.2.5], where this time we allow for at least 30% of the

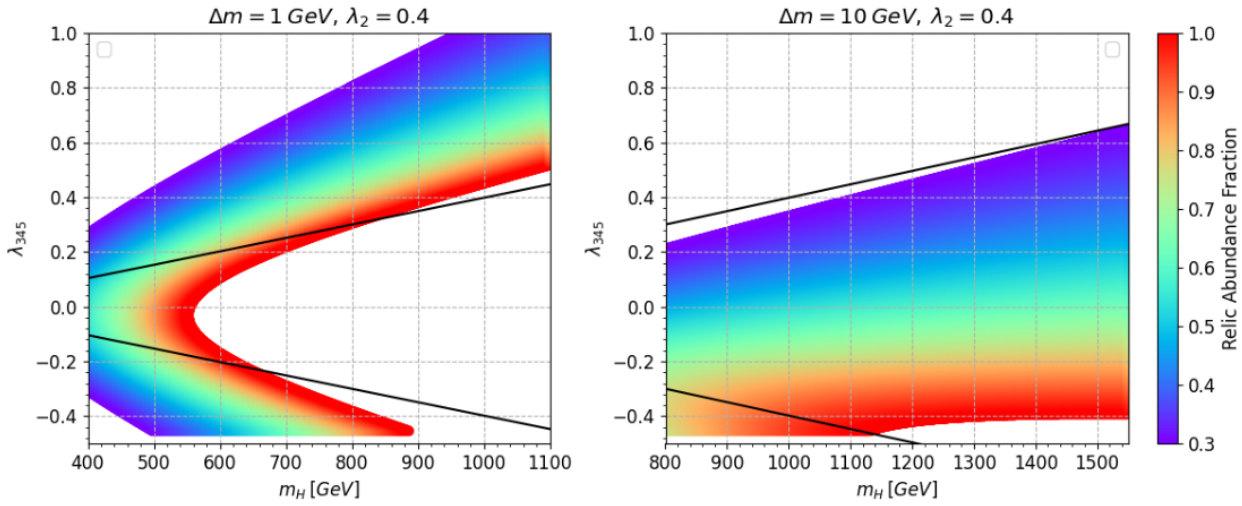

Figure 6.2.5: The relic abundance normalized to $\Omega h^2 = 0.12$ in the $\lambda_{345} - m_H$ plane for different mass splittings $\Delta m = m_{A,H^\pm} - m_H$ in the high mass regime. **Left panel:** $\Delta m = 1$ GeV. **Right panel:** $\Delta m = 10$ GeV. Only points fulfilling $0.3 \cdot 0.1200 \leq \Omega h^2 \leq 0.1200 + 3 \cdot 0.0012$ are shown. The black lines represent the XENON1T limits.

measured relic density. The lower bound in λ_{345} comes from the vacuum stability constrains, particularly from the third condition in Eq. (6.1.1) (for $\lambda_5 < 0$) reading

$$\lambda_{345} > -2\sqrt{\lambda_1 \lambda_2}\,, \tag{6.2.3}$$

which, for $\lambda_2 = 0.4$, it is translated to the condition $\lambda_{345} \gtrsim -0.45$. In Fig. [6.2.5] points for which $\lambda_{345} < -0.45$ are not plotted due to the above constraint.

Again, we can cross-check these results by looking at the behaviour of the thermally averaged cross section with respect to the mass splitting as shown in Fig. [6.2.6]. As expected the most relevant processes in this regime are the annihilations of two DM particles into longitudinal gauge bosons which are largely enhanced by large mass splittings. We also see that negative values of the portal coupling deliver a slightly smaller cross section and thus enhances the relic density, therefore explaining the asymmetric behaviour found in Fig. [6.2.5].

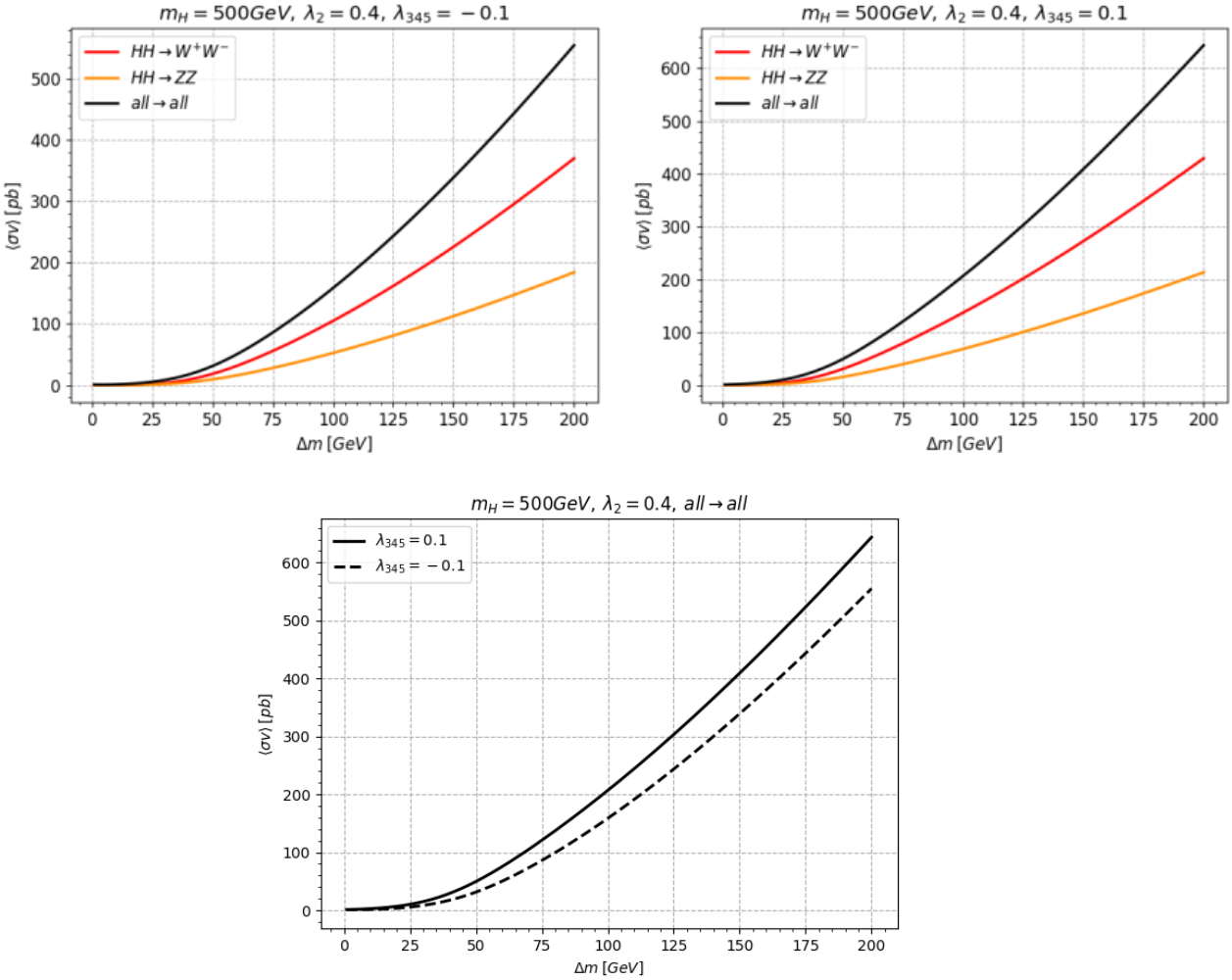

Figure 6.2.6: The evolution of the thermally averaged cross section with respect to the mass splitting for the most important annihilation and co-annihilation channels in the high mass regime. **Left upper panel:** for negative quartic coupling. **Right upper panel:** for positive quartic coupling. **Lower panel:** comparison of the total cross sections for different values of the portal coupling.

6.3 PHASE TRANSITION IN THE IDM

6.3.1 *Finite Temperature Potential*

Having checked that the IDM can indeed accommodate DM physics, we now turn our attention to the nature of the phase transition. For this purpose we need to consider the scalar potential at finite temperature (for a more complete discussion on thermal

corrections to the potential see Appendix [A]). This is given by the effective potential [17]

$$V_{eff}(h, H, T) = V_0(h, H) + V_{CW}(h, H) + V_{CT}(h, H) + V_T(h, H, T) \,, \tag{6.3.1}$$

where V_0 is the tree level potential as given in Eq. (6.0.3), V_{CW} is the Coleman-Weinberg potential, V_{CT} is the counter term potential and V_T contains the leading thermal corrections. As discussed in Appendix [A] the Coleman-Weinberg potential encloses the one-loop corrections to the potential at zero temperature. In the IDM (in Landau gauge and $\overline{MS}$-scheme) this is given by [19, 42]

$$V_{CW} = \sum_i \frac{n_i}{64\pi^2} \hat{m}_i^4(h, H) \left[\ln \left(\frac{\hat{m}_i^2(h, H)}{Q^2} - C_i \right) \right] \,, \tag{6.3.2}$$

where the sum runs over the gauge bosons $W^\pm$ and Z, the top quark t (assuming that the contributions from other fermions are small), the Higgs h, the Goldstone bosons ϕ and $\phi^\pm$ and the inert scalars $H, A, H^\pm$. In the same way, n_i is the number of fermionic or bosonic degrees of freedom, Q is a renormalization scale and C_i are renormalization-scheme dependent constants. The corresponding values of n_i and C_i are summarized in table [6.3.1].

PARTICLE	n_i	C_i
W	6	5/6
Z	3	5/6
t	-12	3/2
h, H, A, ϕ	1	3/2
$\phi^\pm, H^\pm$	2	3/2

Table 6.3.1: Number of degrees of freedom and parameters C_i appearing in the Coleman-Weinberg potential for the IDM. The values can be found in Ref.[42].

On the other hand, the field-dependent masses for the gauge bosons $v = W^{\pm}, Z$ and the fermions read

$$\hat{m}_v^2(h,H) = \frac{h^2+H^2}{v^2} m_v^2 \,, \qquad \hat{m}_f^2(h) = \frac{h^2}{2} y_f^2 \,, \tag{6.3.3}$$

where m_v are the masses at zero temperature and y_f are the usual Yukawa couplings. The rest of the masses are computed by diagonalizing the scalar mass matrices

$$\begin{aligned}
\hat{M}_{h,H}^2 &= \frac{1}{2}\begin{pmatrix} 6\lambda_1 h^2 - 2\lambda_1 v^2 + \lambda_{345} H^2 & 2hH\lambda_{345} \\ 2hH\lambda_{345} & 6\lambda_2 H^2 + \lambda_{345} h^2 + 2\mu_2^2 \end{pmatrix}, \\
\hat{M}_{\phi,A}^2 &= \frac{1}{2}\begin{pmatrix} 2\lambda_1 h^2 - 2\lambda_1 v^2 + \overline{\lambda}_{345} H^2 & 2hH\lambda_5 \\ 2hH\lambda_5 & 2\lambda_2 H^2 + \overline{\lambda}_{345} h^2 + 2\mu_2^2 \end{pmatrix}, \\
\hat{M}_{\phi^{\pm},H^{\pm}}^2 &= \frac{1}{2}\begin{pmatrix} 2\lambda_1 h^2 - 2\lambda_1 v^2 + \lambda_3 H^2 & hH(\lambda_4+\lambda_5) \\ hH(\lambda_4+\lambda_5) & \lambda_2 H^2 + \lambda_3 h^2 + 2\mu_2^2 \end{pmatrix},
\end{aligned} \tag{6.3.4}$$

which coincide with the masses in the EW vacuum $(h,H) = (v,0)$ at zero temperature. In addition, to compensate shifts of the vacuum due to the one-loop corrections, we add a counter-term potential which reads

$$V_{CT}(h,H) = \delta m_h^2 h^2 + \delta m_H^2 H^2 + \delta\lambda_1 h^4 \,, \tag{6.3.5}$$

where the coefficients are computed using a set of appropriate renormalization conditions

$$\begin{aligned}
\left.\frac{\partial V_{CT}}{\partial h}\right|_{VEV} &= -\left.\frac{\partial V_{CW}}{\partial h}\right|_{VEV}, \\
\left.\frac{\partial^2 V_{CT}}{\partial h^2}\right|_{VEV} &= -\left.\frac{\partial^2 V_{CW}}{\partial h^2}\right|_{VEV}, \\
\left.\frac{\partial^2 V_{CT}}{\partial H^2}\right|_{VEV} &= -\left.\frac{\partial^2 V_{CW}}{\partial H^2}\right|_{VEV}.
\end{aligned} \tag{6.3.6}$$

Note that the couplings λ_2 and λ_{345} are running $\overline{MS}$ couplings, while the masses for $H^{\pm}$ and A are assumed to be one-loop corrected.

At this point we encounter a technical issue [17] involving the inclusion of the Goldstone bosons in the Coleman-Weinberg potential which, in Landau gauge, acquire a mass at finite temperature but are massless at zero temperature. The inclusion leads to infrared (IR) divergences due to the second derivatives of the Coleman-Weinberg potential in Eq. (6.3.6). To treat these divergences one then imposes an IR cutoff for the Goldstones

at the SM Higgs mass, *i.e.* $m_h^2 = m_{IR}^2$. In practice this just means that the Goldstone modes are removed from the sum in the derivatives of the Coleman-Weinberg potential, and their contribution is added as a regularized extra term on the right-hand side of Eq. (6.3.6) as [32]

$$\begin{aligned}
\left.\frac{\partial V_{CT}}{\partial h}\right|_{VEV} &= -\left.\frac{\partial V_{CW}}{\partial h}\right|_{VEV}, \\
\left.\frac{\partial^2 V_{CT}}{\partial h^2}\right|_{VEV} &= -\left.\left(\frac{\partial^2 V_{CW}}{\partial h^2} + \frac{1}{32\pi^2}\sum_{i=\phi,\phi^\pm}\frac{\partial^2 \hat{m}_i^2(h,H)}{\partial h^2}\ln\left(\frac{m_{IR}^2}{Q^2}\right)\right)\right|_{VEV}, \\
\left.\frac{\partial^2 V_{CT}}{\partial H^2}\right|_{VEV} &= -\left.\left(\frac{\partial^2 V_{CW}}{\partial H^2} + \frac{1}{32\pi^2}\sum_{i=\phi,\phi^\pm}\frac{\partial^2 \hat{m}_i^2(h,H)}{\partial H^2}\ln\left(\frac{m_{IR}^2}{Q^2}\right)\right)\right|_{VEV}.
\end{aligned} \tag{6.3.7}$$

Finally, the finite temperature contributions are given by

$$V_T(h,H) = \frac{T^4}{2\pi^2}\left[\sum_i n_i^B J_B\left(\frac{\hat{m}_i^2(h,H)}{T^2}\right) + \sum_i n_i^F J_F\left(\frac{\hat{m}_i^2(h,H)}{T^2}\right)\right], \tag{6.3.8}$$

where the thermal functions $J_{B,F}$ are defined in Eq. (A.2.2). As an extra step, however, we must include the corrections coming from the resummation of daisy diagrams, which can be done by two distinct approaches. On one hand, the approach proposed by Arnold and Espinosa [7] consists of adding the following contribution to the potential

In the analysis of [42] which is discussed in the following section, the Parwani approach was used.

$$V^{daisy} = -\frac{T}{12\pi}\sum_{i=bosons} n_i\left(\left[\overline{m}_i^2(h,H,T)\right]^{3/2} - \left[\hat{m}_i^2(h,H)\right]^{3/2}\right), \tag{6.3.9}$$

with $\overline{m}^2(h,H,T)$ the corresponding thermal masses. The other approach proposed by Parwani [85] consists of replacing the field-dependent masses by the thermal masses directly in V_T. Since the transversal parts of the SM gauge bosons are not af-

fected by finite temperature corrections, we consider only the Debye masses for the longitudinal components [19, 42]

$$\begin{aligned}
\overline{m}^2_{W_L} &= \frac{h^2+H^2}{v^2} m^2_W + 2g^2T^2 \\
\overline{m}^2_{Z_L,\gamma_L} &= \frac{h^2+H^2}{8}\left(g^2+g'^2\right) + \left(g^2+g'^2\right)T^2 \pm \Delta \\
\Delta^2 &= \frac{\left(h^2+H^2+8T^2\right)^2}{64}\left(g^2+g'^2\right)^2 - g^2g'^2T^2\left(h^2+H^2+4T^2\right).
\end{aligned} \tag{6.3.10}$$

The remaining terms are computed by diagonalizing the scalar thermal mass matrices

$$\overline{M}^2_X = \hat{M}^2_X + \hat{\Pi}(T)\,, \tag{6.3.11}$$

$$\begin{aligned}
\hat{\Pi}_{11}(T) &= \frac{T^2}{24}\left(6y_t^2+6y_b^2+2y_\tau^2+\frac{9}{2}g^2+\frac{3}{2}g'^2+12\lambda_1+4\lambda_3+2\lambda_4\right), \\
\hat{\Pi}_{22}(T) &= \frac{T^4}{24}\left(\frac{9}{2}g^2+\frac{3}{2}g'^2+12\lambda_2+4\lambda_3+2\lambda_4\right).
\end{aligned} \tag{6.3.12}$$

The evolution of the potential in Eq. (6.3.1) with temperature will determine the nature of the phase transition in the IDM.

6.3.2 *The Strength of the Phase Transition*

Without going into too much detail, we now turn to the question of how is the nature of the phase transition in the IDM. For that, in this section, we give a brief review of [42] (see also [49, 50]). The interesting parameter space for the low mass regime is shown in Fig. [6.3.1]. The bright regions correspond to parameter sets that deliver a sufficient amount of DM (at least 60% of the measured value) and satisfy all the theoretical and experimental constraints including the XENON1T bounds. Regions where this is not possible are shaded in gray. In the same way, the dashed lines denote the strength of the EWPhT ξ and the dotted lines indicate the corresponding critical temperatures T_c. In the light of EWBG the green and yellow regions are the most interesting, since they correspond to parameter spaces where we can have a strong first-order one-step PhT or a strong two-step PhT, respectively. In the case of a one-step PhT the inert scalar H does not acquire a VEV and the universe undergoes a single phase transition at the critical temperature when the

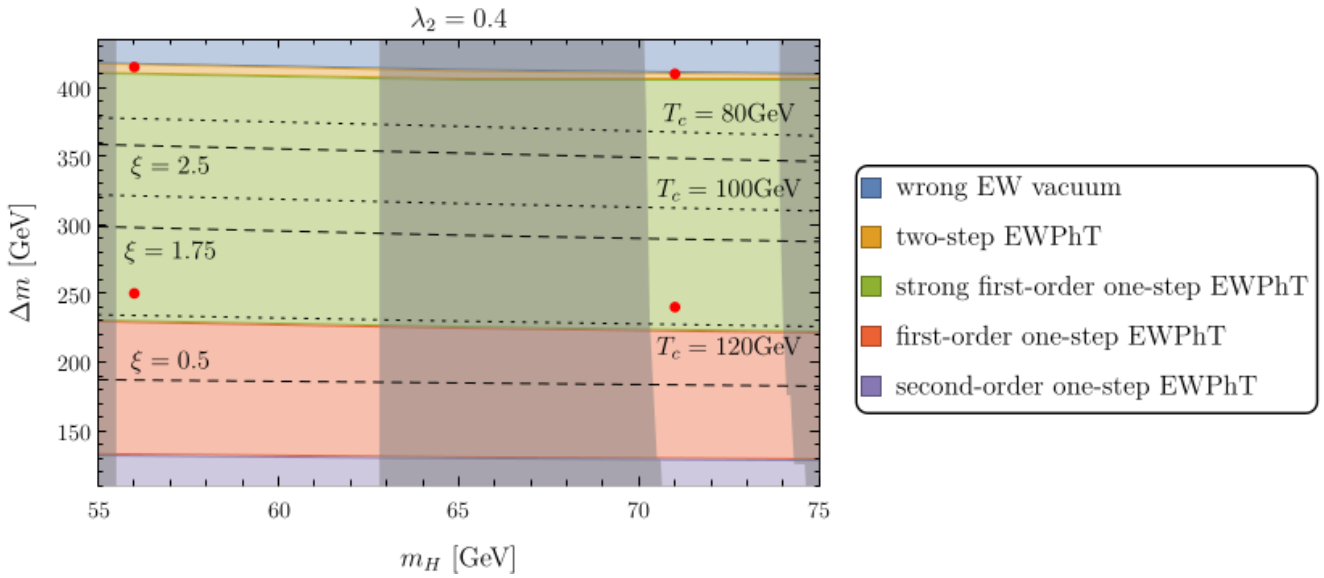

Figure 6.3.1: Characterization of the EWPhT in the $\Delta m - m_H$ plane in the low mass regime for fixed values of $\lambda_2 = 0.4$ and quartic coupling $\lambda_{345} = 0.005$. Taken from [42].

usual Higgs acquires its VEV. The strength of the PhT is then given with the usual ratio of the critical VEV over the critical temperature, *i.e.*

$$\xi = \frac{v_c}{T_c} \,. \tag{6.3.13}$$

On the other hand, for a two-step phase transition the inert scalar H acquires a non-zero VEV at an intermediate temperature T_1. For a lower temperature $T_2 < T_1$ a second transition occurs, where the Higgs will get a non-zero VEV and $\langle H \rangle$ becomes zero once again. For this case the strength of the phase transition will be given by [42]

$$\xi_j = \frac{\sqrt{\langle h \rangle_j^2 + \langle H \rangle_j^2}}{T_j} \,, \tag{6.3.14}$$

with $j = 1, 2$ and the corresponding VEV's $\langle h \rangle_j$ and $\langle H \rangle_j$ at the critical temperatures T_j. We see that the interesting range in the mass splitting for the low mass regime is $230\,\text{GeV} \lesssim \Delta m \lesssim 420\,\text{GeV}$. For the high mass regime, on the contrary, the situation is a bit more complicated. This is because, as discussed in Sec. [6.2.2], for high mass splittings, the DM annihilations into longitudinal gauge bosons are enhanced and the relic abun-

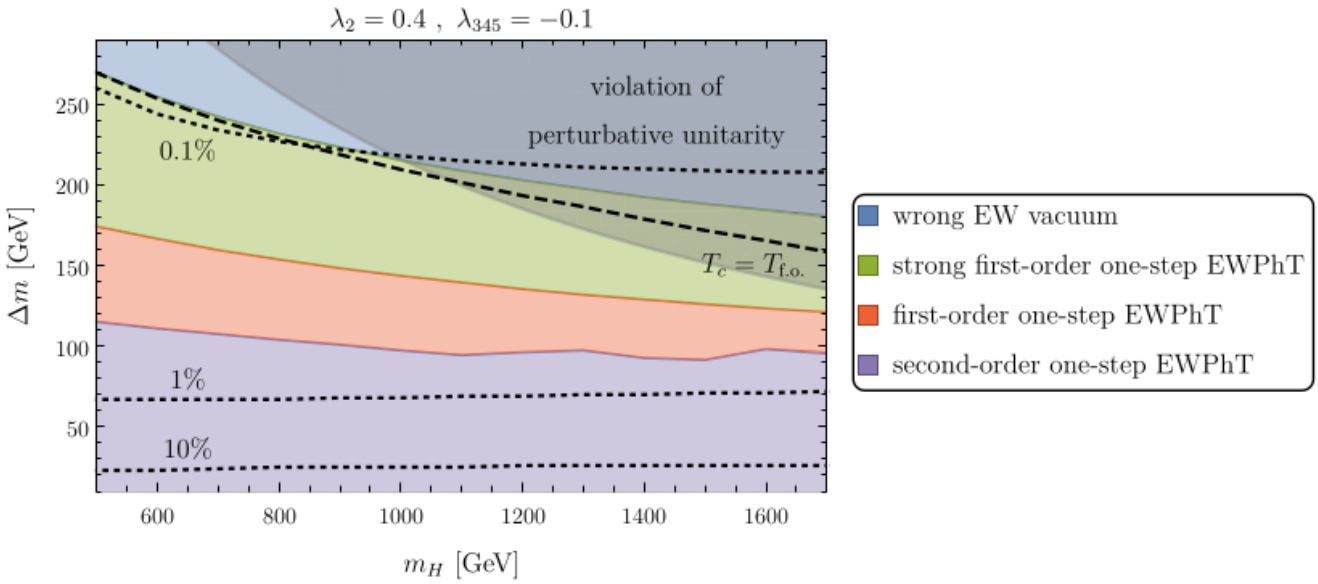

Figure 6.3.2: Characterization of the EWPhT in the $\Delta m - m_H$ plane in the high mass regime for fixed values of $\lambda_2 = 0.4$ and quartic coupling $\lambda_{345} = -0.1$. Taken from [42].

dance becomes negligible. However, this is precisely the region where a strong phase transition can occur as can be seen from Fig. [6.3.2]. This time the dotted contours denote the fractions of the measured relic abundance and we see that, in order to have a successful strong first-order PhT, we need mass splittings larger than ~ 150 GeV. Nonetheless, in these regions we find approximately only around 0.1% and 1% of the relic density. Accommodating a large fraction of DM in the high mass regime for large mass splittings will motivate the introduction of higher-dimensional derivative operators that will be discussed in the following chapters.

7

MINIMAL EXTENSION OF THE SCALAR SECTOR

In the aim to accommodate baryogenesis into the IDM we now extend the model adding higher dimensional CP-violating operators. Note that higher dimensional operators must be used because any other CP-violating dimension four operator is excluded by the $\mathbb{Z}_2$ symmetry. Therefore, we must take dimension six operators into account and we assume the cutoff of the theory to lie in the TeV scale, so the order of the corresponding coefficients must be around 10^{-6}GeV^{-2}. Bearing this in mind, in the first attempt, we will extend the IDM by adding CP-violation directly in the scalar potential in the following way

$$\begin{aligned} V = {} & \mu_1^2 |H_1|^2 + \mu_2^2 |H_2|^2 + \lambda_1 |H_1|^4 + \lambda_2 |H_2|^4 + \lambda_3 |H_1|^2 |H_2|^2 \\ & + \lambda_4 \left| H_1^\dagger H_2 \right|^2 + \frac{1}{2} \left[\hat{\lambda}_5 \left(H_1^\dagger H_2 \right)^2 + \hat{\lambda}_6 |H_1|^2 \left(H_1^\dagger H_2 \right)^2 + \text{h.c.} \right] , \end{aligned} \tag{7.0.1}$$

where $\hat{\lambda}_5, \hat{\lambda}_6 \in \mathbb{C}$, whereas the other parameters are real and the doublets H_1 and H_2 are again given as in Eq. (6.0.1). However, we notice that by performing a rotation of the second Higgs doublet,

$$H_2 \to e^{-i\theta_5/2} H_2 , \tag{7.0.2}$$

The same rotation as in Eq. (7.0.2) can be used in the vanilla IDM to remove the phase from the term proportional to λ_5.

we can choose $\hat{\lambda}_5$ to be real and we rewrite the last two operators as

$$\frac{\lambda_5}{2} \left(H_1^\dagger H_2 \right)^2 + \frac{\lambda_6}{2} |H_1|^2 e^{i\bar{\theta}_{65}} \left(H_1^\dagger H_2 \right)^2 + \text{h.c.} \tag{7.0.3}$$

with the phase difference $\bar{\theta}_{65} \overset{\text{def}}{=} \theta_6 - \theta_5 \in [0, \pi)$. Therefore, we have two additional free parameters in the potential compared to the IDM, namely λ_6 and $\bar{\theta}_{65}$. As we will see, the new opera-

tor induces a mixing between the neutral scalars of the second doublet. In fact, the mass matrix for these components reads

$$\begin{aligned}\mathcal{M} &= -\begin{pmatrix} \partial^2 V/\partial H^2 & \partial^2 V/\partial H \partial A \\ \partial^2 V/\partial A \partial H & \partial^2 V/\partial A^2 \end{pmatrix} \\ &= \begin{pmatrix} \mu_2^2 + \frac{\lambda_{34}}{2} v^2 + \frac{v^2}{2}\lambda_{56} & -\frac{1}{4}\lambda_6 v^4 \sin\bar{\theta}_{65} \\ -\frac{1}{4}\lambda_6 v^4 \sin\bar{\theta}_{65} & \mu_2^2 + \frac{\lambda_{34}}{2} v^2 - \frac{v^2}{2}\lambda_{56} \end{pmatrix}\end{aligned} \tag{7.0.4}$$

with $\lambda_{34} \overset{\text{def}}{=} \lambda_3 + \lambda_4$ and $\lambda_{56} \overset{\text{def}}{=} \lambda_5 + \frac{v^2}{2}\lambda_6 \cos\bar{\theta}_{65}$. After diagonalizing the mass matrix

$$\mathcal{M}_{\text{diag}} = \mathcal{U}^{-1}\mathcal{M}\mathcal{U} = \begin{pmatrix} m_{H'}^2 & 0 \\ 0 & m_{A'}^2 \end{pmatrix}, \tag{7.0.5}$$

the masses of the physical fields H' and A' are given by

$$m_{A',H'}^2 = \mu_2^2 + \frac{v^2}{2}\left(\lambda_{34} \pm \sqrt{\lambda_5^2 + \frac{v^4}{4}\lambda_6^2 + \lambda_5\lambda_6 v^2 \cos\bar{\theta}_{65}}\right). \tag{7.0.6}$$

In this way, we can rewrite the phase difference as

$$\bar{\theta}_{65} = \arccos \frac{\left(\frac{\Delta m^2}{v^2}\right)^2 - \lambda_5^2 - \frac{v^4}{4}\lambda_6^2}{\lambda_5\lambda_6 v^2} \in [0, \pi] \tag{7.0.7}$$

with $\Delta m^2 \overset{\text{def}}{=} m_{A'}^2 - m_{H'}^2 > 0$. Moreover, using the mass matrix $\mathcal{M}$ in Eq. (7.0.4) and the physical masses in Eq. (7.0.6), we find the normalized eigenvectors to be

$$\begin{aligned} u_1 &= \frac{1}{\sqrt{\frac{v^4}{4}\lambda_6^2 \sin^2\bar{\theta}_{65} + \left(\widetilde{\lambda}_{56} - \lambda_{56}\right)^2}} \begin{pmatrix} \widetilde{\lambda}_{56} - \lambda_{56} \\ \frac{v^2}{2}\lambda_6 \sin\bar{\theta}_{65} \end{pmatrix}, \\ u_2 &= \frac{1}{\sqrt{\frac{v^4}{4}\lambda_6^2 \sin^2\bar{\theta}_{65} + \left(\widetilde{\lambda}_{56} - \lambda_{56}\right)^2}} \begin{pmatrix} -\frac{v^2}{2}\lambda_6 \sin\bar{\theta}_{65} \\ \widetilde{\lambda}_{56} - \lambda_{56} \end{pmatrix}, \end{aligned} \tag{7.0.8}$$

with the short-hand notation

$$\widetilde{\lambda}_{56} \overset{\text{def}}{=} \sqrt{\lambda_5^2 + \frac{v^4}{4}\lambda_6^2 + \lambda_5\lambda_6 v^2 \cos\bar{\theta}_{65}} = \sqrt{\lambda_{56}^2 + \frac{v^4}{4}\lambda_6^2 \sin^2\bar{\theta}_{65}} = \frac{\Delta m^2}{v^2} \,. \tag{7.0.9}$$

Therefore, the diagonalization matrix reads

$$\mathcal{U} \propto \begin{pmatrix} \widetilde{\lambda}_{56} - \lambda_{56} & -\frac{v^2}{2}\lambda_6 \sin\bar{\theta}_{65} \\ \frac{v^2}{2}\lambda_6 \sin\bar{\theta}_{65} & \widetilde{\lambda}_{56} - \lambda_{56} \end{pmatrix} = \begin{pmatrix} \cos\eta & \sin\eta \\ -\sin\eta & \cos\eta \end{pmatrix}, \tag{7.0.10}$$

with the mixing angle $\eta \in [0, \frac{\pi}{2})$ and given by

$$\eta = \arctan \frac{-\frac{v^2}{2}\lambda_6 \sin\bar{\theta}_{65}}{\widetilde{\lambda}_{56} - \lambda_{56}} \overset{\text{IDM}}{=} 0 \,. \tag{7.0.11}$$

Eq. (7.0.11) reflects the absent mixing in the IDM where $\lambda_6 \to 0$. The diagonalization matrix $\mathcal{U}$ transforms the mass eigenstates (primed fields) to the weak eigenstates, reading

$$\begin{pmatrix} H \\ A \end{pmatrix} = \mathcal{U} \begin{pmatrix} H' \\ A' \end{pmatrix} \,. \tag{7.0.12}$$

As expected, $\mathcal{U}$ approaches the identity matrix in the limit of small λ_6. That is, the mixing is almost absent for those couplings.

In this model we choose as free parameters a set containing the scalars' masses among others, $\{v, m_h, m_{H'}, m_{A'}, m_{H^\pm}, \lambda_2, \lambda_{34}, \bar{\theta}_{65}, \eta\}$, such that the parameters in the potential are expressed as

$$\begin{aligned}
&\mu_1 = \sqrt{\frac{-m_h^2}{2}} \,, \qquad \mu_2 = \sqrt{\frac{\hat{m}_H^2 + \hat{m}_A^2 - \lambda_{34}v^2}{2}} \,, \qquad \lambda_1 = \frac{m_h^2}{2v^2} \,, \\
&\lambda_3 = \lambda_{34} - \lambda_4 \,, \qquad \lambda_4 = \frac{\hat{m}_H^2 + \hat{m}_A^2 - 2m_{H^\pm}^2}{v^2} \,, \\
&\lambda_5 = -\frac{\Delta m^2}{v^2}\cos 2\eta \left(1 - \tan 2\eta \cot\bar{\theta}_{65}\right) , \\
&\lambda_6 = \frac{2\Delta m^2 \sin 2\eta}{v^4 \sin\bar{\theta}_{65}} \,.
\end{aligned} \tag{7.0.13}$$

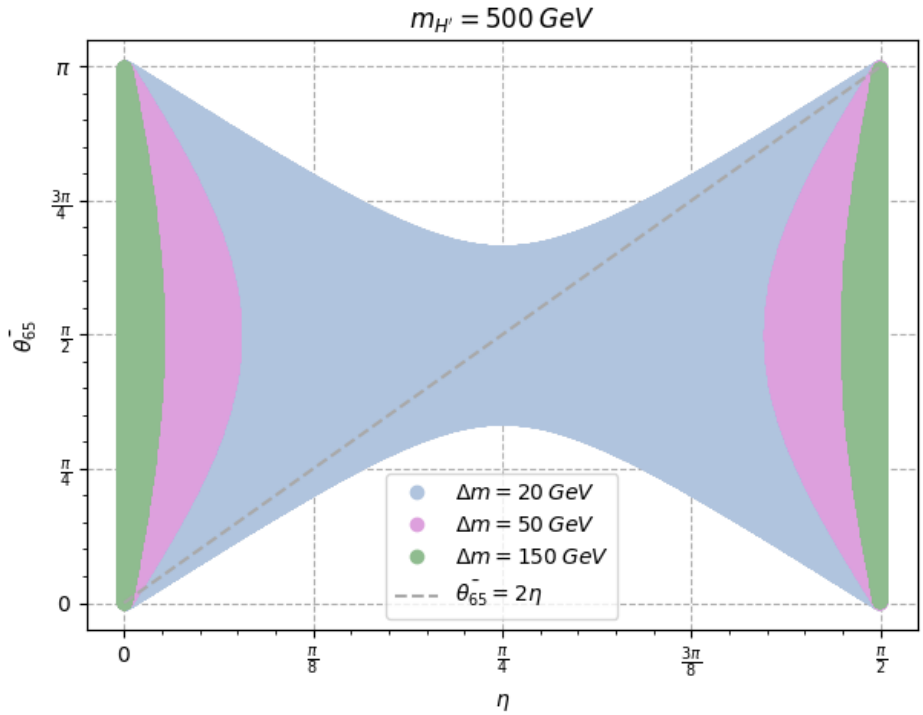

Figure 7.0.1: Allowed parameter space with respect to η and $\bar{\theta}_{65}$ for different mass splittings Δm to allow for the new physics scale, *i.e.* $\lambda_6 \leq 4\pi \cdot 10^{-6}\text{GeV}^{-2}$. The DM mass is set to $m_{H'} = 500\text{GeV}$.

The expression for λ_6 results from Eq. (7.0.9), using the definition for λ_{56} from Eq. (7.0.11), and the one for λ_5 can be derived subsequently from there. One can easily see that the IDM is restored, *i.e.* $\lambda_5 v^2 = -\Delta m^2$ and $\lambda_6 = 0$, for absent mixing.

Furthermore, we need to apply an upper bound on the coupling λ_6 of the dimension six operator due to a lower bound of the new physics scale $\Lambda \gtrsim 1\,\text{TeV}$. Therefore, we have

$$|\lambda_6| \lesssim 4\pi \cdot 10^{-6}\text{GeV}^{-2} \rightarrow \sin 2\eta \lesssim \frac{2\pi v^4 \sin\bar{\theta}_{65}}{\Delta m^2} \cdot 10^{-6}\text{GeV}^{-2}\,, \tag{7.0.14}$$

which is illustrated in Fig. [7.0.1] for different mass splittings. Moreover, since we expect the contribution of the new operator to be fairly small, we assume the constraints in Sec. [6.1] to remain valid for this model and the ones thereafter. Nonetheless, a small comment comes in hand regarding the stability

of the potential. In this case, considering that we are adding a new dimension six term, one might ask whether the stability constraints in Eq. (6.1.1) can still guarantee that the potential is bounded from below. As it turns out, this is indeed the case as long as we also satisfy the condition $\lambda_6 > 0$, which, for our particular choices of mixing angle and CP phase, is immediately fulfilled from Eq. (7.0.13).

7.1 THE RELIC ABUNDANCE

Without further discussion, in this section we investigate the impact of the higher-dimensional CP-violating operator in the DM relic abundance. For the analysis we choose $\bar{\theta}_{65} = \pi/2$ and a small mixing angle such that it satisfies the new physics constraint from Eq. (7.0.14). In Fig. [7.1.1] the results for the low mass regime are shown for a mixing angle of $\eta = 10^{-3}$ and two different mass splittings. Once again it is possible to identify three distinct regions (funnel, resonant and tail) as in the IDM, such that the discussion in Sec. [6.2.1] remains valid. In the left panel of Fig. [7.1.1] identical results as the ones in the vanilla case are obtained. In this instance the mass split-

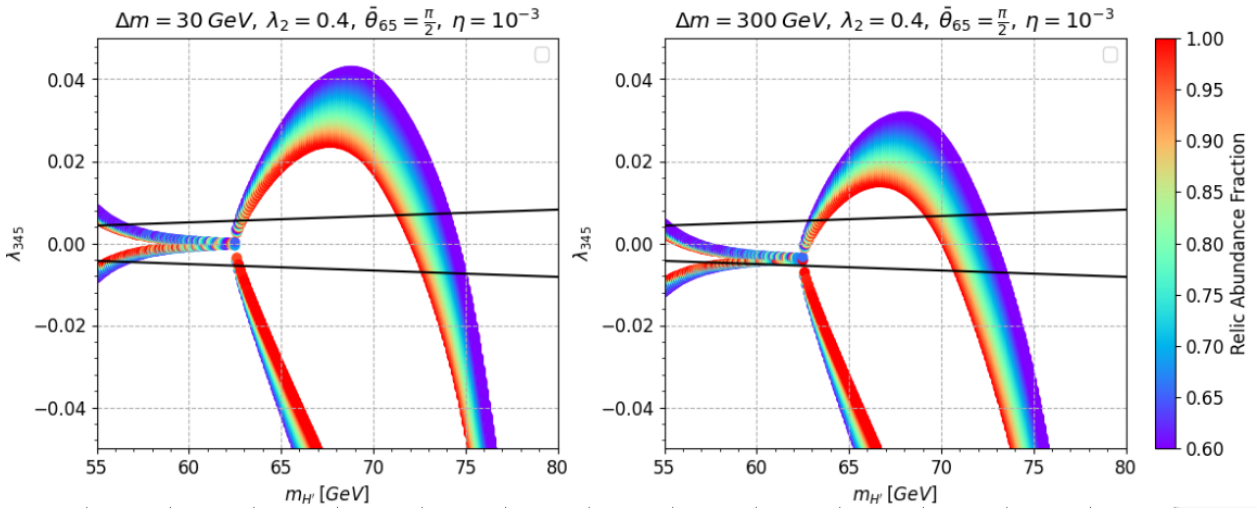

Figure 7.1.1: The relic abundance normalized to $\Omega h^2 = 0.12$ in the $\lambda_{345} - m_{H'}$ plane for different mass splittings $\Delta m = m_{A',H^\pm} - m_{H'}$ and fixed mixing angle in the low mass regime. **Left panel:** $\Delta m = 30$ GeV. **Right panel:** $\Delta m = 300$ GeV. Only points fulfilling $0.6 \cdot 0.1200 \leq \Omega h^2 \leq 0.1200 + 3 \cdot 0.0012$ are shown. The black lines represent the XENON1T limits.

ting is small enough as to greatly suppress the contributions coming from the new CP violating operator (these contributions are studied in detail in Appendix [C]). This can also be cross-checked from Eq. (7.0.13) where, for small η, the numerical value of the new term in the potential essentially goes as $\sim \Delta m^2 \eta / v^4 \sim 10^{-9} \Delta m^2 \eta$ GeV^{-4}. Therefore, unless sizable mass splittings and not too small mixing angles are chosen, the impact of the new operator in the relic abundance is clearly subdominant. In the right panel of Fig. [7.1.1], on the other hand, a greater mass splitting was chosen such that the effects of the λ_6-term kick in and the maximum value of λ_{345} allowing for the right amount of DM relics slightly decreases. It also becomes clear why the funnel region in the right panel is not symmetric with respect to zero coupling anymore; this just shows the interplay between λ_{345} and λ_6 which are the terms contributing to the $HH - h$ processes.

We now turn into the analysis of the relics in the high-mass regime, which already is problematic in the vanilla IDM as discussed in the previous chapter. However, since the new CP-violating operator has contributions to the processes where two DM particles annihilate into longitudinal gauge bosons, it is a rather natural question to ask whether this new term in the potential can relax the small mass splitting constraint discussed in Sec. [6.2.2]. The motivation behind this is to find sufficient DM density in the regions where it is also possible to get a sufficiently strong first order phase transition as required by baryogenesis (see Sec. [6.3.2]). To that end, we set the mass splitting to 150 GeV and we investigate the behavior of the thermally averaged cross section for different channels with respect to the mixing angle and the CP phase $\bar{\theta}_{65}$, which are the two new degrees of freedom in the model. Similarly, the DM mass is fixed to 500 GeV and the comparison of the respective annihilation cross section to that of the vanilla IDM is shown in Fig. [7.1.2]. It can be seen that, even though some regions yield suppressed annihilation cross sections for certain channels, the total annihilation cross section equals the one in the vanilla IDM in the limit $\eta \to 0, \pi/2$, and it is enhanced for all mixing angles in between by a factor of at least 1.5. This happens because, despite the fact that one can obtain a successful cancellation for the $HH \to VV$ processes for a certain combination of parameters, other channels (like $HH \to t\bar{t}$ and $HH \to hh$) become important for that particular combination. Thus, we conclude that in the scalar

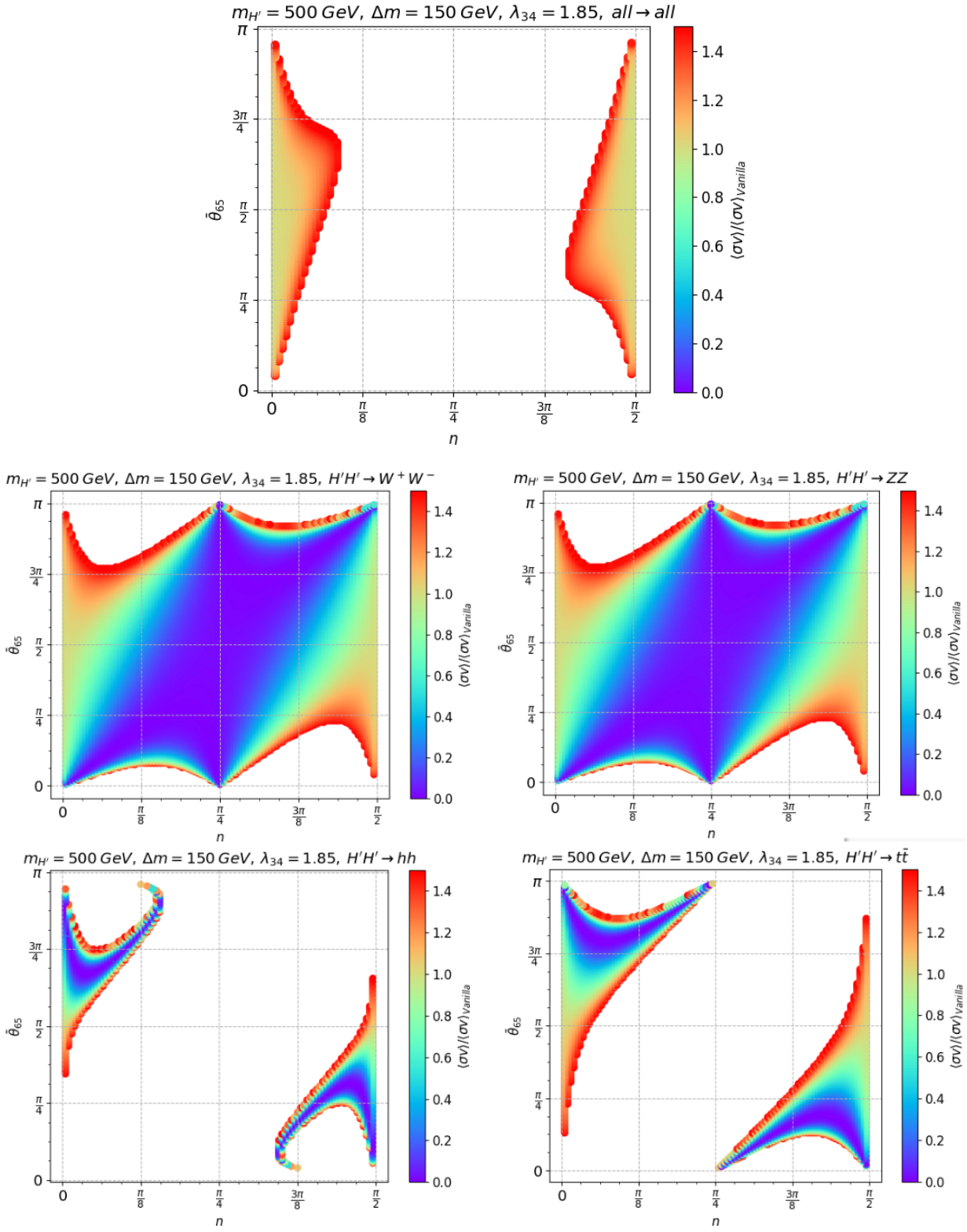

Figure 7.1.2: The thermally averaged cross section with respect to the angles $\bar{\theta}_{65}$ and η for different channels. The cross section is normalized to the corresponding value of the vanilla IDM. The white regions correspond to combinations of parameters for which the cross section is enhanced by more than a factor of 1.5.

extension of the IDM there is no parameter space (in the high mass regime) in which we can find the correct relic abundance for high mass splittings.

7.1.1 *The Derivative Operators*

Given the status in the high mass regime, we are forced to find another way in which to obtain a sizable relic for high mass splittings. As discussed in the last section, the new CP violating term, even though it has contributions to the annihilation of two DM particles into longitudinal gauge bosons, cannot do the trick by itself. Therefore, higher dimensional derivative operators are introduced in the hope that they can interfere in a destructive way as to deliver a sufficient amount of DM. With this in mind, we restrict ourselves in this section to the study of DM, while keeping the λ_6 term as the source of CP violation for completeness. Its impact on the generation of the BAU will be discussed in more detail later on. The new operators read

Note that c_3 and c_4 could, in general, be complex. If this was the case, one would have extra sources of CP violation in the model. Nonetheless, and for the sake of simplicity, we choose all the derivative operators to be CP conserving and we focus only on their impact in the DM relic abundance. The possible impact of the derivative operators in the generation of the BAU is, thus, left for future work.

$$\begin{aligned}\mathcal{L}_c = {} & c_1 \left|H_1\right|^2 \left(D_\mu H_2\right)^\dagger D^\mu H_2 + c_2 \left|H_2\right|^2 \left(D_\mu H_1\right)^\dagger D^\mu H_1 \\ & + c_3 \left[H_1^\dagger H_2 \left(D_\mu H_1\right)^\dagger D^\mu H_2 + \text{h.c.}\right] \\ & + c_4 \left[H_1^\dagger H_2 \left(D_\mu H_2\right)^\dagger D^\mu H_1 + \text{h.c.}\right], \end{aligned} \tag{7.1.1}$$

where the covariant derivative is defined as in Eq. (3.1.3) and we take c_1, c_2, c_3 and c_4 to be real. Again we constrain the size of the operators taking into account the new physics scale such that

$$|c_i| \lesssim 4\pi \cdot 10^{-6}\text{GeV}^{-2}, \qquad \text{with} \quad i = 1,2,3,4\,. \tag{7.1.2}$$

The computations of the contributions from these operators to the DM annihilation cross sections can be found in Appendix [C]. On the other hand, the evolution of the thermally averaged cross section with respect to the c_i coefficients is shown in Fig. [7.1.3] for different channels, where the DM mass and the mass splitting are fixed to 500 GeV and 150 GeV, respectively. From here it can be seen that, for negative values of the c_i's, a decrease in the total cross section is achieved, thus resulting in an enhancement of the relic density. Positive values of the Wilson coefficients, in contrast, only lead to an increment in the cross section. The destructive interference is particularly large

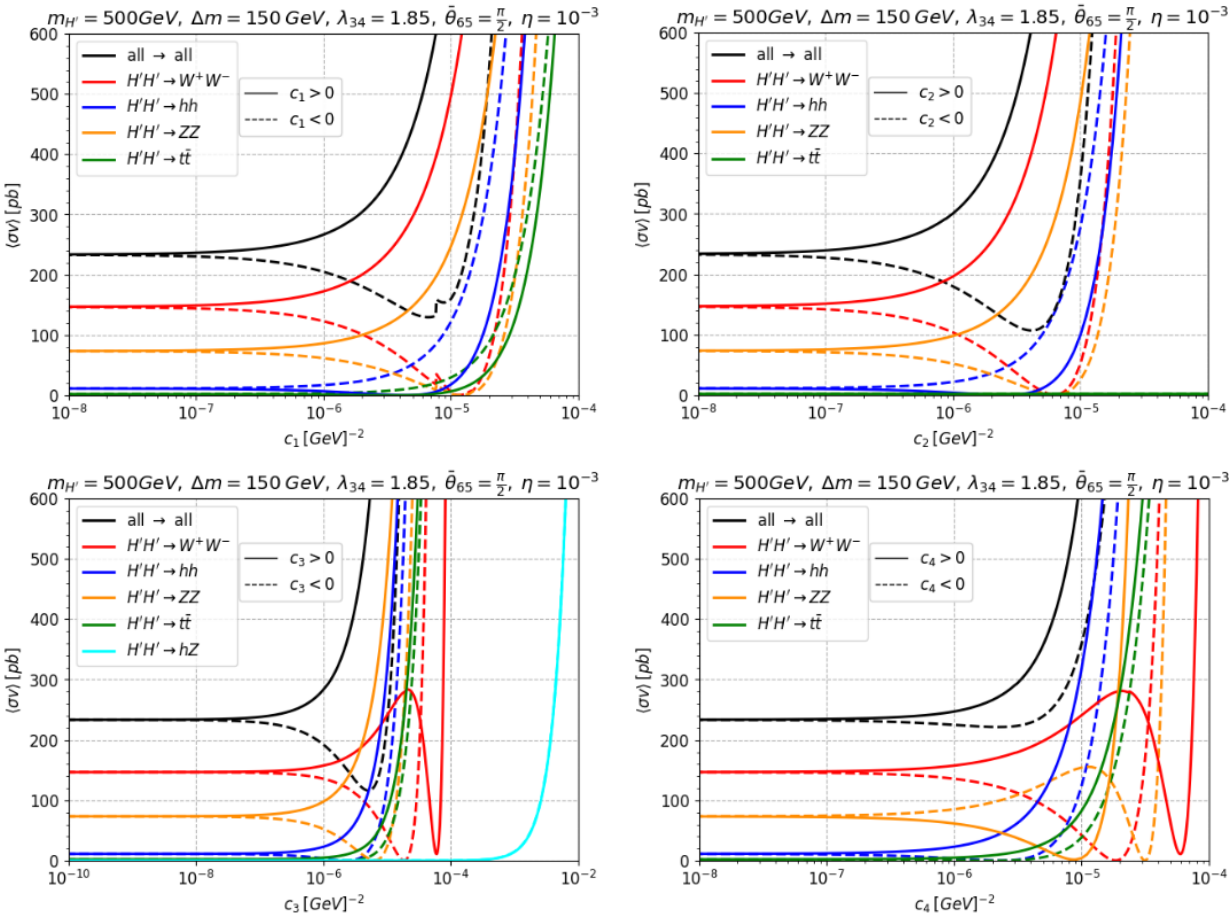

Figure 7.1.3: Evolution of the thermally averaged cross section with respect to each of the different dimension six operators c_i for different channels. Unless it is indicated the values for the other coefficients c_i are set to 0.

for c_2 and c_3, whereas for c_4 it is less prominent. By looking closely into Fig. [7.1.3] one realizes that the behaviour of the total cross section is actually determined by an interplay between the shutting down of the annihilations into longitudinal gauge bosons (represented by the red and yellow lines) and the increase of the annihilations to SM Higgses and top quarks (dark blue and green lines). It can also be pointed out that, even with the respective decrease in the total cross section for each operator, its value is still far too big ($\sim$ 100 pb) as to get the right amount of DM. Therefore, one must try different combinations of operators to see which one works better. In Fig. [7.1.4] for example, we show the evolution of the cross section with respect to c_1 for fixed c_3 and c_4. For this particular combination of operators, one finds a minimum of $\langle \sigma v \rangle \sim 9$ pb which already

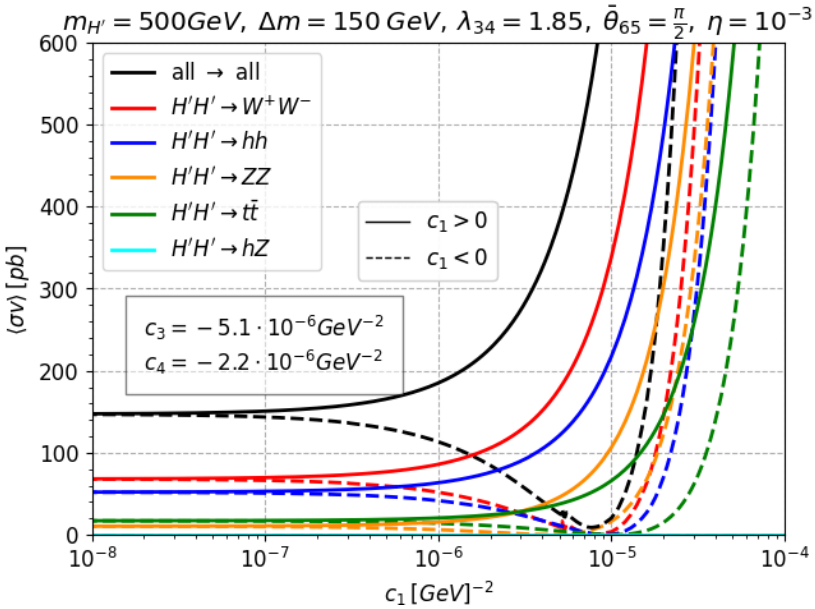

Figure 7.1.4: Evolution of the thermally averaged cross section with respect to c_1 with fixed c_3 and c_4 for different channels. The minimum of the cross section is around 9 pb.

signals a significant improvement by a factor of 10.

Nonetheless, since the cross section must be even smaller in order to accommodate sufficient DM, a suitable combination of operators was yet to be found. To that end, a thorough scan over all possible combinations of the Wilson coefficients c_i was performed for different combinations of DM mass and quartic coupling λ_{345}. As shown in Figs. [7.1.3] and [7.1.4] it was clear that significant changes in the relics were going to be found only for $|c_i|$ of the order 10^{-6}GeV^{-2}. In addition, in order to abide by the theoretical constraints, specifically the vacuum stability conditions, the quartic coupling cannot be arbitrarily small. In fact, for $\lambda_2 < 1$, the boundedness of the potential immediately sets a lower limit of $\lambda_{345} > -0.7$. Nevertheless, for $|\lambda_{345}| \lesssim 0.7$ and $|c_i| \sim 10^{-6}\text{GeV}^{-2}$ no suitable parameter space was found. In particular, allowing for $|c_1| \sim 10^{-6}\text{GeV}^{-2}$ has a significant impact on the spin independent DM-nucleon cross section, making it impossible to get the correct relics while respecting the XENON1T bounds simultaneously (the issue of the XENON1T bounds will be discussed in more detail in the next section). On the other hand, allowing for smaller values of λ_{345} can indeed lead to regions where the XENON1T bounds still hold,

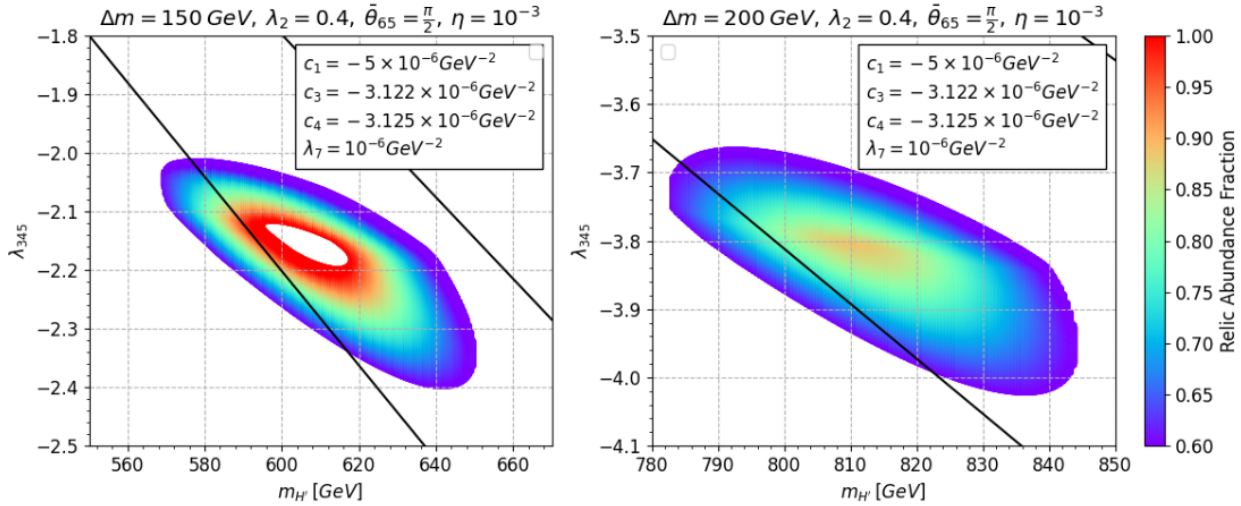

Figure 7.1.5: The relic abundance normalized to $\Omega h^2 = 0.12$ in the $\lambda_{345} - m_{H'}$ plane for different mass splittings and fixed c_i's coefficients and mixing angle in the high mass regime. **Left panel:** $\Delta m = 150$ GeV. **Right panel:** $\Delta m = 200$ GeV. Only points fulfilling $0.6 \cdot 0.1200 \leq \Omega h^2 \leq 0.1200 + 3 \cdot 0.0012$ are shown. The black lines represent the XENON1T limits.

the problem now being that the stability of the potential is no longer guaranteed. In order to solve this issue, we need then to find a way to relax the vacuum stability constraints (see Appendix [E] for more details). One way to achieve this is to add an additional dimension six term in the potential of the form

$$V \supset \lambda_7 |H_2|^6 \,, \tag{7.1.3}$$

where again, $\lambda_7 \lesssim 10^{-6}\text{GeV}^{-2}$ and we take it to be real. If that is the case, then we only need to fulfil the conditions

$$\lambda_1 > 0 \quad \text{and} \quad \lambda_7 > 0 \tag{7.1.4}$$

to guarantee vacuum stability, and no lower limit for λ_{345} is needed. Furthermore, since this new term only has contributions to interactions of six DM particles, it will not have a large impact in the relic abundance giving us some freedom to choose its value. Hence, from now on we fix the size of the new coupling to be $\lambda_7 = 10^{-6}\text{GeV}^{-2}$.

With this in mind, a possible combination of the Wilson coefficients c_i that can deliver the right amount of DM in the high

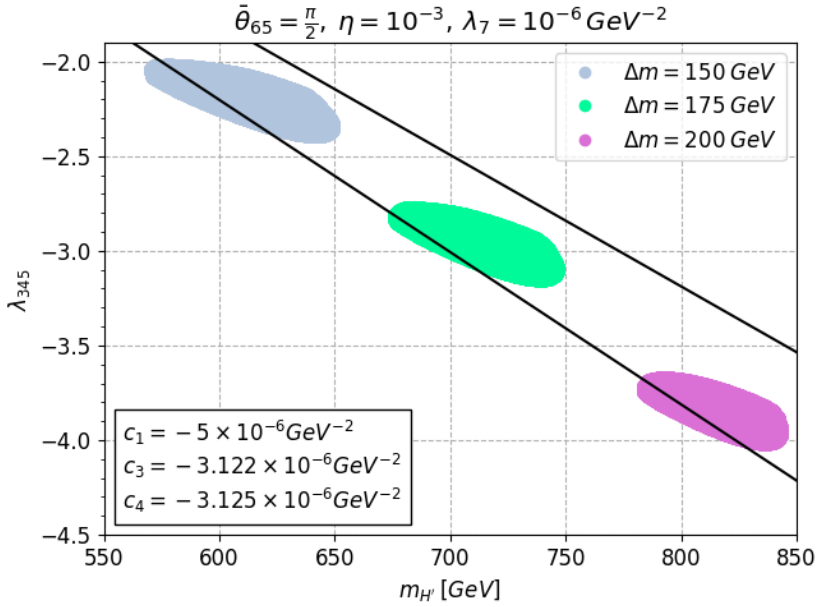

Figure 7.1.6: Allowed regions of relic abundance in the $\lambda_{345} - m'_H$ plane for 3 different mass splittings and fixed c_i's coefficients and mixing angle in the high mass regime. Only points fulfilling $0.6 \cdot 0.1200 \leq \Omega h^2 \leq 0.1200 + 3 \cdot 0.0012$ are shown. The black lines represent the XENON1T limits.

mass regime for high mass splittings, while respecting the theoretical and experimental constraints (with the modified potential), is

$$c_1 = -5 \cdot 10^{-6}\text{GeV}^{-2}, \qquad c_3 = -3.122 \cdot 10^{-6}\text{GeV}^{-2},$$
$$c_4 = -3.125 \cdot 10^{-6}\text{GeV}^{-2}, \tag{7.1.5}$$

with $c_2 = 0$. Accordingly, the results for the relic abundance are shown in Fig. [7.1.5], where it can be seen that the entire relic density can be furnished for a mass splitting of 150 GeV, while we can find regions with up to $\sim 90\%$ of the measured amount of DM for 200 GeV mass splitting. In addition one can observe that, for a fixed set of coefficients, the allowed parameter space moves down towards greater negative values of the quartic coupling λ_{345} and towards higher DM masses when Δm is increased (see Fig. [7.1.6]). This is indeed a great improvement with respect to the vanilla IDM where, for high mass splittings, only around 0.1% of the relic density could be attained.

At this point, nonetheless, one must acknowledge the fact that, even though the small mass splitting constraint was successfully addressed, adding a new operator in the potential and considering larger values of $|\lambda_{345}|$ could lead to a different phenomenology of the phase transition, such that the analysis in Sec. [6.3.2] could not apply to our case anymore. In particular, the characterization of the PhT shown in Fig. [6.3.2] might change notably. A detailed analysis is required to answer these questions. However, despite the possibility of not being able to accommodate DM and a strong first order PhT in the high mass regime, it is still interesting to see that a whole new portion of suitable parameter space is opened up when additional higher dimensional operators are considered; operators which are, regardless, required to make the model viable for baryogenesis.

7.1.2 *A Comment on the XENON1T Bounds*

As briefly discussed in the last section, when using the derivative operators of Eq. (7.1.1), the XENON1T bounds look quite different (see Fig. [7.1.6]) compared to those in the vanilla IDM or the low mass regime, where the bounds are symmetric with respect to the quartic coupling λ_{345}. To understand why this is the case, one must keep in mind that the XENON1T bounds are actually constraints on the spin-independent (SI) DM-nucleon cross section, obtained via direct detection (DD) experiments (see Fig. [4.3.2]) where we have scattering processes of a DM particle with a nucleon. Because the DM does not interact directly with fermions, the SM Higgs is the only possible mediator for these processes (at tree level) in the IDM. Consequently, for the vanilla IDM, the XENON1T bounds translate into constraints for λ_{345}, which is the coupling of the corresponding hHH vertex. This also means that for every operator that is included in the model, one must check whether they have contributions to the direct detection cross section, *i.e.* if they contribute to the three-point interaction of two DM particles with the SM Higgs boson or to direct interactions between DM particles and SM fermions. As can be checked from Appendix [C] the λ_6 term from Eq. (7.0.1) and the derivative operators from Eq. (7.1.1) have indeed these contributions. Nonetheless, for a mixing angle of the order 10^{-3} and for mass splittings up to 300 GeV the change in the SI DM-nucleon cross section is negligible, such that the λ_6 operator in the potential does not affect the

A direct coupling between DM particles and SM fermions is indeed possible if one considers dimension six operators as showed, for example, in the following chapter.

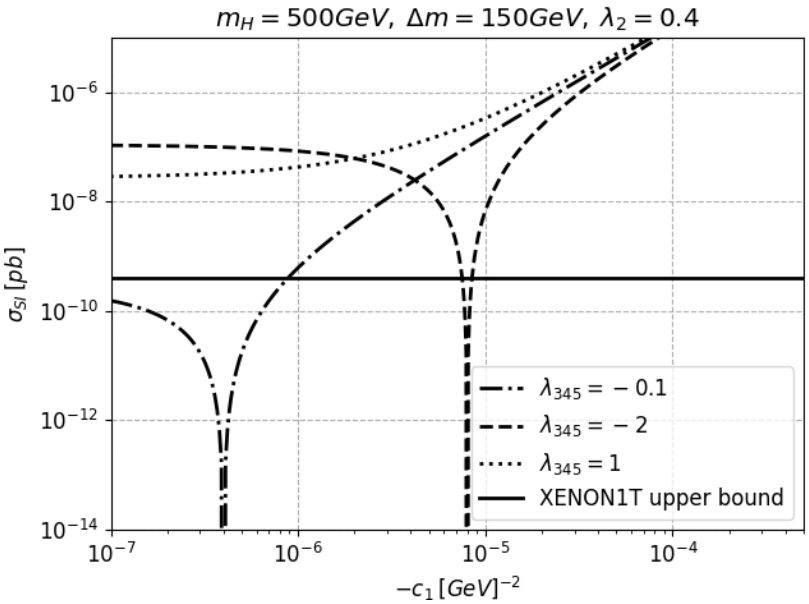

Figure 7.1.7: Dependence of the direct detection cross section with respect to the size of c_1 for fixed DM mass and different values of the quartic coupling. The solid black line represents the upper XENON1T limit on the DD cross section for a DM particle with $m_H = 500$ GeV.

XENON1T bounds in the interesting parameter space. On the other hand, for the derivative operators introduced in the high mass regime in Sec. [7.1.1], one can see from Fig. [7.1.3] that all of them (except for c_2) can in principle contribute to the DD cross section (the contribution is visualized in the $H'H' \to t\bar{t}$ process, where the mediator must be the SM Higgs). Nonetheless, for c_3 and c_4 we find that the corresponding contribution to the hHH vertex goes as

$$(c_3 + c_4)\left(p_{1,\mu}p_2^\mu + p_{1,\mu}p_3^\mu\right) \propto -p_{1,\mu}p_1^\mu \tag{7.1.6}$$

with p_1 and $p_{2,3}$ being the SM Higgs' and the DM particles' momenta, respectively (we take by convention that all the momenta are incoming). By convention, micrOMEGAs computes the DD cross section in the limit of zero momentum transfer, *i.e.* $q^2 \equiv p_{1,\mu}p_1^\mu = 0$, meaning that the contributions from the $c_{3,4}$ operators are exactly zero. The assumption of zero momentum transfer can be justified on the basis that typical values of q^2 in DD scattering processes are of the order $10 - 100$ MeV [107], while the mass of the mediating Higgs is at least three orders

of magnitude larger. Thus, only the c_1 operator can affect the XENON1T bounds and its impact is shown in Fig. [7.1.7] in the limit of the vanilla IDM (without mixing). One can see that the evolution of the DD cross section is smooth for positive values of the the quartic coupling, whereas for negative values we observe a deep fall that moves towards higher values of $-c_1$ for greater negatives values of λ_{345}. This just means that, for each fixed value of c_1, one must adjust the size of the quartic coupling and the DM mass accordingly in order to respect the XENON1T bounds and to obtain the correct relic abundance.

7.2 THE MECHANISM FOR BARYOGENESIS

Having analyzed the DM physics in the new model and having found interesting parameter spaces both, in the low and in the high mass regime, we finally come to the question of whether this model can accommodate sufficient CP violation for successful baryogenesis. One could, for example, go for an EWBG mechanism as discussed in Sec. [5.2.4]. After all, we have all the ingredients: B violation from sphaleron processes, a suitable parameter space where we have a strong-first order phase transition, and our newly introduced CP-violating operator in the scalar potential. The crucial point here is being able to use this CP violation to produce the excess of left-handed particles and antiparticles in front of the bubble wall, which will later be converted into a net baryon number by the sphalerons.

In Appendix [D] we show the computation of the Jarlskog invariant for this particular model.

In EWBG models, in order to produce the desired excess of left-handed particles, one usually relies on the fact that the CP-violating interactions give rise to space and time dependent mass terms for the fermions [30, 31, 59] (for more recent reviews see also [20, 45])

$$m_i(z) = |m_i(z)|e^{i\theta(z)}, \tag{7.2.1}$$

where θ is a complex phase and we assume that the bubble wall is planar and moving in the $+z$ direction. In the rest frame of the bubble, one can describe the particle-wall interactions with a semiclassical force given by

$$F_z = -\frac{(|m|^2)'}{2E} + s\left[\frac{(|m|^2\theta')'}{2EE_z} - \frac{|m|^2(|m|^2)'\theta'}{4E^3E_z}\right], \tag{7.2.2}$$

with $E = (\mathbf{p}^2 + |m|^2)^{1/2}$, $E_z = (p_z^2 + |m|^2)^{1/2}$, $s = \pm 1$ the spin in the z direction, and the primes denoting derivatives with respect to z. It is due to the chiral structure of the mass term in Eq. (7.2.1) that one obtains a spin-dependent part in the force from Eq. (7.2.2). This spin-dependent part will be negative for left-handed particles (or antiparticles), thus decreasing the net force acting on them, whereas it increases the net force acting on right-handed particles ultimately contributing to form the left-handed asymmetry. To get the net baryon number one then needs to solve the corresponding Boltzmann equation containing collision terms that describe particle scattering. Solving the transport equations is, however, out of the scope of this work.

The important point to answer here is whether one can transmit the CP violation that appears in the scalar potential to the fermion sector, such as to get a complex mass contribution. According to [46] this is indeed possible as long as the two doublets acquire a VEV simultaneously, no matter if only one of the doublets couples to fermions. To explain why this is the case, one can first parametrize the neutral components of the doublets as

$$H_1^0 = he^{-i\theta_1}, \qquad H_2^0 = He^{i\theta_2}, \tag{7.2.3}$$

such that $\langle h \rangle = v_1$ and $\langle H \rangle = v_2$. Moreover, in the minimum one can choose a gauge in which $\theta_1 = \theta_2 = \theta/2$. During the phase transition, the equations of motion for the fields h, H and θ are obtained by minimizing the effective action at T_c. Particularly, as argued in [33], the equations of motion for θ will have non-trivial solutions due to the explicit CP violation in the effective potential, given by the complex parameter λ_6. Furthermore, since the CP violating phase in the potential can only appear in terms involving the products of both doublets, then it is clear that if either h or H were to remain zero during the PhT, it would not be possible to generate any CP violation in the bubble wall. This has been carefully studied before in the context of the two Higgs doublet model, for instance, in [32].

Therefore, assuming that both doublets change during the PhT, and taking only into account contributions coming from the top quark, the complex mass term reads

$$m(z)_t = y_t h(z) e^{i\theta(z)/2}, \tag{7.2.4}$$

with y_t the top Yukawa coupling. Keep in mind that the change in θ will be determined by the CP violating phase in the potential as indicated, for example, in [34]. Accordingly, in our model with the extended scalar potential, the generation of the BAU could only proceed via a two-step PhT. In this case, during the second step, the Higgs field will acquire a finite VEV while the already finite VEV of H_2 will evolve to zero. As discussed in [42] this scenario is only possible, in principle, in a small region of parameter space in the low mass regime. Nonetheless, a further complication comes into hand, *i.e.* that one must require the first step of the PhT to be not too strong. Otherwise, sphalerons will be turned off by the time the second transition occurs and the generation of the BAU would be impossible regardless. In [42], unfortunately, no parameter space where the first-step is mild was found. This does not mean, however, that the model does not work altogether; one could still envisage a scenario where the addition of extra dimension six operators change the thermal history of the universe, thus allowing for a different phenomenology of the PhT as the one discussed in Sec. [6.3.2]. Even the addition of the extra λ_7 term in the potential as in Eq. (7.1.3) could lead to a change that could make the model viable for baryogenesis. These ideas are, nonetheless, left for future work.

8

FERMIOPHILIC INERT DOUBLET MODEL

Given the problem we encountered in the last section of the previous chapter, concerning the transmission of the CP violating phase from the scalar potential to the fermion sector, we now discuss another possible source of CP violation that can be added to the IDM and that, potentially, could solve this issue. In this case we consider the following Yukawa-like operator

$$\mathcal{L}_Y^{CPV} = -\tilde{y}\left(H_1^\dagger H_2\right)\left(\bar{Q}H_2 d_R + \bar{Q}\tilde{H}_2 u_R\right) + h.c.\,, \tag{8.0.1}$$

where Q, u_R and d_R are defined in Eq. (3.0.1), $\tilde{y} = |\tilde{y}|e^{i\tilde{\theta}}$ is a complex number with $|\tilde{y}| \lesssim 10^{-6}\text{GeV}^{-2}$, and

$$\tilde{H}_2 = i\sigma_2 H_2^* = \frac{1}{\sqrt{2}}\begin{pmatrix} H - iA \\ -\sqrt{2}H^- \end{pmatrix}\,. \tag{8.0.2}$$

The novel feature of this operator is that it allows us to introduce CP violation directly into the quark sector without breaking the $\mathbb{Z}_2$-symmetry, which prevents a direct coupling of the inert doublet with the fermions at the renormalizable level. The expectation is, thus, that this operator will allow for CP-violating processes which could lead to complex quark masses as discussed in Sec. [7.2]; ideas that will be explored later. For now, we focus our attention on DM physics which is discussed in detail in the following section.

8.1 THE RELIC ABUNDANCE

As in previous models, we start by checking how the DM relics are affected by the new Yukawa-type operator. For that purpose a first step is to check how the thermally averaged cross section evolves with the size of $|\tilde{y}|$. From the start it is clear that the new operator will have new contributions to the processes where two DM particles annihilate into quarks (for more details see Appendix [C]). This is shown in Fig. [8.1.1], where the CP violating angle is fixed to $\tilde{\theta} = \pi/2$ and we explore the two mass regimes. For instance, in the left panel the be-

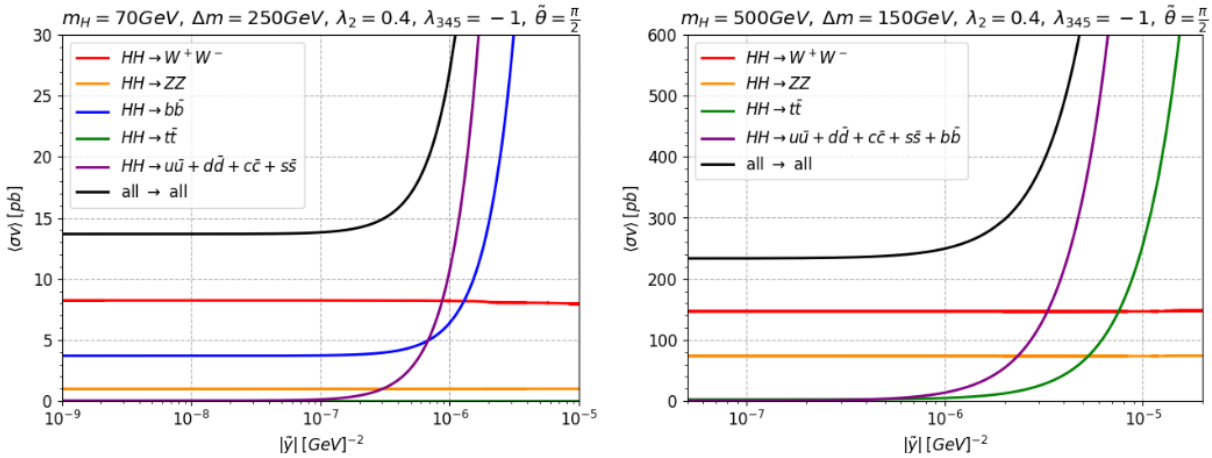

Figure 8.1.1: Evolution of the thermally averaged cross section with respect to $|\tilde{y}|$ for different annihilation channels. **Left panel:** in the low mass regime. **Right panel:** in the high mass regime.

haviour in the low mass regime for a DM mass of 70 GeV and 250 GeV mass splitting is shown, whereas in the right panel the behaviour in the high mass regime is depicted for a DM mass of 500 GeV and 150 GeV mass splitting. In the low mass scenario, for $|\tilde{y}| \sim 10^{-6}\,\text{GeV}^{-2}$, the cross section for processes involving the kinematically accessible quarks (the top quark is to heavy to be produced in this regime) is greatly enhanced. Therefore, the correct relic abundance is expected to be attained only for values of $|\tilde{y}|$ up to $10^{-7}\,\text{GeV}^{-2}$. The situation is similar in the high mass regime. Already for values of $|\tilde{y}|$ around $10^{-6}\,\text{GeV}^{-2}$ annihilations into "light" quarks are enhanced, whereas the contributions coming from annihilations into top quarks become dominant at about $|\tilde{y}| \sim 10^{-5}\text{GeV}^{-2}$. However, if one zooms in the plot on the right panel of Fig. [8.1.1] one realizes that already for $|\tilde{y}|$ around 10^{-7}GeV^{-2} the increment in the cross section is sufficiently important as to expect a sizable reduction in the delivered relic abundance. It is also worth noting here that, since the new operator does not affect the cross section corresponding to the annihilation of DM into gauge bosons (corresponding to the red and yellow lines in Fig. [8.1.1] which remain constant for every value of $|\tilde{y}|$), the Yukawa-like operator alone cannot change the panorama in the high mass regime and derivative operators as in Sec. [7.1.1] must be used. Results of the relic abundance in the low mass regime are shown in Fig. [8.1.2] where $|\tilde{y}|$ is fixed to $10^{-7}\,\text{GeV}^{-2}$ and the CP phase is

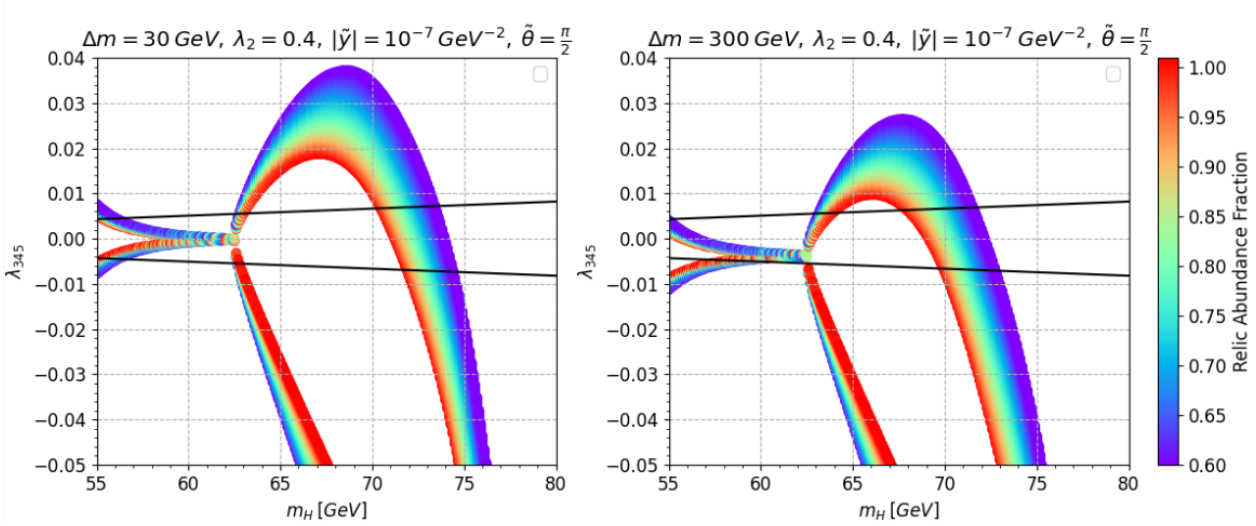

Figure 8.1.2: The relic abundance normalized to $\Omega h^2 = 0.12$ in the $\lambda_{345} - m_H$ plane for different mass splittings and fixed CP violating phase and $|\tilde{y}|$ in the low mass regime. **Left panel:** $\Delta m = 30$GeV. **Right panel:** $\Delta m = 300$GeV. Only points fulfilling $0.6 \cdot 0.1200 \leq \Omega h^2 \leq 0.1200 + 3 \cdot 0.0012$ are shown. The black lines represent the XENON1T limits.

fixed to $\tilde{\theta} = \pi/2$. Once again the three distinctive regions can be identified as in the vanilla IDM. Nonetheless, due to a slight increase in the total cross section, the maximum value of λ_{345} (compared to the vanilla IDM) allowing for the correct relics decreases. Increments of the size of $|\tilde{y}|$ result in a further increase of the total cross section, and the entire parameter space disappears once we reach $|\tilde{y}| \sim 10^{-6}\,\text{GeV}^{-2}$.

On the other hand, we finally show the results for the relics in the high mass regime in Fig. [8.1.3], where the values of the derivative operators are fixed as in Eq. (7.1.5) and we choose a high mass splitting of 200 GeV. In this case we also need to include the extra term in the potential as given in Eq. (7.1.3) in order to guarantee vacuum stability; its size is fixed to $\lambda_7 = 10^{-6}\,\text{GeV}^{-2}$. In the left panel of Fig. [8.1.3], for $|\tilde{y}| = 10^{-8}\text{GeV}^{-2}$, up to 90% of the measured relic density can be obtained, which is a comparable result as in the previous model and an important improvement with respect to the vanilla IDM. Also, as we expected from the cross section analysis, when increasing the value of $|\tilde{y}|$ to 10^{-7}GeV^{-2} (see right panel of Fig. [8.1.3]), the available parameter space is considerably reduced. In addi-

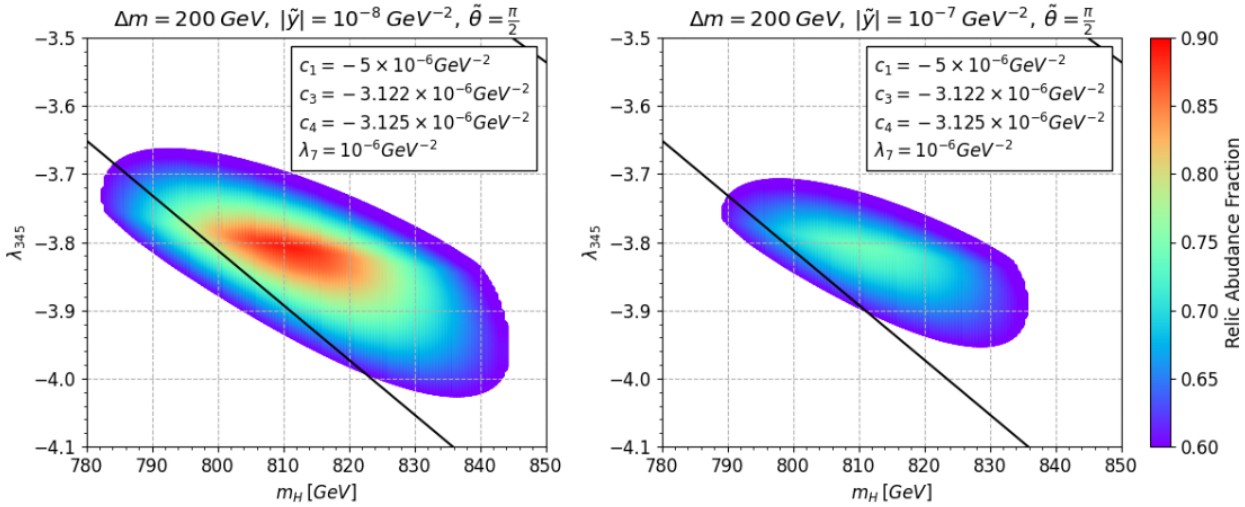

Figure 8.1.3: The relic abundance normalized to $\Omega h^2 = 0.12$ in the $\lambda_{345} - m_H$ plane for different values of $|\tilde{y}|$ and fixed c_i's coefficients and mass splitting in the high mass regime. **Left panel:** $|\tilde{y}| = 10^{-8}\text{GeV}^{-2}$. **Right panel:** $|\tilde{y}| = 10^{-7}\text{GeV}^{-2}$. Only points fulfilling $0.6 \cdot 0.1200 \leq \Omega h^2 \leq 0.1200 + 3 \cdot 0.0012$ are shown. The black lines represent the XENON1T limits.

tion, the maximum fraction of DM relic abundance decreases by approximately 20%, as one can obtain a relic density only up to 70% of the present value. Decreasing the mass splitting to around 150 GeV leads to regions where the full relic density can be found for $|\tilde{y}| = 10^{-8}\text{GeV}^{-2}$, whereas for $|\tilde{y}| = 10^{-7}\text{GeV}^{-2}$ one can find up to 90% of the measured value.

As a final comment in this section, one must bare in mind that, similarly as in the extended IDM, adding a new term in the potential and considering larger values of $|\lambda_{345}|$ in the high mass regime, could completely change the nature of the phase transition. For more details about this issue the reader is referred to the final discussion in Sec. [7.1].

8.2 A BRIEF COMMENT ON THE EDM'S

So far we have delayed a very important issue that must be addressed in any model that includes new sources of CP violation: Electric Dipole Moments (EDMs). As we have previously seen, CP violation is a key ingredient in any EWBG model, however, it is usual that models containing new sources of CP violation are

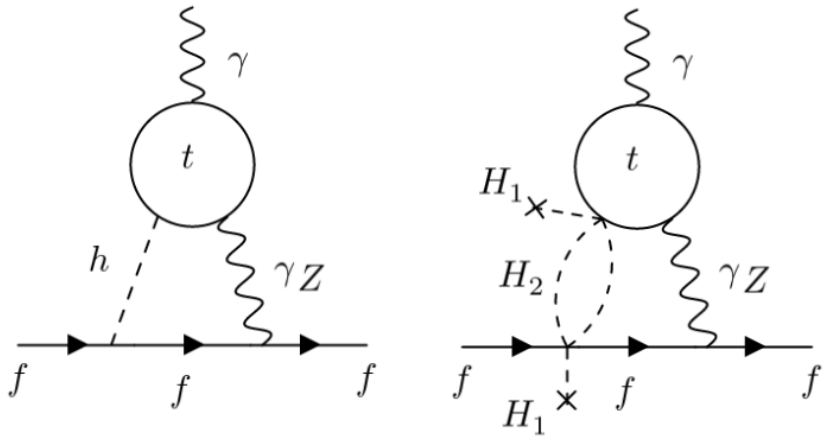

Figure 8.2.1: Two-loop Barr-Zee diagrams contributing to the EDMs. **Left panel:** when there is CP violation in the Higgs sector. **Right panel:** in the Fermiophilic IDM.

heavily constrained by negative searches of EDMs [11], particularly for the electron, the neutron and for neutral atoms. For instance, a precise measurement of the electron EDM by the ACME collaboration yields [2]

$$d_e < 1.11 \times 10^{-29} e \text{ cm} , \tag{8.2.1}$$

where e is the electric charge of the electron. In the SM, contributions to the EDMs associated with the CKM matrix occur first a three-loop level, resulting in a natural suppression below the current bounds [80]. Thus, one can say that EDMs are excellent tools to probe for new physics [47]. For example, in the presence of CP violation in the quark-Higgs sector, contributions to the EDMs are generally induced via two-loop Barr-Zee [12] diagrams as the one shown in the left panel of Fig. [8.2.1]. Meanwhile, in our particular model, one could obtain a contribution given by the diagram in the right panel of Fig. [8.2.1], where the two vertices in the H_2 loop will be proportional to $\tilde{y}$. The good news is that the contribution appears already at three-loop level which could mean it is suppressed and no new constrains would appear in the model. Nonetheless, a detailed analysis is still lacking and it is out of the scope of this work.

As a final remark in this section it must be pointed out that, since leading contributions to the EDMs usually come from CP violating operators in the quark-Higgs sector [9], the models

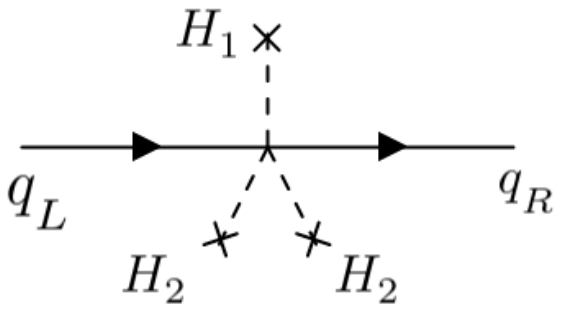

Figure 8.3.1: Feynman diagram contributing to the quark mass terms in the fermiophilic IDM.

discussed in Chapters [7] and [9] should have negligible contributions at zero temperature and therefore be left unconstrained.

8.3 CREATING THE BARYON ASYMMETRY

Having finished the discussion on DM physics, once again we ask ourselves if this model can accommodate enough CP violation as required by baryogenesis. After all, we are adding CP violation directly into the fermion sector such that, in principle, the mechanism described in Sec. [7.2] for complex fermion masses should work. Indeed, the operator in Eq. (8.0.1) has contributions to the mass terms, in particular if both doublets acquire a VEV simultaneously one has

$$m_t = \left(\frac{v_1}{\sqrt{2}} y_t + |\tilde{y}| e^{i\tilde{\theta}} \frac{v_1 v_2^2}{2\sqrt{2}} \right) \bar{t}_L t_R + h.c. \,, \tag{8.3.1}$$

where v_1 and v_2 are the VEVs corresponding to H_1 and H_2 respectively, and we have taken only the contribution from the top quark as an example. This contribution is shown in Fig. [8.3.1]. It is clear that, during the phase transition, the term in Eq. (8.3.1) will become an spatially varying complex mass depending on the respective profiles for h and H around the bubble wall. Therefore, the fermiophilic IDM could generate the baryon asymmetry in the second step of a two-step PhT, as it was also discussed in the last section of chapter [7]. Nonetheless, we again encounter the problem of finding a suitable parameter space where the first transition does not wash out the sphaleron processes, which must be sufficiently active during the second

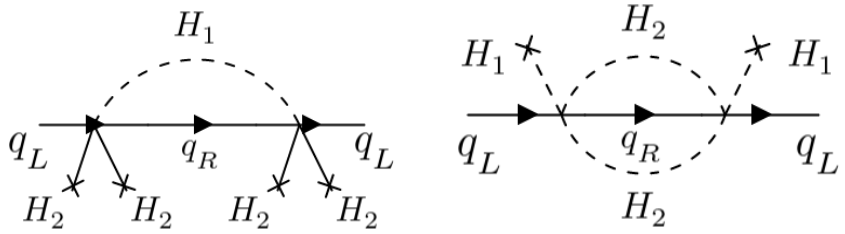

Figure 8.3.2: Feynman diagrams appearing at intermediate stages in the evolution of the universe. **Left panel:** when only H_2 acquires a VEV. **Right panel:** when only H_1 acquires a VEV.

phase transition. The questions is, thus, whether the fermiophilic IDM could work in other scenarios as well; scenarios where each doublet acquires a VEV independently.

Accordingly, let us suppose that only one of the doublets acquires a VEV at a time. However, it is not hard to check that when this happens, we do not obtain a contribution to the mass terms at all. For instance, if the doublet acquiring the VEV is H_2, then from Eq. (8.0.1) we have a contribution given by

$$\mathcal{L}_Y^{CPV} \supset \tilde{y}\frac{v_2^2}{2\sqrt{2}}\, h\, \bar{q}_L\, q_R\ , \tag{8.3.2}$$

which would correspond to a transition of the form $\bar{q}_L q_L$ rather than the required $\bar{q}_L q_R$ interaction, as depicted in the left panel of Fig. [8.3.2]. The undesired change in chirality results from the need of closing the h-loop. The situation is similar when H_1 is the doublet acquiring the VEV. The corresponding Feynman diagram is shown in the right panel of Fig. [8.3.2] where, this time, we need to close two H_2 loops. It is easily seen that this also results in a $\bar{q}_L q_L$ transition. We must conclude, then, that the new operator does not represent any improvement with respect to the scalar extension of the IDM (see Chapter [7]) and, at this point, we are still lacking of a clear mechanism to generate the asymmetry.

We must point out that a similar operator of the form $|H_1|^2\,(\bar{q}_L H_1 q_R)$ could work and generate the asymmetry during the H_1 transition [11, 103]. Nonetheless, since the SM doublet has a VEV at zero temperature, we expect the contributions to the EDMs from this operator to be greater and, thus, the size of the operator itself to be more constrained.

9

CP VIOLATION IN THE GAUGE SECTOR

In a last attempt to extend the IDM as to have new sources of CP violation and account for baryogenesis we choose the following operator

$$\mathcal{L}_{dual} = \tilde{c}|H_2|^2 F_{\mu\nu}\tilde{F}^{\mu\nu} \ , \tag{9.0.1}$$

where $F_{\mu\nu}\tilde{F}^{\mu\nu} = W^a_{\mu\nu}\tilde{W}^{a,\mu\nu} + B_{\mu\nu}\tilde{B}^{\mu\nu}$ is a sum over the $SU(2)$ field strength tensors. These are defined as

$$W^a_{\mu\nu} = \partial_\mu W^a_\nu - \partial_\nu W^a_\mu + g\varepsilon^{abc}W^b_\mu W^c_\nu, \tag{9.0.2}$$

$$B_{\mu\nu} = \partial_\mu B_\nu - \partial_\nu B_\mu \ , \tag{9.0.3}$$

with ε^{ijk} the Levi-Civita tensor, and their corresponding duals given by

$$\widetilde{W}^{a,\mu\nu} = \frac{1}{2}\varepsilon^{\mu\nu\rho\sigma}W^a_{\rho\sigma} \ . \tag{9.0.4}$$

Once more, given the constraint coming from the new physics scale, we force the coefficient $\tilde{c}$ to be of the order $\sim 10^{-6}\text{GeV}^{-2}$. Note that this operator closely resembles the one leading to the strong CP problem in QCD.

9.1 THE RELIC ABUNDANCE

As done for the the previous models, we first check the impact of the new CP violating operator in the relic abundance. An important feature of this operator is that it couples the inert doublet directly to the gauge bosons (therefore contributing to the $HH \to VV$ processes), which could lead to a possible interference in the high mass regime decreasing the annihilation cross section and relaxing the small mass splitting constraint. We will discuss this issue in more detail later. For now, we start with the low mass regime which is shown in Fig. [9.1.1], where the corresponding parameter spaces for two different values of the coefficient $\tilde{c}$ and different mass splittings are compared. In the upper row, for $\tilde{c} = -10^{-7}\,\text{GeV}^{-2}$, identical results com-

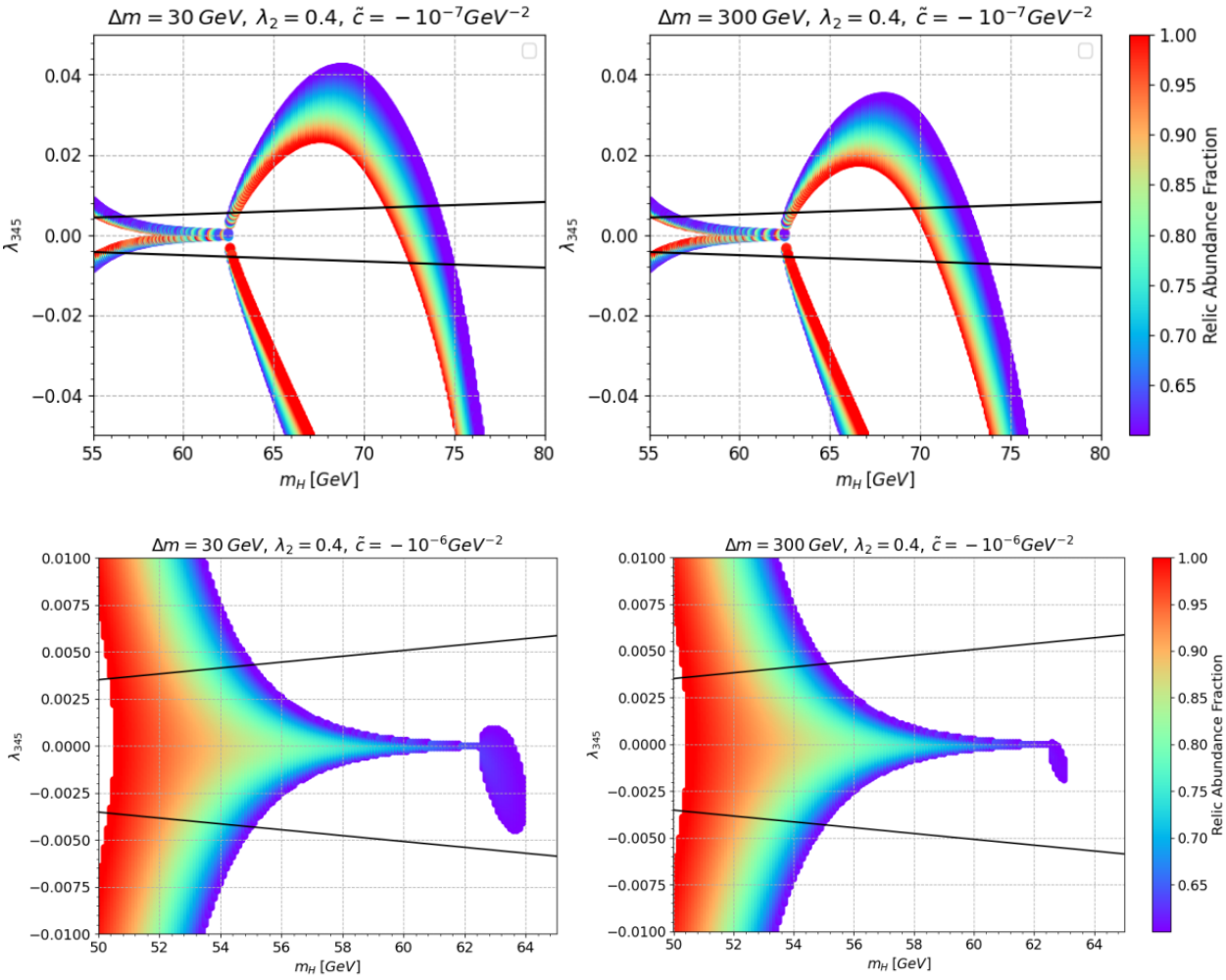

Figure 9.1.1: The relic abundance normalized to $\Omega h^2 = 0.12$ in the $\lambda_{345} - m_H$ plane for different mass splittings and values of $\tilde{c}$ in the low mass regime. **Upper row:** $\tilde{c} = -10^{-7}\text{GeV}^{-2}$. **Lower row:** $\tilde{c} = -10^{-6}\text{GeV}^{-2}$. Only points fulfilling $0.6 \cdot 0.1200 \leq \Omega h^2 \leq 0.1200 + 3 \cdot 0.0012$ are shown. The black lines represent the XENON1T limits.

pared to those in the vanilla IDM are obtained (see Fig. [6.2.3]), such that the physics in the three known regions (funnel, resonant and tail) remains practically unchanged (see Sec.[6.2.1]). This tells us that, for $|\tilde{c}|$ of the order $10^{-7}\,\text{GeV}^{-2}$, the contributions coming from the new operator are negligible and the delivered relic density matches the one in the vanilla IDM (contributions to the annihilation cross section from this operator can be found in Appendix [C]). However, in the lower row, for $\tilde{c} = -10^{-6}\,\text{GeV}^{-2}$, an appreciable change can be seen. For this

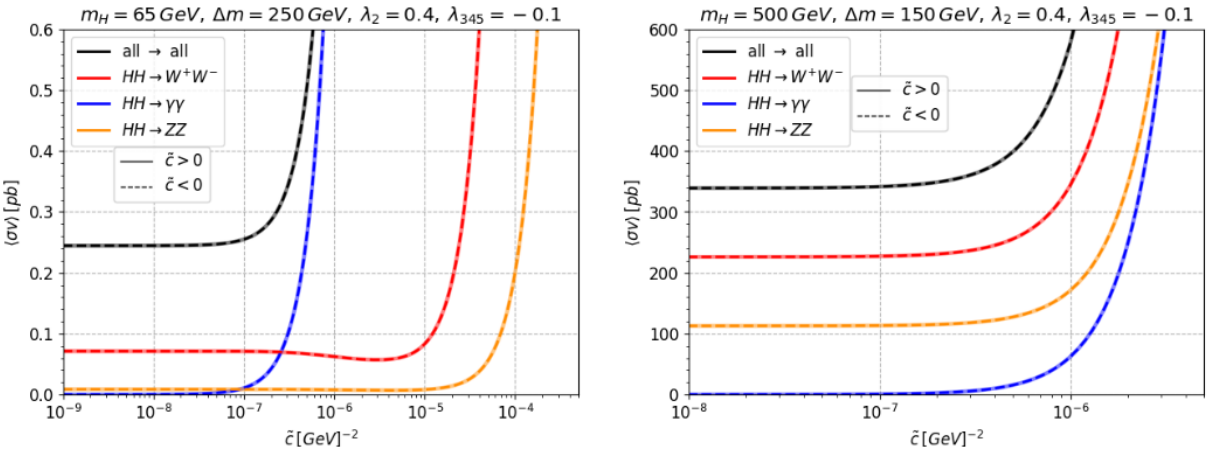

Figure 9.1.2: Evolution of the thermally averaged cross section with respect to $\tilde{c}$ for different annihilation channels. **Left panel:** in the low mass regime. **Right panel:** in the high mass regime.

case the contributions coming from the new operator do become important and they significantly impact the parameter space, opening up the possibility for the DM mass to be as low as ~ 50 GeV, which was excluded in the vanilla IDM due to the XENON1T bounds. In this case, sufficient relic density can not longer be attained for DM masses over ~ 64 GeV. This behavior can be cross checked by looking at Fig. [9.1.2] where, in the left panel, the evolution of the thermally averaged cross section with respect to $\tilde{c}$ is shown in the low mass regime for $m_H = 65$ GeV and a mass splitting of 250 GeV. Already for values of $\tilde{c}$ around $-10^{-6}\,\text{GeV}^{-2}$, annihilations of two DM particles into two photons increase appreciably, whereas annihilations into W bosons are enhanced for $\tilde{c} \sim -10^{-5}\,\text{GeV}^{-2}$. Another important result one can deduce from Fig. [9.1.2] is that the cross section must be proportional to $\tilde{c}^2$, since the sign of the coefficient clearly does not affect the result.

If that is indeed the case, this also means that the new operator contributes only to increasing the total annihilation cross section in the high mass regime, as also shown in the right panel of Fig. [9.1.2], where the DM mass and the mass splitting are fixed to 500 GeV and 150 GeV, respectively. Therefore, no improvement relative to the vanilla IDM for the DM relics can be expected. In fact, it can be seen that the annihilation cross section increases with the increase of the absolute value of $\tilde{c}$ such that,

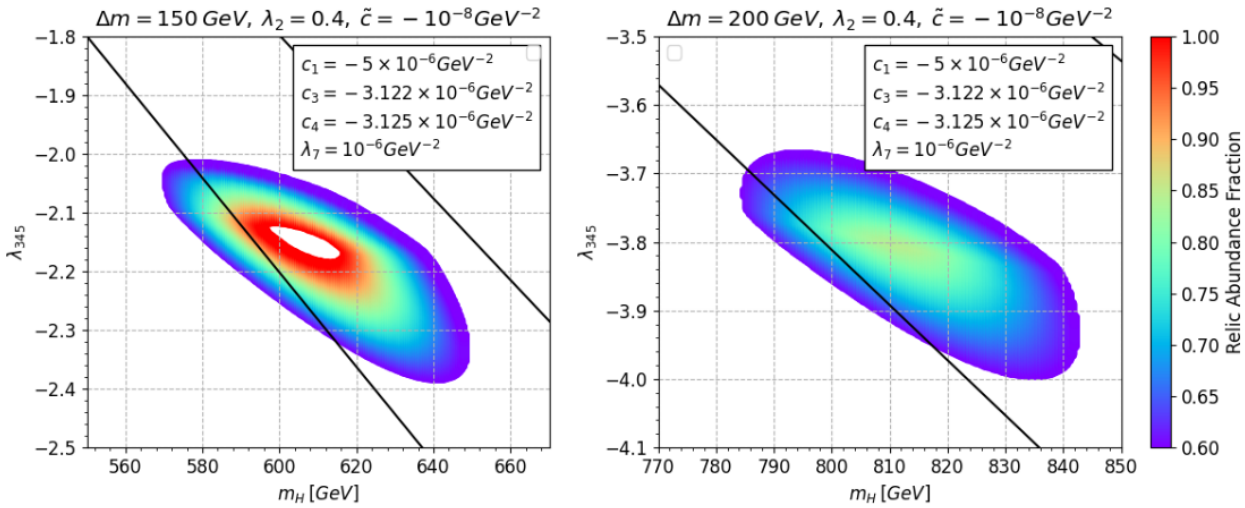

Figure 9.1.3: The relic abundance normalized to $\Omega h^2 = 0.12$ in the $\lambda_{345} - m_H$ plane for different mass splittings and fixed c_i's coefficients and $\tilde{c}$ in the high mass regime. **Left panel:** $\Delta m = 150$ GeV. **Right panel:** $\Delta m = 200$ GeV. Only points fulfilling $0.6 \cdot 0.1200 \leq \Omega h^2 \leq 0.1200 + 3 \cdot 0.0012$ are shown. The black lines represent the XENON1T limits.

around $|\tilde{c}| \sim 10^{-6}\text{GeV}^{-2}$, there is a significant enhancement of $\langle \sigma v \rangle$. Consequently this implies that the new CP violating operator alone does not change the situation in the high mass regime and the entire model still suffers from the existent problems in the vanilla IDM, *i.e.* only small mass splittings lead to sizable relics for heavy DM. Thus, as done in the previous cases, we must rely on the use of the derivative operators defined in Sec. [7.1.1] and the dimension six term defined in Eq. (7.1.3) to find the correct relics for high mass splittings. For example, in Fig. [9.1.3] the allowed parameter space for $\tilde{c} = -10^{-8}\text{GeV}^{-2}$ and fixed c_i's is shown for 150 GeV and 200 GeV mass splittings. The chosen values of the coefficients are the same as in Eq. (7.1.5) and, once more, λ_7 is fixed to $10^{-6}\,\text{GeV}^{-2}$. The results are similar as the ones obtained for the scalar extension and the fermiophilic IDM where, for 150 GeV mass splitting the entire measured relic density can be attained, while it decreases to around 90% for 200 GeV mass splitting. Once we increment the size of the coefficient $\tilde{c}$ the allowed parameter space shrinks until at around $\tilde{c} \sim -10^{-7}\text{GeV}^{-2}$ where a sizable relic can no longer be delivered and the entire region disappears.

The important thing to keep in mind is that the IDM, extended with CP violation in the gauge sector, still serves as a suitable DM model as long as one keeps the size of the Wilson coefficient around $\tilde{c} \sim 10^{-7}\,\mathrm{GeV}^{-2}$ in the low mass regime (for which similar results as in the vanilla IDM are obtained), and around $\tilde{c} \sim 10^{-8}\,\mathrm{GeV}^{-2}$ in the high mass regime (this is because for $\tilde{c} \sim 10^{-7}\mathrm{GeV}^{-2}$ the increment in the cross section is enough as to produce underabundant DM for any combination of parameters).

9.2 BARYON ASYMMETRY À LA SPONTANEOUS BARYOGENESIS

Once more, and a final time, we come to the question of whether we can accommodate sufficient CP violation in the model as to allow for baryogenesis. As discussed in Sec. [7.2], if we want to use the conventional realization of EWBG we would need of a mechanism capable of transferring the CP violation from the gauge sector to the fermion sector, such that we can obtain a complex mass contribution as in Eq. (7.2.1). However, due to the absence of such mechanism and since our CP-violating operator does not involve any fermions directly, we do not expect this idea to work. This means that, so far, there is no clear advantage between this model and the ones discussed earlier.

An interesting feature of spontaneous baryogenesis is that, contrary to the predetermined intuition of the Sakharov conditions, ***the BAU can be produced in equilibrium and with no CP violation at all****. This is the case because spontaneous baryogenesis relies on an spontaneous breaking of CPT symmetry, whereas CPT symmetry is one of the requirements for Sakharov's criteria to hold.*

Nevertheless, there could be another possibility, for example, if another mechanism of EWBG was used to produce the baryon asymmetry; if one could transfer the CP violation to the generation of the BAU without necessarily having a complex mass. In [38], for instance, a similar effective operator was added to the SM involving the usual Higgs doublet, *i.e.*

$$\frac{1}{M^2}\frac{g^2}{32\pi^2}|H_1|^2 W_{\mu\nu}\widetilde{W}^{\mu\nu}\ , \tag{9.2.1}$$

where M is a typical mass-scale squared and g is the $SU(2)_L$ coupling constant. In this way a mechanism analogous to the one known as **spontaneous baryogenesis** [35] can be used in order to estimate the total baryon number density. Without go-

ing into too much detail, the key idea is to have a term in the Lagrangian of the form [5]

$$\mathcal{L} \supset \partial_\mu \theta j_B^\mu \,, \tag{9.2.2}$$

where θ is a scalar field and j_B is the baryon current. When one considers an spatially homogeneous field such that $\theta = \theta(t)$ the interaction in Eq. (9.2.2) is reduced to the form $\dot{\theta} j_B^0$. In this way $\dot{\theta}$ acts as a sort of chemical potential for baryon number, shifting the energy levels of baryons with respect to those of antibaryons. Thus, as long as baryon number violating processes are in thermal equilibrium, a non-zero baryon number will be produced. Once baryon number violating processes fall out of equilibrium **the BAU freezes in**. The picture is, then, as follows:

In the model of [38], the realization of spontaneous baryogenesis still needs of the three Sakharov conditions: CP violation is present in the operator involving dual fields and the BAU is still created during the EWPhT. Therefore, calling the mechanism as spontaneous baryogenesis could be misleading. Nonetheless, the name is still used for historical reasons.

- At very high temperatures we assume the field θ to remain constant (as we will see later, the second doublet H_2 will play the role of θ in the mechanism). If this is the case, a term as in Eq. (9.2.2) is not present and the system remains in the usual minimum with zero baryon number density, even though sphalerons are very active and in equilibrium for these temperatures.
- At some point in the thermal history of the universe, the field θ acquires a space-time dependence (for example, if a PhT occurs). This will lead to a term as in Eq. (9.2.2), acting as an effective chemical potential and changing the minimum of the free energy with a non-zero baryon number density.
- Accordingly, since sphalerons are the only B violating processes, they will start building up the asymmetry by driving the system towards the new minimum.
- Finally, once the EWPhT occurs, and assuming it is a strong first-order PhT, the sphalerons will turn off and the produced baryon asymmetry will be ultimately conserved.

For the particular case in [38], and similar to our case, one can use the anomaly equation

$$\partial_\mu j_B^\mu = \frac{3g^2}{32\pi^2} W_{\mu\nu} \widetilde{W}^{\mu\nu} \,, \tag{9.2.3}$$

to rewrite the operator in Eq. (9.2.1) in the form of Eq. (9.2.2) as

$$\frac{1}{M^2}\frac{g^2}{32\pi^2}|H_1|^2 W_{\mu\nu}\widetilde{W}^{\mu\nu} = \frac{1}{3M^2}\partial_\mu|H_1|^2 j_B^\mu \,. \tag{9.2.4}$$

As mentioned before, this term in the Lagrangian changes the minimum of the free energy, such that the entire system will try to relax to the new minimum where [5]

$$n_B^0 = \frac{T^2}{12M^2}\partial_0|H_1|^2. \tag{9.2.5}$$

Given that sphalerons are the only sources of B violation in the model, they need enough time to create the asymmetry. Nonetheless, one must keep in mind that, in this realization of spontaneous baryogenesis, the entire process takes place during the EWPhT where the Higgs field acquires a VEV, changing near the bubble walls. Thus, baryon number must satisfy the equation [37]

$$\frac{dn_B}{dt} = -18\Gamma T^{-3}\left(n_B - n_B^0\right) \,, \tag{9.2.6}$$

where Γ is the sphaleron rate which we assume to be

$$\Gamma = \begin{cases} \kappa(\alpha_W T)^4 & \text{if } m_W < \alpha_W T \\ 0 & \text{if } m_W > \alpha_W T \,. \end{cases} \tag{9.2.7}$$

Eq. (9.2.6) is crucial: the rate of change of baryon number stops at the minimum and it is directly proportional to the sphaleron rate. When the change in H_1 is sudden, such as in a strong first order phase transition, the baryon number density will go simply as [38]

$$n_B \sim \frac{|v_c|^2}{M^2}\alpha_W^5 \, \Delta t \, T^4 \,, \tag{9.2.8}$$

with Δt being the amount of time needed for the Higgs field to rise from $\langle H_1\rangle = 0$ to $\langle H_1\rangle = v_c$. More precisely, Δt will be the amount of time needed for the Higgs field to change over a correlation volume $\xi^3 \sim (\alpha_W T_c)^{-3}$, such that

$$\Delta t = \xi / v_w \,, \tag{9.2.9}$$

where v_w is the bubble wall velocity. In our model, the operator in Eq. (9.0.1) is proportional to $|H_2|$ rather than the usual Higgs doublet; adjusting the factors of $\frac{3g^2}{32\pi^2}$ to make use of the anomaly equation and including the coefficient $\tilde{c}$ one finds that the baryon number density will be given by

$$n_B \sim \frac{8\pi}{3}\tilde{c}\,|v_c|^2\alpha_W^4\,\Delta t\,T^4\,, \tag{9.2.10}$$

where we keep the definition of Δt as in Eq. (9.2.9) and v_c now denotes the critical VEV corresponding to H_2. Furthermore, since the number density of photons is defined as

$$n_\gamma = \frac{2\zeta(3)}{\pi^2}T^3\,, \tag{9.2.11}$$

with $\zeta(3) \approx 1.2$ the Riemann zeta function, one obtains for the baryon-to-photon ratio

$$\eta \sim \frac{4\pi^3}{3\,\zeta(3)\,v_w}\tilde{c}\,\alpha_W^3\,|v_c|^2\,. \tag{9.2.12}$$

The key finding of this section is that the new doublet H_2 not only allows us to explain DM and to accommodate a strong first-order PhT, but it also allows us to introduce CP violating operators that work in explaining the BAU; all of it simultaneously.

Surprisingly the ratio in Eq. (9.2.12) does not explicitly depend on the temperature but, on the size of the CP-violating operator, the critical VEV and the bubble wall velocity. Accordingly, in Fig. [9.2.1] the results for the normalized BAU with respect to $\tilde{c}$ and the critical VEV are shown for a fixed value of the bubble wall velocity. The black solid line represents the combination of parameters for which one can obtain the measured value of the BAU. This means that the region that lies over this line signals overabundant matter, whereas the region under the line corresponds to underabundant matter. Then, if we expect the critical VEV to be of the order 100 GeV, the size of the CP-violating operator must be in between 10^{-11}GeV^{-2} and 10^{-10}GeV^{-2}; values which in turn allow for a sufficient amount of DM (see Sec. [9.1]). On the other hand, by increasing the size of $\tilde{c}$ the generation of the measured BAU requires an even smaller value of the critical VEV. However, since we also aim to have a strong first order PhT, even smaller values of T_c are needed in order to satisfy the condition in Eq. (6.3.13). Nonetheless, if the critical temperature is very low, scenarios where the DM freeze out occurs before the EWPhT could appear. In those cases, a new detailed analysis will be necessary in order to study the impact on the DM relics, given that one must replace the longitudinal components of the

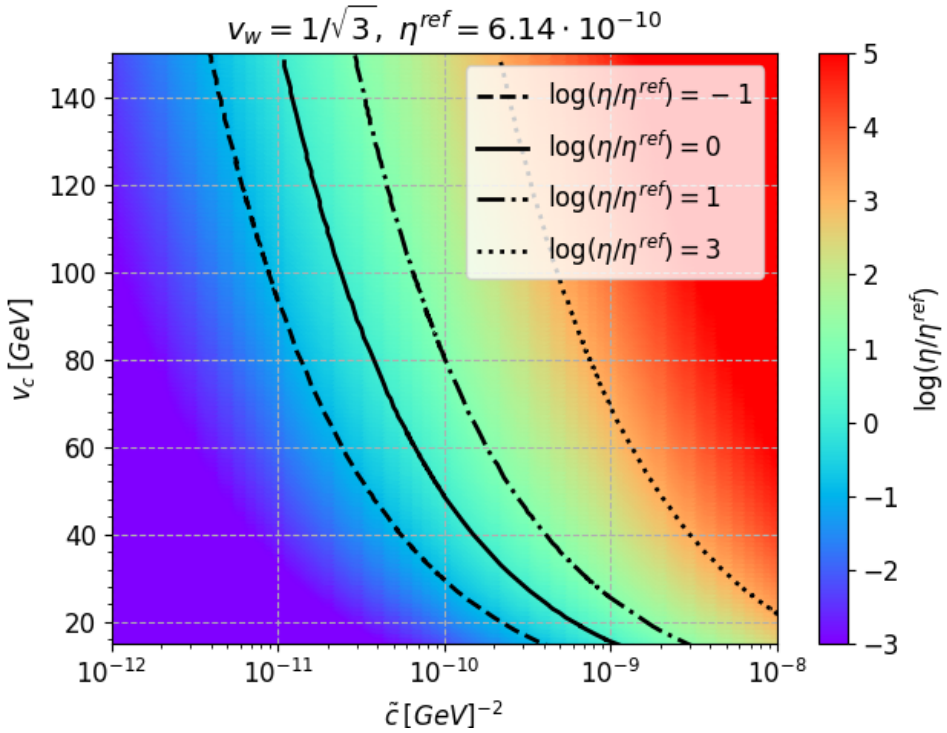

Figure 9.2.1: The BAU normalized to the measured value with respect to $\tilde{c}$ and the critical VEV for a fixed value of the bubble wall velocity.

gauge bosons with the scalar fields $\phi^{(\pm)}$. Therefore, we restrict ourselves to consider only sufficiently large values of v_c, which require the CP-violating operator to be, at most, of the order 10^{-10}GeV^{-2}.

Now, to complete the analysis in this section, in Fig. [9.2.2] the dependence of the BAU with respect to the bubble wall velocity is shown for a fixed value of $\tilde{c}$ and different values of v_c. We notice that if the critical VEV is too small, then we need of a rather slow bubble wall to compensate and obtain the correct BAU. On the other hand, increasing the critical VEV allows for larger values of v_w. Nonetheless, for very large values of v_c (in this case already for $v_c = 150$ GeV), one obtains a way too large asymmetry for any value of the bubble wall velocity. This is in accordance with the results from Fig. [9.2.1], where allowing for a large VEV requires the CP-violating operator to be even smaller.

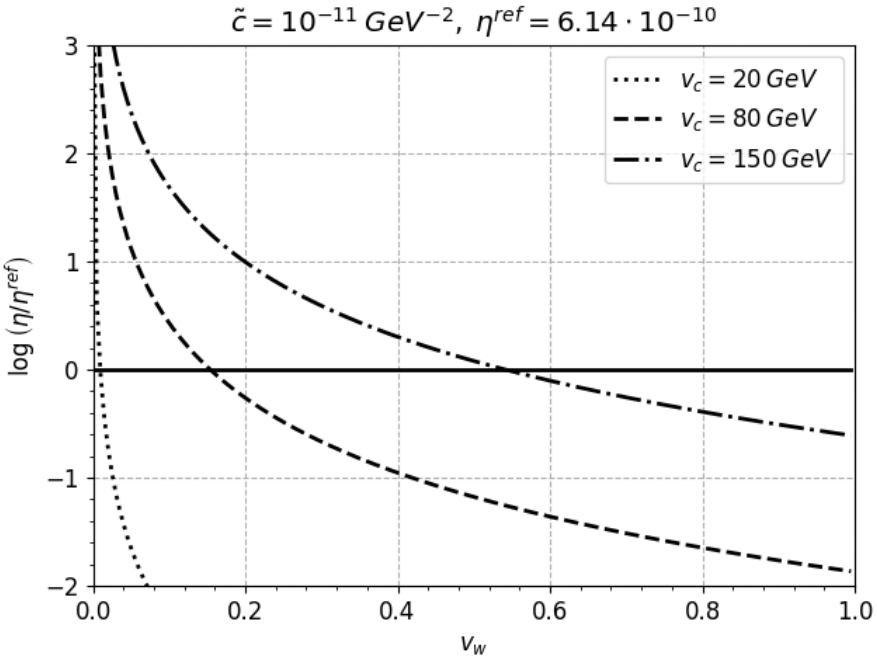

Figure 9.2.2: The BAU normalized to the measured value with respect to the bubble wall velocity for a fixed value of $\tilde{c}$ and different values of the critical VEV.

As a final remark here, one must keep in mind that for the analysis in this section to be valid and to obtain the correct BAU by means of the mechanism described previously, a two-step PhT is required. Given that the CP-violating operator of Eq. (9.0.1) is proportional to H_2, the entire mechanism to produce the BAU relies on the fact that H_2 must acquire a VEV at some point in the history of the universe, which would correspond to the first step of the PhT. As discussed in Sec. [6.3.2] this is possible in the low mass regime. In particular, one can make use of the benchmark scenarios studied in [42] for which one can obtain a two-step PhT, while satisfying all the theoretical and experimental constraints. These are given in Tab. [9.2.1], where ξ_1 and ξ_2 correspond to the strength of the first and second step respectively, and similarly for $T_{1,2}$. Since we assume that baryogenesis takes place at the first step, we are only interested in the critical VEV of H_2 which has a value of $v_c \approx 117.6$ GeV and $v_c \approx 112.2$ GeV for the first and second benchmark points, respectively. By keeping the wall velocity at $v_w = 1/\sqrt{3}$

m_H	Δm	λ_{345}	Ωh^2	ξ_1	ξ_2	T_1	T_2
56 GeV	415 GeV	0.0037	0.1188	1.68	6.12	70 GeV	40 GeV
71 GeV	410 GeV	0.0020	0.1177	2.04	6.58	55 GeV	35 GeV

Table 9.2.1: Benchmark points where a two-step PhT is present in the low mass regime for $\lambda_2 = 0.4$. All theoretical and experimental constraints are satisfied. Taken from [42].

one can find the corresponding size of $\tilde{c}$ in order to obtain the measured BAU as

$$\tilde{c} \approx \begin{cases} 1.78 \times 10^{-11}\,\text{GeV}^{-2} & \text{if} \quad v_c = 117.6\,\text{GeV} \\ 1.95 \times 10^{-11}\,\text{GeV}^{-2} & \text{if} \quad v_c = 112.2\,\text{GeV}\,. \end{cases} \tag{9.2.13}$$

Since these values of $\tilde{c}$ are fairly small, no noticeable change in the relic abundance is expected (as discussed in the previous section already for values of $\tilde{c} = 10^{-7}\text{GeV}^{-2}$ one can reproduce the vanilla IDM results). Thus, it is shown that suitable benchmark points can be found in the model (particularly in the low mass regime) for which both DM and baryogenesis are, in principle, accounted for.

The situation in the high mass regime, on the other hand, requires of a more careful treatment. In particular, from the discussion in Sec. [6.3.2], in the high mass regime no suitable parameter space accommodating a two-step PhT was found. This, in principle, completely rules out the possibility of creating the asymmetry by means of the mechanism and the operator discussed in this section. Nonetheless, as also discussed in Sec. [9.1], the introduction of the additional dimension six term in the potential- as in Eq. (7.1.3)- could lead to a change in the nature of the PhT. Specifically, investigating the impact of choosing rather large values for $|\lambda_{345}|$ and different combinations of λ_2 (which is no longer required to be strictly positive) could entail new interesting findings. This, however, will require of a more detailed analysis and it is left for future work.

One could think of using the operator in Eq (9.2.1) involving the SM Higgs doublet in order to create the asymmetry in the high mass regime (or in the low mass regime) during a single H_1 transition. This is indeed possible and it has been studied in previous works [37, 38, 63]. Nonetheless, since H_2 has no VEV at zero temperature, we expect our operator to be less constrained, for example, by EDMs.

10

CONCLUSIONS AND OUTLOOK

In order to accommodate DM and baryogenesis into the IDM, in this work different extensions of the model with new sources of CP violation were studied in detail. In particular, CP violation was added by means of higher dimensional operators in different sectors of the theory, *i.e.* in the scalar potential, the Yukawa Lagrangian and the gauge sector. The dimension six CP-violating operators were constrained to be at most of the order $10^{-6}\,\text{GeV}^{-2}$, assuming the new physics scale is around 1 TeV. First, in each case, the impact of the new operators in the DM relic abundance was thoroughly examined. It was found that, as in the vanilla IDM, two distinct regimes for DM masses allow for at least 60% of the measured relic density. In the low mass regime, *i.e.* for $55\,\text{GeV} \lesssim m_H \lesssim 75\,\text{GeV}$, similar results as in the vanilla IDM can be achieved as long as the size of the CP-violating operators is not particularly large. For instance, in the scalar extension and the fermiophilic IDM, with a mixing angle of $\eta \sim 10^{-3}$ and $|\tilde{y}| \sim 10^{-7}\,\text{GeV}^{-2}$ respectively, a sufficient amount of DM can be attained (independently of the value of the CP violating phase), whereas in the model with CP violation in the gauge sector, one can allow for $\tilde{c}$ to be at most of the order $10^{-7}\,\text{GeV}^{-2}$. As pointed out in [42], this regime allows either for a one-step or a two-step strong first order PhT and this continues to be valid for each of the extensions.

In the high mass regime (for $m_H \gtrsim 500\,\text{GeV}$), on the other hand, and following the discussion in [42] about the nature of the PhT in this regime, new higher dimensional derivative operators were introduced in order to obtain sufficient amounts of DM with non-(quasi)degenerate scalar masses, which correspond to the interesting parameter space where also a sufficiently strong first order PhT can take place. These operators, when used in appropriate combinations, lead to a destructive interference in the thermally averaged annihilation cross section, allowing one to find up to 90% of the measured relic density even for 200 GeV mass splittings. Nonetheless, obtaining the correct relic density while respecting the XENON1T bounds

is only possible for large negative values of the quartic coupling λ_{345}, therefore violating vacuum stability constraints. To solve this issue a new term in the potential proportional to $|H_2|^6$ was added. This new term, when positive, allows for the potential to be bounded from below even for $|\lambda_{345}| \gtrsim 1$ and, since it only involves interactions of six DM particles, its size is completely irrelevant in the computation of the relic abundance. Consequently, viable parameter spaces for DM in the $m_H - \lambda_{345}$ plane for high mass splittings were found in each model, for fixed sizes of the higher derivative operators and the CP-violating operators. At this point, however, the results for the PhT from [42] might no longer be valid. Indeed, considering large values of $|\lambda_{345}|$ and allowing for negative values of λ_2 could lead to a different phenomenology in the phase transition. A deep study on the nature of the PhT in this regime is, nevertheless, left for future work.

Regarding the generation of the BAU, in the scalar extension and the fermiophilic IDM it was argued that baryogenesis could take place if both doublets acquire a VEV at the same time, for example, in the second step of a two-step PhT. This situation will require, nonetheless, of a scenario where the first transition is weak enough as to not turn off the sphaleron processes; a scenario that, unfortunately, was not found for any combination of parameters. In this respect one could think of the possibility to add further dimension six operators in the model, particularly in the potential, which could lead to a change in the thermal history of our universe and make the situation of having simultaneous VEVs feasible, maybe even in the high mass regime.

On the other hand, in the last extension, where CP violation is added in the gauge sector one can use a mechanism analogous to "spontaneous baryogenesis" in order to generate the BAU. This is possible only at the first step of a two-step phase transition which, so far, it is only present in the low mass regime. Accordingly, two different benchmarks were analysed in this regime and it was shown that, in principle, it is plausible to account for both DM and baryogenesis (a situation that was not possible in the vanilla IDM due to the lack of CP violation). In the high mass regime, nonetheless, a more careful treatment is needed. Together with the derivative operators, which ensure enough relics and a strong first-order PhT, one could con-

sider the operators of the form $|H_1|^2 q_L H_1 q_R$ and $|H_1|^2 W_{\mu\nu}\widetilde{W}^{\mu\nu}$ – which we expect to be more constrained by the EDMs – as the sources to generate the BAU. Alternatively, studying the impact of complex derivative operators could also be interesting for future works.

Needless to say, in this work we only had a glimpse of all the possibilities that are opened up when considering dimension six operators in the IDM, a longer and more detailed analysis will be required to get the full picture. Having the IDM as an effective model serving to explain DM and baryogenesis simultaneously is, certainly, an idea worth further investigations.

Part III

APPENDICES

A

FINITE TEMPERATURE EFFECTIVE POTENTIAL

In order to fully understand the EWPhT and all the interesting phenomena happening in the early Universe we must introduce concepts of thermal quantum field theory. In this context, a very important tool to study phase transitions is the effective potential at finite temperature. In particular, to understand the behaviour of the Higgs potential we usually choose the one-loop effective potential at finite temperature because it allows us to include next-to-leading order and finite temperature effects in the theory [81]. In general the effective potential can be written as [80]

$$V_{eff}(\phi_c, T) = V_{eff}(\phi_c) + \Delta V_1^{(T)}(\phi_c, T)', \tag{A.0.1}$$

where ϕ_c is the expectation value of the field, $V_{eff}(\phi_c)$ is the effective potential at zero temperature, and $\Delta V_1^{(T)}$ is a term containing the leading thermal corrections. In this this appendix we will discuss each of the terms appearing in Eq. (A.0.1) in detail.

A.1 ZERO TEMPERATURE EFFECTIVE POTENTIAL

A.1.1 *The Generating Functional*

In a QFT the effective action is defined as the Legendre transform of the generating functional for the connected Green functions $W[J]$. For simplicity we will consider here a theory for a scalar field, for which the effective action can be written as [102]

$$\Gamma[\bar{\phi}] = W[J] - \int d^4x \bar{\phi}(x) J(x) \,, \tag{A.1.1}$$

where $J(x)$ is the source and the corresponding field is defined in the following way

$$\bar{\phi} = \frac{\delta W[J]}{\delta J(x)} \, . \tag{A.1.2}$$

The effective action then satisfies the equation

$$J(x) = -\frac{\delta \Gamma[\bar{\phi}]}{\delta \bar{\phi}} \, , \tag{A.1.3}$$

meaning that the vacuum of the theory in the absence of any sources will be characterized by [91]

$$\frac{\delta \Gamma[\bar{\phi}]}{\delta \bar{\phi}} = 0 \, . \tag{A.1.4}$$

For a translationally invariant theory, the field $\bar{\phi}$ is a constant ϕ_c such that we can define the effective potential $V_{eff}(\phi_c)$ of the theory as

$$\Gamma[\phi_c] = -\int d^4x V_{eff}(\phi_c) \, . \tag{A.1.5}$$

In this way, the equation leading to the vacua of the theory reduces to [102]

$$\frac{\partial V_{eff}(\phi_c)}{\partial \phi_c} = 0 \, . \tag{A.1.6}$$

A.1.2 *The One-Loop Effective Potential*

Now, we would like to compute the effective potential appearing in Eq. (A.1.6) so we start at zero temperature. In this case, the effective potential will only have two contributions, *i.e.*

$$V_{eff}(\phi_c) = V_0(\phi_c) + V_1(\phi_c) \, , \tag{A.1.7}$$

where the zero-loop effective potential V_0 will simply be given by the classical tree-level potential, as in Eq. (3.1.1), and the one-loop correction will be the sum of all 1PI diagrams with a single loop and zero external momenta as shown, for instance,

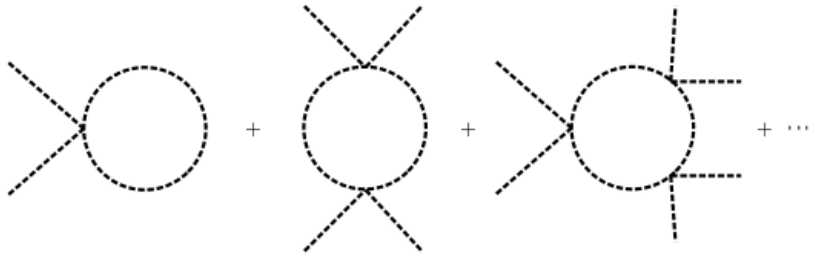

Figure A.1.1: 1PI diagrams contributing to the one-loop effective potential. Taken from Ref.[91].

in Fig. [A.1.1] for scalars. In the case of a massive gauge boson one can show that that V_1 will be given by [81, 91]

$$V_1(\phi_c) = \frac{3}{2} Tr \int \frac{d^4p}{(2\pi)^4} \log\left(p^2 + M^2(\phi_c)\right) \ , \tag{A.1.8}$$

with $M(\phi_c)$ the field-dependent mass. However, this one-loop contribution must be renormalized since it is UV-divergent. Using the $\overline{MS}$ renormalization scheme in Landau gauge, the one-loop potential takes the form of the Coleman-Weinberg potential defined as [17, 19]

$$V_{CW} = \sum_i \frac{n_i}{64\pi^2} \hat{m}_i{}^4(\phi_c) \left[\log\left(\frac{\hat{m}_i{}^2(\phi_c)}{Q^2}\right) - C_i\right] \ , \tag{A.1.9}$$

where n_i is the number of degrees of freedom (positive for bosons and negative for fermions), C_i are renormalization scheme dependent constants and Q is a renormalization scale. In the case of the SM where the Higgs doublet can be expanded as

$$\Phi = \frac{1}{\sqrt{2}} \begin{pmatrix} \sqrt{2}\phi^+ \\ v + h + i\phi \end{pmatrix} \ , \tag{A.1.10}$$

the sum in Eq. (A.1.9) runs over the top quark, the W and the Z bosons, the Higgs h and the Goldstones ϕ. In the same way Q is fixed to the Higgs VEV, *i.e.* $v \approx 246\,\text{GeV}$.

Furthermore, the field-dependent masses are given by

$$\begin{aligned} &\hat{m}_W^2 = \frac{1}{4} g^2 \phi_c^2 \ , \qquad \hat{m}_Z^2 = \frac{1}{4}(g^2 + g'^2)\phi_c^2, \qquad \hat{m}_t^2 = \frac{1}{2} y_t^2 \phi_c^2 \ , \\ &\hat{m}_h^2 = 2\lambda\phi_c^2, \qquad \hat{m}_{\phi,\phi^\pm}^2 = 0, \end{aligned} \tag{A.1.11}$$

PARTICLE	n_i	C_i
W boson	6	5/6
Z boson	3	5/6
Top quark	-12	3/2
Higgs boson	1	3/2
Goldstone bosons	3	3/2

Table A.1.1: Number of degrees of freedom and parameters C_i appearing in the Coleman-Weinberg potential for the SM. The values can be found in Ref.[91].

where y_t is top Yukawa coupling. The masses then approach the predicted values at $T = 0$ where $\phi_c = v$. In table [A.1.1] we summarize the numbers appearing int the Coleman-Weinberg potential for the SM.

A.1.3 *The Counter-Term Potential*

To be more precise V_{CW}, as in Eq. (A.1.9), is already finite. The counter-term potential is added in order to compensate for shifts on the vacuum due to the one-loop corrections.

The counter term potential V_{CT} must be added now in order to absorb the divergences and make the theory finite. This will also ensure that the relationships between masses and vacuum expectations values remain the same as in the tree-level case. In general counterterms must be found by solving the appropriate set of renormalization conditions. For example, in the SM it is enough to impose that [81]

$$\begin{aligned} \frac{\partial(V_{CW}+V_{CT})}{\partial\phi_c}\Big|_{\phi_c=v} &= 0 \\ \frac{\partial^2(V_{CW}+V_{CT})}{\partial\phi_c^2}\Big|_{\phi_c=v} &= 0\,. \end{aligned} \tag{A.1.12}$$

In this way all divergences in the SM potential can be absorbed with only two counterterms [91]

$$V_{CT} = \frac{\delta m^2}{2}\phi_c^2 + \frac{\delta\lambda}{4}\phi_c^4\,. \tag{A.1.13}$$

The amount of counterterms needed will depend on the theory under consideration.

Gathering all the contributions we finally can write the zero-temperature effective potential as

$$V_{eff}(\phi_c) = V_0 + V_{CW} + V_{CT} \,. \tag{A.1.14}$$

A.2 FINITE TEMPERATURE EFFECTIVE POTENTIAL

We now aim to introduce thermal effects in our theory. Following the discussion in [19, 25, 80, 91] the leading order temperature-dependent contributions to the effective potential will be given by

$$V_T = \frac{T^4}{2\pi^2}\left[\sum_{i=boson} n_i J_B\left(\frac{\hat{m}_i^2(\phi_c)}{T^2}\right) + \sum_{j=fermion} n_j J_F\left(\frac{\hat{m}_j^2(\phi_c)}{T^2}\right)\right], \tag{A.2.1}$$

with the field-dependent masses $\hat{m}(\phi_c)$ and the thermal bosonic and fermionic functions defined as

$$\begin{aligned} J_B(x) &= \int_0^\infty dt\, t^2 \log\left[1 - e^{-\sqrt{t^2+x^2}}\right] \\ J_F(x) &= \int_0^\infty dt\, t^2 \log\left[1 + e^{-\sqrt{t^2+x^2}}\right] \,. \end{aligned} \tag{A.2.2}$$

These thermal integrals can be expanded in the high temperature limit, *i.e.* $|x| << 1$ as

$$\begin{aligned} J_B(x) &= -\frac{\pi^4}{45} + \frac{\pi^2}{12}x - \frac{\pi}{6}x^{3/2} - \frac{1}{32}x^2 \log\left(\frac{x}{a_b}\right) \\ &\quad - 2\pi^{7/2}\sum_{l=1}^{\infty}(-1)^l \frac{\zeta(2l+1)}{(l+1)!}\Gamma\left(l+\frac{1}{2}\right)\left(\frac{x}{4\pi^2}\right)^{l+2} \\ J_F(x) &= \frac{7\pi^4}{360} - \frac{\pi^2}{24}x - \frac{1}{32}x^2 \log\left(\frac{x}{a_f}\right) \\ &\quad - \frac{\pi^{7/2}}{4}\sum_{l=1}^{\infty}(-1)^l \frac{\zeta(2l+1)}{(l+1)!}\left(1 - 2^{-2l-1}\right)\Gamma\left(l+\frac{1}{2}\right)\left(\frac{x}{\pi^2}\right)^{l+2} , \end{aligned} \tag{A.2.3}$$

where $a_b = 16\pi^2 e^{(3/2-2\gamma_E)}$ and $a_f = \pi^2 e^{(3/2-2\gamma_E)}$, with the Euler-Mascheroni constant γ_E, the Riemann ζ-function and the

Γ-function. On the other hand, in the low temperature regime, both functions reduce to [17]

$$J_{B,F}(x) = -\left(\frac{\pi}{2}\right)^{1/2} x^{3/4} e^{-x^{1/2}} \left(1 + \frac{15}{8} x^{-1/2}\right) , \qquad \text{(A.2.4)}$$

explicitly showing the typical Boltzmann suppression for particles much heavier than the temperature.

A.2.1 *Daisy Resummation*

Note that symmetry restoration takes place because it might happen that, at sufficiently high T, the minimum of the effective potential at finite temperature occurs at $\langle \phi(T) \rangle = 0$. EW symmetry is, therefore, restored for high temperatures.

Now we must turn into an issue we have not discussed before, *i.e.* that symmetry restoration signals the breakdown of perturbation theory at high temperatures [17]. This happens because higher order diagrams become important and their effects must be taken into account by resummation [7, 85]. One can show that, to a fixed order in the loop expansion, the largest contributions come from the diagrams with the maximum number of quadratically divergent loops like in Fig[A.2.1], *i.e.* the so-called Daisy diagrams [91].

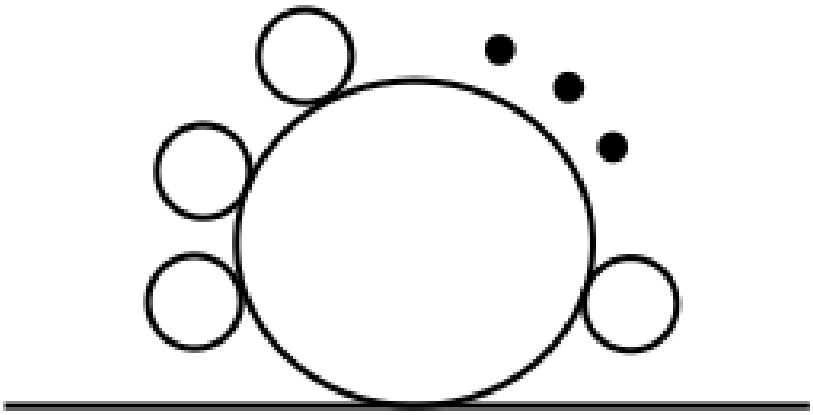

Figure A.2.1: Daisy $(n+1)$-loop contribution to the self energy for a scalar theory. Taken from Ref.[91].

The resummation of these diagrams is performed, then, by adding temperature corrections to the boson masses [19]. This can be done following two different approaches. The first ap-

proach, proposed by Arnold and Espinosa [7], consists of adding the following net contribution to the thermal effective potential [41]

$$V^{daisy} = -\frac{T}{12\pi}\sum_b n_b \left(\left[\overline{m}_b^2(\phi_c, T)\right]^{3/2} - \left[\hat{m}_b^2(\phi_c)\right]^{3/2} \right) , \quad \text{(A.2.5)}$$

where, in the SM, the sum runs only over the longitudinal degrees of freedom of gauge bosons for which we have

$$\frac{1}{2} n_{WL} = n_{ZL} = n_{\gamma L} = 1. \quad \text{(A.2.6)}$$

The second approach, on the other hand, was proposed by Parwani [85] and consists of replacing the field-dependent masses by the corresponding thermal masses directly in V_T. In the SM, the thermal Debye masses are given by

$$\begin{aligned} \overline{m}_{WL}^2 &= \hat{m}_W^2(\phi_c) + \frac{11}{6} g^2 T^2 \\ \overline{m}_{ZL}^2 &= \frac{1}{2}\left(\hat{m}_Z^2(\phi_c) + \frac{11}{6}\frac{g^2}{\cos^2\theta_W} T^2 + \Delta(\phi_c, T) \right) \\ \overline{m}_{\gamma L}^2 &= \frac{1}{2}\left(\hat{m}_Z^2(\phi_c) - \frac{11}{6}\frac{g^2}{\cos^2\theta_W} T^2 + \Delta(\phi_c, T) \right) , \end{aligned} \quad \text{(A.2.7)}$$

with

$$\Delta^2(\phi_c, T) = \hat{m}_Z^4(\phi_c) + \frac{11}{3}\frac{\cos^2 2\theta_W}{\cos^2\theta_W}\left[\hat{m}_Z^2(\phi_c) + \frac{11}{2}\frac{g^2}{\cos^2\theta_W} T^2 \right] T^2 . \quad \text{(A.2.8)}$$

Finally, putting all the ingredients together, we can write the one-loop effective potential at finite temperature as

$$V_{eff}(\phi_c, T) = V_0 + V_{CW} + V_{CT} + V_T + V^{daisy} . \quad \text{(A.2.9)}$$

B

DISCRETE SYMMETRIES

Symmetries are a central topic in all branches of physics. Just imposing symmetries in a theory leads to profound and immediate consequences that even allow us to predict the existence of new particles, new processes and explain why certain things can never happen in nature. In this appendix we briefly describe two of the most important discrete symmetries in the SM, *i.e.* charge conjugation and parity. For a detailed treatment see *e.g.* Ref.[21].

B.1 CHARGE CONJUGATION

Charge conjugation (C) is a transformation that essentially changes a particle by its antiparticle [94]. More specifically it changes all the "internal" quantum numbers - charge, baryon and lepton numbers, strangeness and so on - while leaving the mass, energy, momentum and spin untouched [51]. C-symmetry, thus, asserts that particles and antiparticles behave in the same way and that it is just a convention which of them we call particles and which we call antiparticles. Particularly, under charge conjugation Dirac fields change as [98]

$$\begin{aligned} C &: \Psi \to -i\gamma_2 \Psi^* \\ C &: \Psi^* \to -i\gamma_2 \Psi \ , \end{aligned} \tag{B.1.1}$$

where γ_2 is the second gamma or Dirac matrix given by

$$\gamma^2 = \begin{pmatrix} 0 & 0 & 0 & -i \\ 0 & 0 & i & 0 \\ 0 & i & 0 & 0 \\ -i & 0 & 0 & 0 \end{pmatrix} = -\gamma_2 \ . \tag{B.1.2}$$

In the same way, C acts on complex scalars fields and on vector fields in the following way

$$C : \phi \to \phi^* \qquad C : A_\mu \to -A_\mu \ . \tag{B.1.3}$$

BILINEAR	P	C	CP
$\overline{\Psi}\chi$	$\overline{\Psi}\chi$	$\overline{\chi}\Psi$	$\overline{\chi}\Psi$
$\overline{\Psi}\gamma^5\chi$	$-\overline{\Psi}\gamma^5\chi$	$\overline{\chi}\gamma^5\Psi$	$-\overline{\chi}\gamma^5\Psi$
$\overline{\Psi}\gamma^\mu\chi$	$\overline{\Psi}\gamma_\mu\chi$	$-\overline{\chi}\gamma^\mu\Psi$	$-\overline{\chi}\gamma_\mu\Psi$
$\overline{\Psi}\gamma^\mu\gamma^5\chi$	$-\overline{\Psi}\gamma_\mu\gamma^5\chi$	$\overline{\chi}\gamma^\mu\gamma^5\Psi$	$-\overline{\chi}\gamma_\mu\gamma^5\Psi$

Table B.1.1: Action of some discrete symmetries on fermion bilinears. Both Ψ and χ are Dirac fields.

The transformation properties of fermions bilinears are summarized in table [B.1.1].

B.2 PARITY

A parity transformation is a discrete transformation consisting on the flip of the sign of all three spatial coordinates, *i.e.* we reverse the momentum of a particle leaving its spin unchanged [94]. This means we change the handedness of the system of axes in two steps: first we perform a mirror reflection on a coordinate plane and, second, we do a rotation by an angle π around the axis perpendicular to that plane (see Fig. [B.2.1]) [21]. Since we assume physics is isotropic (invariant under rotations) the questions about P parity is concerned on whether physics is invariant under a mirror reflection or not. In general, complex scalar fields, Dirac fields and vector fields transform under parity as [98]

$$\begin{aligned} &P : \phi(t,\vec{x}) \to \eta\phi(t,-\vec{x}) \\ &P : \Psi(t,\vec{x}) \to \eta\gamma_0\Psi(t,-\vec{x}) \\ &P : A_\mu(t,\vec{x}) \to A_\mu(t,-\vec{x}) \ , \end{aligned} \tag{B.2.1}$$

where η is a pure phase.

B.3 CP TRANSFORMATION

Finally, a CP transformation consists of simultaneously performing a parity transformation together with charge conjugation. CP violation is a fascinating concept in physics as it is required by the Sakharov conditions in order to generate the

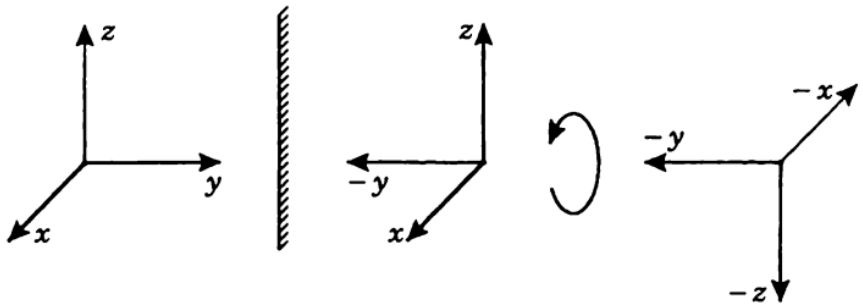

Figure B.2.1: A parity transformation consists of a mirror reflection followed by a rotation. Taken from Ref.[21].

observed baryon asymmetry. It also implies the possibility for elementary particles to have electric dipole moments. Yet, CP violation remains as one of the most elusive subjects in particle physics partly because our knowledge about it is rather limited.

C

CONTRIBUTIONS TO THE DM ANNIHILATION CROSS SECTIONS

In this appendix we deal with the contributions of the non-SM terms to the annihilation cross sections of two DM particles in the models discussed in chapters [6, 7, 8, 9]. To that end we expand the doublets as

$$H_1 = \frac{1}{\sqrt{2}}\begin{pmatrix} \sqrt{2}\phi^+ \\ v + h + i\phi \end{pmatrix} \qquad H_2 = \frac{1}{\sqrt{2}}\begin{pmatrix} \sqrt{2}H^+ \\ H + iA \end{pmatrix} , \tag{C.0.1}$$

with the SM VEV $v \approx 246$ GeV. Furthermore, we consider only those processes involving up to four particles and at least two DM particles.

C.1 OPERATORS IN THE SCALAR POTENTIAL

Starting with the vanilla IDM we find that the terms of the potential have the following contributions (for the moment we leave aside coannihilation processes)

$$\lambda_3 |H_1|^2 |H_2|^2 \supset \frac{H^2}{4}\lambda_3 \left[2\phi^+\phi^- + \phi^2 + (v+h)^2\right] , \tag{C.1.1}$$

$$\lambda_4 |H_1^\dagger H_2|^2 \supset \frac{H^2}{4}\lambda_4 \left[\phi^2 + (v+h)^2\right] , \tag{C.1.2}$$

$$\frac{\lambda_5}{2}\left[\left(H_1^\dagger H_2\right)^2 + \text{h.c.}\right] \supset \frac{\lambda_5 H^2}{4}\left((v+h)^2 - \phi^2\right) . \tag{C.1.3}$$

Now, since we have mixing in the extended IDM (see chapter [7]), we have a different expression for the λ_5 term as well as an additional expression for the extra dim-6 operator λ_6 containing angle-dependent interactions; these are given by

$$\frac{\lambda_5}{2}\left[\left(H_1^\dagger H_2\right)^2 + \text{h.c.}\right] \supset \frac{\lambda_5 H'^{\,2}}{4}\Big(\left[(v+h)^2 - \phi^2\right]\cos 2\eta \\ -2(v+h)\phi \sin 2\eta\Big) \tag{C.1.4}$$

and

$$\frac{\lambda_6}{2}|H_1|^2\left[e^{i\bar{\theta}_{65}}\left(H_1^\dagger H_2\right)^2+\text{h.c.}\right]\supset\frac{\lambda_6 H'^2}{8}\left(2\phi^+\phi^-+(v+h)^2+\phi^2\right)\cdot\left[\left((v+h)^2-\phi^2\right)\cos\left(2\eta-\bar{\theta}_{65}\right)-2\,(v+h)\,\phi\sin\left(2\eta-\bar{\theta}_{65}\right)\right]\,, \tag{C.1.5}$$

where, in this case, H' is the corresponding mass eigenstate and η is the corresponding mixing angle.

Then, from Eqs.(C.1.1)-(C.1.5), the vertex factors for particular interaction channels (coming only from the scalar potential) can be extracted. For instance, the vertex factors containing Goldstone bosons in the final state read

$$\begin{aligned} H'H'\phi^+\phi^- &: -\left(\lambda_3+\frac{\lambda_6}{2}v^2\cos(2\eta-\bar{\theta}_{65})\right)\,, \\ H'H'\phi\phi &: -(\lambda_{34}-\lambda_5\cos 2\eta)\,. \end{aligned} \tag{C.1.6}$$

and those with at least one SM Higgs boson in the final state are

$$\begin{aligned} H'H'hh &: -\left[\lambda_{34}+\lambda_5\cos 2\eta+3\lambda_6 v^2\cos(2\eta-\bar{\theta}_{65})\right]\,, \\ H'H'h &: -v\left[\lambda_{34}+\lambda_5\cos 2\eta+\lambda_6 v^2\cos\left(2\eta-\bar{\theta}_{65}\right)\right]\,, \\ H'H'\phi h &: \lambda_5\sin 2\eta+\frac{3}{2}\lambda_6 v^2\sin\left(2\eta-\bar{\theta}_{65}\right)\,. \end{aligned} \tag{C.1.7}$$

To recover the corresponding vertex factors for the IDM and other models without mixing, we just need to set $\eta\to 0$ and $H'\to H$.

C.2 DERIVATIVE OPERATORS

We now turn to the operators that are not part of the scalar potential. We start with the c-like operators used in the high-mass regime. The covariant derivative is defined as

$$D_\mu=\begin{pmatrix}\partial_\mu-\frac{i}{2}\left(gW_\mu^3+g'B_\mu\right) & -\frac{i}{\sqrt{2}}gW_\mu^+ \\ -\frac{i}{\sqrt{2}}gW_\mu^- & \partial_\mu-\frac{i}{2}\left(-gW_\mu^3+g'B_\mu\right)\end{pmatrix}\,, \tag{C.2.1}$$

with the fields

$$\begin{pmatrix} B_\mu \\ W_\mu^3 \end{pmatrix} = \begin{pmatrix} \cos\theta_W & -\sin\theta_W \\ \sin\theta_W & \cos\theta_W \end{pmatrix} \begin{pmatrix} A_\mu \\ Z_\mu \end{pmatrix} . \tag{C.2.2}$$

In the model without mixing the derivative operators are expanded to

$$\begin{aligned} c_1 \left|H_1\right|^2 \left|D_\mu H_2\right|^2 \supset & \frac{g^2 v^2}{16\cos^2\theta_W} H^2 Z_\mu Z^\mu + \frac{g^2 v^2}{8} H^2 W_\mu^- W^{+\mu} \\ & + \frac{1}{4}\partial_\mu H \partial^\mu H \left[(h+v)^2 + \phi^2 + 2\phi^-\phi^+\right] , \end{aligned} \tag{C.2.3}$$

where the contributions to the channels with longitudinal gauge bosons in the final state are apparent. In the same way

$$\begin{aligned} c_2 \left|H_2\right|^2 \left|D_\mu H_1\right|^2 \supset & \frac{H^2\left(1+2\cos 2\theta_W\right)}{16\cos^2\theta_W}\left(\partial_\mu h \partial^\mu h + \partial_\mu \phi \partial^\mu \phi\right) \\ & + \frac{H^2}{4\cos^2\theta_W}\partial_\mu\phi^+\partial^\mu\phi^- + \frac{H^2}{16\cos^2\theta_W}\left|gvW_\mu^- - 2i\partial_\mu\phi^-\right|^2 \\ & + \frac{gvH^2}{8\cos^2\theta_W}\left(iW_\mu^-\partial^\mu\phi^+ + \text{c.c.}\right) + \frac{g^2v^2H^2}{16\cos^2\theta_W}\left(W_\mu^- W^{+\mu} + Z_\mu Z^\mu\right) \\ & + \frac{gvH^2}{4\cos\theta_W} Z_\mu \partial^\mu \phi , \end{aligned} \tag{C.2.4}$$

where we have used $g' \to g\tan\theta_W$. The third operator reads

$$\begin{aligned} c_3 \left[H_1^\dagger H_2 \left(D_\mu H_1\right)^\dagger D^\mu H_2 + \text{h.c.}\right] \supset & \frac{g^2v^2}{4} H^2 W_\mu^- W^{+\mu} \\ & + \frac{gvH}{8}\left(W_\mu^-\left(2H\partial^\mu\phi^+ - \sqrt{2}\phi^+\partial^\mu H\right) + \text{c.c.}\right) \\ & + \frac{H\partial_\mu H}{4}\left(\left(\partial^\mu h + i\partial^\mu\phi\right)\left(v + h + i\phi\right) + \text{c.c.}\right) \\ & + \frac{gvZ_\mu H}{4\cos\theta_W}\left(H\partial^\mu\phi - 2\phi\partial^\mu H\right) \\ & + \frac{g^2v^2}{8\cos^2\theta_W} H^2 Z_\mu Z^\mu . \end{aligned} \tag{C.2.5}$$

Finally, the last derivative operator is

$$c_4\left[H_1^\dagger H_2\left(D_\mu H_2\right)^\dagger D^\mu H_1+\text{h.c.}\right]\supset\frac{g^2v^2}{4}H^2W_\mu^-W^{+\mu}+\frac{H\partial^\mu H}{2}\left(\left(v+h\right)\partial_\mu h+\phi\partial_\mu\phi\right)+\frac{gvH}{4}\left(2iHW_\mu^-\partial^\mu\phi^++\text{c.c.}\right)+\frac{\sqrt{2}gvH\partial^\mu H}{8}\left(iW_\mu^+\phi^-+\text{c.c.}\right)+\frac{gvH^2Z^\mu}{\cos\theta_W}\left(2\partial_\mu\phi+\frac{gvZ_\mu}{\cos\theta_W}\right)\,. \tag{C.2.6}$$

In the case there is mixing in the potential as in the extended IDM, the expressions for the operators c_1, c_2 and c_4 remain equal (with the corresponding replacement $H\to H'$), while the presence of the mixing angle modifies the expression for c_3 including a new $H'H'\to hZ$ interaction, reading

$$\begin{aligned}c_3\left[H_1^\dagger H_2\left(D_\mu H_1\right)^\dagger D^\mu H_2+\text{h.c.}\right]\supset{}&\frac{g^2v^2\cos\left(2\eta+\theta_5\right)}{4}H'^2W_\mu^-W^{+\mu}\\&+\frac{gvH'}{8}\left(W_\mu^-\left(2H'\partial^\mu\phi^+-\sqrt{2}\phi^+\partial^\mu H'\right)e^{i(2\eta+\theta_5)}+\text{c.c.}\right)\\&+\frac{H'\partial_\mu H'}{4}\left(\left(\partial^\mu h+i\partial^\mu\phi\right)\left(v+h+i\phi\right)e^{i(2\eta+\theta_5)}+\text{c.c.}\right)\\&+\frac{gvZ_\mu H'}{4\cos\theta_W}\left(H'\partial^\mu\phi-2\phi\partial^\mu H'\right)\cos\left(2\eta+\theta_5\right)\\&+\frac{gvZ_\mu H'}{4\cos\theta_W}\left(H'\partial^\mu h-\left(v+2h\right)\partial^\mu H'\right)\sin\left(2\eta+\theta_5\right)\\&+\frac{g^2v^2\cos\left(2\eta+\theta_5\right)}{8\cos^2\theta_W}H'^2Z_\mu Z^\mu\,.\end{aligned} \tag{C.2.7}$$

C.3 THE YUKAWA-LIKE OPERATOR

The contribution of the Yukawa-like operator is straightforward. It is given as

$$\mathcal{L}_Y^{CPV}=-|\tilde{y}|e^{i\tilde{\theta}}\left(H_1^\dagger H_2\right)\left(\bar{Q}H_2d_R+\bar{Q}\tilde{H}_2u_R\right)+h.c.\,, \tag{C.3.1}$$

where Q, u_R and d_R are defined in Eq. (3.0.1) and

$$\tilde{H}_2=i\sigma_2H_2^*=\frac{1}{\sqrt{2}}\begin{pmatrix}H-iA\\-\sqrt{2}H^-\end{pmatrix}\,. \tag{C.3.2}$$

After expanding, and taking into account only one family of quarks to make it simpler, one obtains

$$-|\tilde{y}|e^{i\tilde{\theta}}\left(H_1^\dagger H_2\right)\left(\bar{Q}H_2 d_R + \bar{Q}\tilde{H}_2 u_R\right) + h.c. \supset \frac{-|\tilde{y}|e^{i\tilde{\theta}}v}{2\sqrt{2}}H^2\left(\bar{d}_L d_R + \bar{u}_L u_R\right) + c.c. \tag{C.3.3}$$

C.4 CP VIOLATION IN THE GAUGE SECTOR

The computation of the interesting terms for the CP violating operator in the gauge sector is a bit more involved. The operator is defined as

$$\tilde{c}|H_2|^2 F_{\mu\nu}\tilde{F}^{\mu\nu} \tag{C.4.1}$$

where $F_{\mu\nu}\tilde{F}^{\mu\nu} = W^a_{\mu\nu}\tilde{W}^{a,\mu\nu} + B_{\mu\nu}\tilde{B}^{\mu\nu}$, and the corresponding field strength tensors are

$$W^a_{\mu\nu} = \partial_\mu W^a_\nu - \partial_\nu W^a_\mu + g\varepsilon^{abc}W^b_\mu W^c_\nu, \tag{C.4.2}$$

$$B_{\mu\nu} = \partial_\mu B_\nu - \partial_\nu B_\mu \ . \tag{C.4.3}$$

with ε^{ijk} the Levi-Civita tensor. In the same way the dual field strength tensors read

$$W^a_{\mu\nu}\widetilde{W}^{a,\mu\nu} = \frac{1}{2}W^a_{\mu\nu}\varepsilon^{\mu\nu\rho\sigma}W^a_{\rho\sigma} \ . \tag{C.4.4}$$

Putting everything together, and exploiting the symmetries of the Levi-Civita tensor, one finally finds

$$\begin{aligned}\tilde{c}|H_2|^2 F^a_{\mu\nu}\tilde{F}^{\mu\nu,a} \supset \tilde{c}H^2\,[\ &\varepsilon^{\mu\nu\rho\sigma}\left(\partial_\mu A_\nu \partial_\rho A_\sigma + \partial_\mu Z_\nu \partial_\rho Z_\sigma\right) \\ &+2ig\varepsilon^{\mu\nu\rho\sigma}\left(\sin\theta_W A_\rho + \cos\theta_W Z_\rho\right)\left(W^-_\sigma \partial_\mu W^+_\nu - W^+_\sigma \partial_\mu W^-_\nu\right) \\ +2g^2\varepsilon^{\mu\nu\rho\sigma}&\left(\sin\theta_W A_\mu + \cos\theta_W Z_\mu\right)W^-_\nu\left(\sin\theta_W A_\rho + \cos\theta_W Z_\rho\right)W^+_\sigma \\ &+2\varepsilon^{\mu\nu\rho\sigma}\partial_\rho W^-_\sigma \partial_\mu W^+_\nu - g^2\varepsilon^{\mu\nu\rho\sigma}W^+_\mu W^-_\nu W^+_\rho W^-_\sigma \\ &-2ig\varepsilon^{\mu\nu\rho\sigma}W^+_\rho W^-_\sigma \partial_\mu\left(\sin\theta_W A_\nu + \cos\theta_W Z_\nu\right)\ ] \ .\end{aligned} \tag{C.4.5}$$

D

THE JARLSKOG INVARIANT FOR THE EXTENDED IDM

In this appendix we try to find a CP-odd invariant (invariant under a basis transformation) that effectively measures the amount of CP violation in the scalar extension of the IDM from Chapter [7]. This is analogous to the Jarlskog invariant in the SM characterized by the mixing in the quark sector [61]. We closely follow the steps in Ref. [67].

To that end, when expanding the potential in Eq. (7.0.1) using the doublets defined in Eq. (6.0.1), we find a term in the form

$$\begin{aligned}
&\frac{1}{2}\hat{\lambda}_5\left(H_1^\dagger H_2\right)^2 + \frac{1}{2}\hat{\lambda}_6\left|H_1\right|^2\left(H_1^\dagger H_2\right)^2 + \text{h.c.} \\
&\supset \left(\frac{vh}{2}\left(\lambda_5 + \lambda_6 v^2\cos\bar{\theta}_{65}\right) - \frac{\lambda_5}{4}\phi^2\right)\left(H^2 - A^2\right) \\
&\quad - \lambda_6 v^3 \sin\bar{\theta}_{65} HAh\,. \qquad \text{(D.0.1)}
\end{aligned}$$

These correspond to terms in the form $c_{ij}\xi_i\xi_j S$, where ξ_i is either $H = \xi_1$ or $A = \xi_2$ and S is a CP-even monomial (h, $\phi\phi$, H^+H^-, $\phi^+\phi^-$). Specifically, we define

$$\begin{aligned}
c_{11} &= -c_{22} = \frac{v}{2}\left(\lambda_5 + \lambda_6 v^2\cos\bar{\theta}_{65}\right) \\
c_{12} &= c_{21} = -\lambda_6 v^3 \sin\bar{\theta}_{65} \\
c'_{11} &= -c'_{22} = \frac{\lambda_5}{4} \\
c'_{12} &= c'_{21} = 0\,, \qquad \text{(D.0.2)}
\end{aligned}$$

where we have used the primes to distinguish between the coefficients involving h and the coefficients involving ϕ^2. One can then construct the CP-odd invariant, using the Levi-Civita symbol contracted with c and c', which reads

$$J = c'_{ki}c_{ij}\varepsilon_{jk} = -\frac{v^3}{2}\lambda_5\lambda_6\sin\bar{\theta}_{65}\,. \qquad \text{(D.0.3)}$$

Similarly to the SM, all CP-violating quantities will be proportional to the invariant J. According to Ref. [28], the baryon-to-photon ratio η is, in the absence of BSM physics, given by

$$\eta \overset{\text{def}}{=} \frac{n_B}{s} \overset{\text{SM}}{\sim} \frac{\alpha_w^4 T^3}{s} \delta_{CP} \sim 10^{-8} \delta_{CP} \,, \tag{D.0.4}$$

where $n_B = n_b - n_{\bar{b}}$ is the difference between the number density of baryons and antibaryons, s is the entropy density of the Universe, and δ_{CP} is a dimensionless suppression factor due to CP violation.

Thus, assuming there is a direct mechanism that allows us to transmit the CP violation from the scalar potential to the quark sector and, since all CP-violation in the model must be proportional to J, one can estimate δ_{CP} via dimensional analysis in Eq. (D.0.4). Since J has mass dimension 1, the dimensionless number can be estimated by

$$\delta_{CP} = \frac{J}{T_c} \sim 10^{-2} J \,\text{GeV}^{-1} \,, \tag{D.0.5}$$

where $T_c \approx 100$ GeV is the temperature of the electroweak phase transition. Since the observed baryon asymmetry is of the order of $\eta \sim 10^{-10}$, we find the requirement $J \sim \mathcal{O}\left(10^{-8}\text{GeV}\right)$ for the CP-odd invariant found above. Using the definitions in Eq. (7.0.13), we find a constraint in the mixing angle, reading

$$J = -\frac{\left(\Delta m^2\right)^2 \sin 4\eta \left(1 - \tan 2\eta \cot \bar{\theta}_{65}\right)}{2v^3} \overset{!}{\sim} \mathcal{O}\left(10^{-8}\text{GeV}\right) \,, \tag{D.0.6}$$

which is easily attained for the relevant parameters allowing for the correct DM relics. This finding in Eq. (D.0.6) signals absent CP violation for zero mixing between the two non-SM neutral scalars, *i.e.*, $\eta = 0$.

E

VACUUM STABILITY

This appendix is dedicated to the derivation of the vacuum stability constraints from the vanilla IDM and the corresponding extensions studied after. In general the vacuum stability constraints appear when we require the potential of a particular model to be bounded from below. Checking the boundedness of a particular potential can be a complicated task, specially when we have many parameters to take into account. However, the procedure is essentially the same in each case; one needs to make sure the potential is always positive for any possible field configurations. As an example, let us start with the potential from the IDM given in Eq. (6.0.3) and rewritten in terms of the neutral scalars h and H

Note that one must require the potential to be bounded from below in every field direction. Nonetheless, for simplicity, in this appendix we only consider the h and H directions.

$$V(h,H) = \frac{\mu_1^2}{2}h^2 + \frac{\mu_2^2}{a}H^2 + \frac{\lambda_1}{4}h^4 + \frac{\lambda_{345}}{4}H^2h^2 + \frac{\lambda_2}{4}H^4. \tag{E.0.1}$$

Guaranteeing the potential being bounded from below, only the terms with highest power in the respective fields h, H are relevant such that we can neglect the terms proportional to μ_1^2 and μ_2^2 from now on. Following the discussion in [6] the potential in Eq. (E.0.1) can be recast as

$$V(\chi) = a + b\chi + c\chi^2, \tag{E.0.2}$$

where $\chi = h^4/H^4$. Now, finding conditions for the stability of the potential requires finding conditions on a, b and c such that $V(\chi) > 0$ for every value of $\chi \in [0,\infty)$. These read

$$\begin{aligned} a &> 0, \\ c &> 0, \\ b + 2\sqrt{ac} &> 0. \end{aligned} \tag{E.0.3}$$

In the case of the potential given in Eq. (E.0.1) the conditions in Eq. (E.0.3) translate into the known vacuum stability constraints for the IDM

$$\lambda_1 > 0, \quad \lambda_2 > 0, \quad \lambda_{345} > -2\sqrt{\lambda_1\lambda_2}. \tag{E.0.4}$$

The requirement of having $V(\chi) > 0$ for the potential to be bounded from below may appear, at first sight, arbitrary. Nonetheless, this is easy to understand by keeping in mind that, when considering large values of the fields (either in the positive or the negative direction), we must ensure that the potential does not tend to $-\infty$ justifying, therefore, the $V > 0$ condition.

We can derive this results in another way. For example, by completing the square in Eq. (E.0.1) the potential can be written as

$$V(h,H) \supset \left(\frac{\sqrt{\lambda_1}}{2}h^2 + \frac{\sqrt{\lambda_2}}{2}H^2\right)^2 + \left(\frac{\lambda_{345}}{4} - \frac{\sqrt{\lambda_1\lambda_2}}{2}\right)h^2H^2. \tag{E.0.5}$$

Since the first term in Eq. (E.0.5) is non-negative but vanishes for the particular field configuration $h^2 = -\sqrt{\frac{\lambda_2}{\lambda_1}}H^2$, one can immediately read off the stability constraints as

$$\frac{\lambda_{345}}{4} - \frac{\sqrt{\lambda_1\lambda_2}}{2} > 0, \tag{E.0.6}$$

in addition to the more trivial conditions

$$\frac{\lambda_1}{4} > 0, \quad \frac{\lambda_2}{4} > 0, \tag{E.0.7}$$

which again reduces to the constraints given in Eq. (E.0.4). A similar analysis can be done for other field directions.

Now, in the presence of the dim-6 operator given in Eq. (7.1.3) it is convenient to consider the potential written as

$$V \supset \frac{\lambda_1}{4}\left(h^2 + \frac{\lambda_{345}}{2\lambda_1}H^2\right)^2 + \frac{\lambda_2}{4}\left(1 - \frac{\lambda_{345}^2}{4\lambda_1\lambda_2}\right)H^4 + \frac{\lambda_7}{8}H^6. \tag{E.0.8}$$

At this point it is clear then that the second term in Eq. (E.0.8) is not relevant for vacuum stability anymore since the H^6 term dominates the course of the potential for large field values. Thus, the constraints for vacuum stability of the augmented IDM potential simply read

$$\lambda_1 > 0, \quad \lambda_7 > 0\,. \tag{E.0.9}$$

BIBLIOGRAPHY

[1] N. Aghanim, Y. Akrami, M. Ashdown, J. Aumont, C. Baccigalupi, M. Ballardini, A. J. Banday, R. B. Barreiro, N. Bartolo, and et al. "Planck 2018 results." In: *Astronomy Astrophysics* 641 (2020), A6. ISSN: 1432-0746. DOI: 10.1051/0004-6361/201833910. arXiv: 1807.06209v3 [hep-ph].

[2] V. Andreev et al. "Improved limit on the electric dipole moment of the electron." In: *Nature* 562.7727 (2018), pp. 355–360. DOI: 10.1038/s41586-018-0599-8.

[3] E. Aprile, J. Aalbers, F. Agostini, M. Alfonsi, F. D. Amaro, M. Anthony, B. Antunes, F. Arneodo, M. Balata, and et al. "The XENON1T dark matter experiment." In: *The European Physical Journal C* 77.12 (2017). ISSN: 1434-6052. DOI: 10.1140/epjc/s10052-017-5326-3. arXiv: 1708.07051v1 [hep-ph].

[4] E. Aprile et al. "Dark Matter Search Results from a One Ton-Year Exposure of XENON1T." In: *Physical Review Letters* 121.11 (2018). ISSN: 1079-7114. DOI: 10.1103/physrevlett.121.111302. arXiv: 1805.12562v2 [hep-ph].

[5] E. V. Arbuzova, A. D. Dolgov, and V. A. Novikov. "General properties and kinetics of spontaneous baryogenesis." In: *Phys. Rev. D* 94.12 (2016), p. 123501. DOI: 10.1103/PhysRevD.94.123501. arXiv: 1607.01247 [astro-ph.CO].

[6] A. Arhrib, R. Benbrik, M. Chabab, G. Moultaka, M. C. Peyranere, L. Rahili, and J. Ramadan. "The Higgs Potential in the Type II Seesaw Model." In: *Phys. Rev. D* 84 (2011), p. 095005. DOI: 10.1103/PhysRevD.84.095005. arXiv: 1105.1925 [hep-ph].

[7] Peter Brockway Arnold and Olivier Espinosa. "The Effective potential and first order phase transitions: Beyond leading-order." In: *Phys. Rev. D* 47 (1993). [Erratum: Phys.Rev.D 50, 6662 (1994)], p. 3546. DOI: 10.1103/PhysRevD.47.3546. arXiv: hep-ph/9212235.

[8] Peter Brockway Arnold and Larry D. McLerran. "Sphalerons, Small Fluctuations and Baryon Number Violation in Electroweak Theory." In: *Phys. Rev. D* 36 (1987), p. 581. DOI: 10.1103/PhysRevD.36.581.

[9] Duarte Azevedo, Pedro M. Ferreira, M. Margarete Muhlleitner, Shruti Patel, Rui Santos, and Jonas Wittbrodt. "CP in the dark." In: *JHEP* 11 (2018), p. 091. DOI: 10.1007/JHEP11(2018)091. arXiv: 1807.10322 [hep-ph].

[10] M. Baak, J. Cúth, J. Haller, A. Hoecker, R. Kogler, K. Mönig, M. Schott, and J. Stelzer. "The global electroweak fit at NNLO and prospects for the LHC and ILC." In: *Eur. Phys. J. C* 74 (2014), p. 3046. DOI: 10.1140/epjc/s10052-014-3046-5. arXiv: 1407.3792 [hep-ph].

[11] Csaba Balazs, Graham White, and Jason Yue. "Effective field theory, electric dipole moments and electroweak baryogenesis." In: *JHEP* 03 (2017), p. 030. DOI: 10.1007/JHEP03(2017)030. arXiv: 1612.01270 [hep-ph].

[12] Stephen M. Barr and A. Zee. "Electric Dipole Moment of the Electron and of the Neutron." In: *Phys. Rev. Lett.* 65 (1990). [Erratum: Phys.Rev.Lett. 65, 2920 (1990)], pp. 21–24. DOI: 10.1103/PhysRevLett.65.21.

[13] Steven D. Bass, Albert De Roeck, and Marumi Kado. "The Higgs boson – its implications and prospects for future discoveries." In: (Apr. 2021). DOI: 10.1038/s42254-021-00341-2. arXiv: 2104.06821 [hep-ph].

[14] Daniel Baumann. *Lectures notes on Cosmology*. Amsterdam.

[15] Alexander Belyaev, Giacomo Cacciapaglia, Igor P. Ivanov, Felipe Rojas-Abatte, and Marc Thomas. "Anatomy of the Inert Two Higgs Doublet Model in the light of the LHC and non-LHC Dark Matter Searches." In: *Phys. Rev. D* 97.3 (2018), p. 035011. DOI: 10.1103/PhysRevD.97.035011. arXiv: 1612.00511 [hep-ph].

[16] L. Bergström. "Dark matter evidence, particle physics candidates and detection methods." In: *Annalen der Physik* 524.9-10 (2012), 479–496. ISSN: 0003-3804. DOI: 10.1002/andp.201200116. arXiv: 1205.4882 [hep-ph].

[17] Jérémy Bernon, Ligong Bian, and Yun Jiang. "A new insight into the phase transition in the early Universe with two Higgs doublets." In: *JHEP* 05 (2018), p. 151. DOI: 10.1007/JHEP05(2018)151. arXiv: 1712.08430 [hep-ph].

[18] Gianfranco Bertone and Dan Hooper. "History of dark matter." In: *Reviews of Modern Physics* 90.4 (2018). ISSN: 1539-0756. DOI: 10.1103/revmodphys.90.045002. arXiv: 1605.04909v2 [hep-ph].

[19] Nikita Blinov, Stefano Profumo, and Tim Stefaniak. "The Electroweak Phase Transition in the Inert Doublet Model." In: *JCAP* 07 (2015), p. 028. DOI: 10.1088/1475-7516/2015/07/028. arXiv: 1504.05949 [hep-ph].

[20] Dietrich Bodeker and Wilfried Buchmuller. "Baryogenesis from the weak scale to the grand unification scale." In: *Rev. Mod. Phys.* 93.3 (2021), p. 035004. DOI: 10.1103/RevModPhys.93.035004. arXiv: 2009.07294 [hep-ph].

[21] Gustavo C. Branco, Luis Lavoura, and Joao P. Silva. *CP Violation*. Vol. 103. 1999.

[22] Sebastian Bruggisser, Thomas Konstandin, and Geraldine Servant. "CP-violation for Electroweak Baryogenesis from Dynamical CKM Matrix." In: *JCAP* 11 (2017), p. 034. DOI: 10.1088/1475-7516/2017/11/034. arXiv: 1706.08534 [hep-ph].

[23] C. P. Burgess. "Introduction to Effective Field Theory." In: *Ann. Rev. Nucl. Part. Sci.* 57 (2007), pp. 329–362. DOI: 10.1146/annurev.nucl.56.080805.140508. arXiv: hep-th/0701053.

[24] J. M. Butterworth. "The Standard Model: how far can it go and how can we tell?" In: *Philosophical Transactions of the Royal Society A: Mathematical, Physical and Engineering Sciences* 374.2075 (2016), p. 20150260. ISSN: 1471-2962. DOI: 10.1098/rsta.2015.0260. arXiv: 1601.02759 [hep-ph].

[25] M. E. Carrington. "Effective potential at finite temperature in the standard model." In: *Phys. Rev. D* 45 (8 1992), pp. 2933–2944. DOI: 10.1103/PhysRevD.45.2933. URL: https://link.aps.org/doi/10.1103/PhysRevD.45.2933.

[26] Sean M. Carroll. "The Cosmological Constant." In: *Living Reviews in Relativity* 4.1 (2001). ISSN: 1433-8351. DOI: 10.12942/lrr-2001-1. arXiv: astro-ph/0004075v2 [astro-ph].

[27] Sean M. Carroll. *Spacetime and Geometry*. Cambridge University Press, July 2004. ISBN: 978-0-8053-8732-2, 978-1-108-48839-6, 978-1-108-77555-7.

[28] Mu-Chun Chen. "TASI 2006 Lectures on Leptogenesis." In: *Theoretical Advanced Study Institute in Elementary Particle Physics: Exploring New Frontiers Using Colliders and Neutrinos*. Mar. 2007. arXiv: hep-ph/0703087.

[29] James M. Cline. "Baryogenesis." In: *Les Houches Summer School - Session 86: Particle Physics and Cosmology: The Fabric of Spacetime*. Sept. 2006. arXiv: hep-ph/0609145.

[30] James M. Cline, Michael Joyce, and Kimmo Kainulainen. "Supersymmetric electroweak baryogenesis." In: *JHEP* 07 (2000), p. 018. DOI: 10.1088/1126-6708/2000/07/018. arXiv: hep-ph/0006119.

[31] James M. Cline and Kimmo Kainulainen. "A New source for electroweak baryogenesis in the MSSM." In: *Phys. Rev. Lett.* 85 (2000), pp. 5519–5522. DOI: 10.1103/PhysRevLett.85.5519. arXiv: hep-ph/0002272.

[32] James M. Cline, Kimmo Kainulainen, and Michael Trott. "Electroweak Baryogenesis in Two Higgs Doublet Models and B meson anomalies." In: *JHEP* 11 (2011), p. 089. DOI: 10.1007/JHEP11(2011)089. arXiv: 1107.3559 [hep-ph].

[33] James M. Cline, Kimmo Kainulainen, and Axel P. Vischer. "Dynamics of two Higgs doublet CP violation and baryogenesis at the electroweak phase transition." In: *Phys. Rev. D* 54 (1996), pp. 2451–2472. DOI: 10.1103/PhysRevD.54.2451. arXiv: hep-ph/9506284.

[34] A.G. Cohen, D.B. Kaplan, and A.E. Nelson. "Spontaneous Baryogenesis at the Weak Phase Transition." In: *Physics Letters B* 263.1 (1991), pp. 86–92. DOI: 10.1016/0370-2693(91)91711-4.

[35] Andrew G. Cohen and David B. Kaplan. "SPONTANEOUS BARYOGENESIS." In: 308.4 (1988), pp. 913–928. DOI: 10.1016/0550-3213(88)90134-4.

[36] W. N. Cottingham and D. A. Greenwood. *An introduction to the standard model of particle physics*. Cambridge University Press, Apr. 2007. ISBN: 978-0-511-27136-6, 978-0-521-85249-4.

[37] Michael Dine. "Electroweak baryogenesis: An Overview (where are we now?)" In: *1st Yale-Texas Workshop on Baryon Number Violation at the Electroweak Scale*. June 1992. arXiv: hep-ph/9206220.

[38] Michael Dine, Patrick Huet, Robert Singleton, and Leonard Susskind. "Creating the baryon asymmetry at the electroweak phase transition." In: 257.3-4 (1991), pp. 351–356. DOI: 10.1016/0370-2693(91)91905-B.

[39] Ethan M. Dolle and Shufang Su. "The Inert Dark Matter." In: *Phys. Rev. D* 80 (2009), p. 055012. DOI: 10.1103/PhysRevD.80.055012. arXiv: 0906.1609 [hep-ph].

[40] F. Englert and R. Brout. "Broken Symmetry and the Mass of Gauge Vector Mesons." In: *Phys. Rev. Lett.* 13 (1964). Ed. by J. C. Taylor, pp. 321–323. DOI: 10.1103/PhysRevLett.13.321.

[41] J. R. Espinosa and M. Quiros. "Improved metastability bounds on the standard model Higgs mass." In: *Phys. Lett. B* 353 (1995), pp. 257–266. DOI: 10.1016/0370-2693(95)00572-3. arXiv: hep-ph/9504241.

[42] Sven Fabian, Florian Goertz, and Yun Jiang. "Dark matter and nature of electroweak phase transition with an inert doublet." In: *JCAP* 09 (2021), p. 011. DOI: 10.1088/1475-7516/2021/09/011. arXiv: 2012.12847 [hep-ph].

[43] Glennys R. Farrar and M. E. Shaposhnikov. "Baryon asymmetry of the universe in the minimal Standard Model." In: *Phys. Rev. Lett.* 70 (1993). [Erratum: Phys.Rev.Lett. 71, 210 (1993)], pp. 2833–2836. DOI: 10.1103/PhysRevLett.70.2833. arXiv: hep-ph/9305274.

[44] Katherine Freese. "Status of dark matter in the universe." In: *International Journal of Modern Physics D* 26.06 (2017), p. 1730012. ISSN: 1793-6594. DOI: 10.1142/s0218271817300129. arXiv: 1701.01840 [hep-ph].

[45] Lars Fromme and Stephan J. Huber. "Top transport in electroweak baryogenesis." In: *JHEP* 03 (2007), p. 049. DOI: 10.1088/1126-6708/2007/03/049. arXiv: hep-ph/0604159.

[46] Lars Fromme, Stephan J. Huber, and Michael Seniuch. "Baryogenesis in the two-Higgs doublet model." In: *JHEP* 11 (2006), p. 038. DOI: 10.1088/1126-6708/2006/11/038. arXiv: hep-ph/0605242.

[47] Kaori Fuyuto. "Electroweak Baryogenesis and Its Phenomenology." PhD thesis. Nagoya U., 2016. DOI: 10.1007/978-981-13-1008-9.

[48] H. Georgi. "Effective field theory." In: *Ann. Rev. Nucl. Part. Sci.* 43 (1993), pp. 209–252. DOI: 10.1146/annurev.ns.43.120193.001233.

[49] Grzegorz Gil, Piotr Chankowski, and Maria Krawczyk. "Inert Dark Matter and Strong Electroweak Phase Transition." In: *Phys. Lett. B* 717 (2012), pp. 396–402. DOI: 10.1016/j.physletb.2012.09.052. arXiv: 1207.0084 [hep-ph].

[50] I. F. Ginzburg, K. A. Kanishev, M. Krawczyk, and D. Sokolowska. "Evolution of Universe to the present inert phase." In: *Phys. Rev. D* 82 (2010), p. 123533. DOI: 10.1103/PhysRevD.82.123533. arXiv: 1009.4593 [hep-ph].

[51] David Griffiths. *Introduction to elementary particles*. 2008. ISBN: 978-3-527-40601-2.

[52] Ben Gripaios. *Lectures on Physics Beyond the Standard Model*. 2015. arXiv: 1503.02636 [hep-ph].

[53] B. Grzadkowski, O. M. Ogreid, P. Osland, A. Pukhov, and M. Purmohammadi. "Exploring the CP-Violating Inert-Doublet Model." In: *JHEP* 06 (2011), p. 003. DOI: 10.1007/JHEP06(2011)003. arXiv: 1012.4680 [hep-ph].

[54] J. L. Hewett. "The Standard model and why we believe it." In: *Theoretical Advanced Study Institute in Elementary Particle Physics (TASI 97): Supersymmetry, Supergravity and Supercolliders*. June 1997. arXiv: hep-ph/9810316.

[55] Peter W. Higgs. "Broken Symmetries and the Masses of Gauge Bosons." In: *Phys. Rev. Lett.* 13 (1964). Ed. by J. C. Taylor, pp. 508–509. DOI: 10.1103/PhysRevLett.13.508.

[56] Peter W. Higgs. "Broken symmetries, massless particles and gauge fields." In: *Phys. Lett.* 12 (1964), pp. 132–133. DOI: 10.1016/0031-9163(64)91136-9.

[57] Peter W. Higgs. "Spontaneous Symmetry Breakdown without Massless Bosons." In: *Phys. Rev.* 145 (4 1966), pp. 1156–1163. DOI: 10.1103/PhysRev.145.1156.

[58] Gerard 't Hooft. "Symmetry Breaking Through Bell-Jackiw Anomalies." In: *Phys. Rev. Lett.* 37 (1976). Ed. by Mikhail A. Shifman, pp. 8–11. DOI: 10.1103/PhysRevLett.37.8.

[59] S. J. Huber and M. G. Schmidt. "Electroweak baryogenesis: Concrete in a SUSY model with a gauge singlet." In: *Nucl. Phys. B* 606 (2001), pp. 183–230. DOI: 10.1016/S0550-3213(01)00250-4. arXiv: hep-ph/0003122.

[60] Agnieszka Ilnicka, Maria Krawczyk, and Tania Robens. "Inert Doublet Model in light of LHC Run I and astrophysical data." In: *Phys. Rev. D* 93.5 (2016), p. 055026. DOI: 10.1103/PhysRevD.93.055026. arXiv: 1508.01671 [hep-ph].

[61] C. Jarlskog. "Commutator of the Quark Mass Matrices in the Standard Electroweak Model and a Measure of Maximal CP Violation." In: *Phys. Rev. Lett.* 55 (1985), p. 1039. DOI: 10.1103/PhysRevLett.55.1039.

[62] David B. Kaplan. "Five lectures on effective field theory." In: Oct. 2005. arXiv: nucl-th/0510023.

[63] Jonathan Kley, Tobias Theil, Elena Venturini, and Andreas Weiler. "Electric dipole moments at one-loop in the dimension-6 SMEFT." In: (Sept. 2021). arXiv: 2109.15085 [hep-ph].

[64] Edward W. Kolb and Michael S. Turner. *The Early Universe*. Vol. 69. 1990. ISBN: 978-0-201-62674-2.

[65] Maria Krawczyk, Neda Darvishi, and Dorota Sokolowska. "The Inert Doublet Model and its extensions." In: *Acta Phys. Polon. B* 47 (2016). Ed. by Michal Praszalowicz, p. 183. DOI: 10.5506/APhysPolB.47.183. arXiv: 1512.06437 [hep-ph].

[66] V. A. Kuzmin, V. A. Rubakov, and M. E. Shaposhnikov. "On the Anomalous Electroweak Baryon Number Nonconservation in the Early Universe." In: *Phys. Lett. B* 155 (1985), p. 36. DOI: 10.1016/0370-2693(85)91028-7.

[67] L. Lavoura and Joao P. Silva. "Fundamental CP violating quantities in a SU(2) x U(1) model with many Higgs doublets." In: *Phys. Rev. D* 50 (1994), pp. 4619–4624. DOI: 10.1103/PhysRevD.50.4619. arXiv: hep-ph/9404276.

[68] Hyun Min Lee. "Lectures on physics beyond the Standard Model." In: *Journal of the Korean Physical Society* 78.11 (2021), 985–1017. ISSN: 1976-8524. DOI: 10.1007/s40042-021-00188-x. arXiv: 1907.12409 [hep-ph].

[69] Laura Lopez Honorez, Emmanuel Nezri, Josep F. Oliver, and Michel H. G. Tytgat. "The Inert Doublet Model: An Archetype for Dark Matter." In: *JCAP* 02 (2007), p. 028. DOI: 10.1088/1475-7516/2007/02/028. arXiv: hep-ph/0612275.

[70] Laura Lopez Honorez and Carlos E. Yaguna. "The inert doublet model of dark matter revisited." In: *JHEP* 09 (2010), p. 046. DOI: 10.1007/JHEP09(2010)046. arXiv: 1003.3125 [hep-ph].

[71] Erik Lundstrom, Michael Gustafsson, and Joakim Edsjo. "The Inert Doublet Model and LEP II Limits." In: *Phys. Rev. D* 79 (2009), p. 035013. DOI: 10.1103/PhysRevD.79.035013. arXiv: 0810.3924 [hep-ph].

[72] Yu-Gang Ma, Jin-Hui Chen, and Liang Xue. "A brief review of antimatter production." In: *Frontiers of Physics* 7.6 (2012), 637–646. ISSN: 2095-0470. DOI: 10.1007/s11467-012-0273-9. arXiv: 1301.4902 [nucl-ex].

[73] Michele Maggiore. *A Modern introduction to quantum field theory*. 2005.

[74] Franz Mandl and Graham Shaw. *QUANTUM FIELD THEORY*. 1985.

[75] Aneesh V. Manohar. "Introduction to Effective Field Theories." In: (Apr. 2018). Ed. by Sacha Davidson, Paolo Gambino, Mikko Laine, Matthias Neubert, and Christophe Salomon. DOI: 10.1093/oso/9780198855743.003.0002. arXiv: 1804.05863 [hep-ph].

[76] Matthew McCullough. "Lectures on Physics Beyond the Standard Model." In: *6th Tri-Institute Summer School on Elementary Particles*. 2018. URL: https://inspirehep.net/literature/1684708.

[77] Guy D. Moore. "The Sphaleron rate: Where we stand." In: *3rd International Conference on Strong and Electroweak Matter*. Dec. 1998, pp. 23–33. arXiv: hep-ph/9902464.

[78] Guy D. Moore, Chao-ran Hu, and Berndt Muller. "Chern-Simons number diffusion with hard thermal loops." In: *Phys. Rev. D* 58 (1998), p. 045001. DOI: 10.1103/PhysRevD.58.045001. arXiv: hep-ph/9710436.

[79] J.M. Moreno, D.H. Oaknin, and M. Quirós. "Sphalerons in the MSSM." In: *Nuclear Physics B* 483.1-2 (1997), 267–287. ISSN: 0550-3213. DOI: 10.1016/s0550-3213(96)00562-7. arXiv: hep-ph/9605387.

[80] David E. Morrissey and Michael J. Ramsey-Musolf. "Electroweak baryogenesis." In: *New J. Phys.* 14 (2012), p. 125003. DOI: 10.1088/1367-2630/14/12/125003. arXiv: 1206.2942 [hep-ph].

[81] Jonas Müller. "Linking Cosmology with Collider Phenomenology." PhD thesis. KIT, Karlsruhe, 2021. DOI: 10.5445/IR/1000131249.

[82] Hitoshi Murayama. *Physics Beyond the Standard Model and Dark Matter*. 2007. arXiv: 0704.2276 [hep-ph].

[83] Yosef Nir. "CP violation in and beyond the standard model." In: *27th SLAC Summer Institute on Particle Physics: CP Violation in and Beyond the Standard Model*. July 1999, pp. 165–243. arXiv: hep-ph/9911321.

[84] Yosef Nir. "CP violation: A New era." In: *55th Scottish Universities Summer School in Physics: Heavy Flavor Physics (SUSSP 2001)*. Sept. 2001, pp. 147–200. arXiv: hep-ph/0109090.

[85] Rajesh R. Parwani. "Resummation in a hot scalar field theory." In: *Phys. Rev. D* 45 (1992). [Erratum: Phys.Rev.D 48, 5965 (1993)], p. 4695. DOI: 10.1103/PhysRevD.45.4695. arXiv: hep-ph/9204216.

[86] Michael E. Peskin and Daniel V. Schroeder. *An Introduction to quantum field theory*. Reading, USA: Addison-Wesley, 1995. ISBN: 978-0-201-50397-5.

[87] Antonio Pich. "Effective field theory: Course." In: *Les Houches Summer School in Theoretical Physics, Session 68: Probing the Standard Model of Particle Interactions*. June 1998, pp. 949–1049. arXiv: hep-ph/9806303.

[88] Aaron Pierce and Jesse Thaler. "Natural Dark Matter from an Unnatural Higgs Boson and New Colored Particles at the TeV Scale." In: *JHEP* 08 (2007), p. 026. DOI: 10.1088/1126-6708/2007/08/026. arXiv: hep-ph/0703056.

[89] Stefano Profumo. *An Introduction to Particle Dark Matter*. World Scientific, 2017. ISBN: 978-1-78634-000-9, 978-1-78634-001-6, 978-1-78634-001-6. DOI: 10.1142/q0001.

[90] Stefano Profumo, Leonardo Giani, and Oliver F. Piattella. *An Introduction to Particle Dark Matter*. 2019. arXiv: 1910.05610 [hep-ph].

[91] Mariano Quiros. "Finite temperature field theory and phase transitions." In: *ICTP Summer School in High-Energy Physics and Cosmology*. Jan. 1999, pp. 187–259. arXiv: hep-ph/9901312.

[92] Adam G. Riess, Stefano Casertano, Wenlong Yuan, Lucas M. Macri, and Dan Scolnic. "Large Magellanic Cloud Cepheid Standards Provide a 1% Foundation for the Determination of the Hubble Constant and Stronger Evidence for Physics beyond CDM." In: *The Astrophysical Journal* 876.1 (2019), p. 85. ISSN: 1538-4357. DOI: 10.3847/1538-4357/ab1422. arXiv: 1903.07603 [hep-ph].

[93] Antonio Riotto. "Theories of baryogenesis." In: *ICTP Summer School in High-Energy Physics and Cosmology*. July 1998. arXiv: hep-ph/9807454.

[94] Camilo Alejandro Rojas Pacheco. "CP Symmetry Violation in Scalar Sector in 2HDM and 331 model." PhD thesis. Colombia, U. Natl., 2017.

[95] Ira Z. Rothstein. "TASI lectures on effective field theories." In: Aug. 2003. arXiv: hep-ph/0308266.

[96] Vera C. Rubin and Jr. Ford W. Kent. "Rotation of the Andromeda Nebula from a Spectroscopic Survey of Emission Regions." In: 159 (Feb. 1970), p. 379. DOI: 10.1086/150317.

[97] A. D. Sakharov. "Violation of CP Invariance, C asymmetry, and baryon asymmetry of the universe." In: *Pisma Zh. Eksp. Teor. Fiz.* 5 (1967), pp. 32–35. DOI: 10.1070/PU1991v034n05ABEH002497.

[98] Matthew D. Schwartz. *Quantum Field Theory and the Standard Model*. Cambridge University Press, Mar. 2014. ISBN: 978-1-107-03473-0, 978-1-107-03473-0.

[99] Alessandro Strumia. "Baryogenesis via leptogenesis." In: *Les Houches Summer School on Theoretical Physics: Session 84: Particle Physics Beyond the Standard Model*. Aug. 2006. arXiv: hep-ph/0608347.

[100] Mark Thomson. *Modern particle physics*. New York: Cambridge University Press, 2013. ISBN: 978-1-107-03426-6.

[101] David Tong. *Lectures on Cosmology*. Cambridge, 2019. URL: http://www.damtp.cam.ac.uk/user/tong/cosmo.html.

[102] Mark Trodden. "Electroweak baryogenesis." In: *Rev. Mod. Phys.* 71 (1999), pp. 1463–1500. DOI: 10.1103/RevModPhys.71.1463. arXiv: hep-ph/9803479.

[103] Jordy de Vries, Marieke Postma, Jorinde van de Vis, and Graham White. "Electroweak Baryogenesis and the Standard Model Effective Field Theory." In: *JHEP* 01 (2018), p. 089. DOI: 10.1007/JHEP01(2018)089. arXiv: 1710.04061 [hep-ph].

[104] Jan Weenink and Tomislav Prokopec. *Baryogenesis*. Seminar Cosmology 2008-2009. Utrecht University, 2009.

[105] S. Weinberg. "The making of the Standard Model." In: *The European Physical Journal C* 34.1 (2004), 5–13. ISSN: 1434-6052. DOI: 10.1140/epjc/s2004-01761-1. arXiv: hep-ph/0401010 [hep-ph].

[106] Steven Weinberg. "Effective Gauge Theories." In: *Phys. Lett. B* 91 (1980), pp. 51–55. DOI: 10.1016/0370-2693(80)90660-7.

[107] P.A. Zyla et al. "Review of Particle Physics." In: *PTEP* 2020.8 (2020), p. 083C01. DOI: 10.1093/ptep/ptaa104.

[108] D. Barducci et al. *The micrOMEGAs user's manual, version 5.2*. 2021. URL: https://lapth.cnrs.fr/micromegas/.

DECLARATION

I hereby declare that the submitted thesis is my own work and I did not use any but the acknowledged sources.

Ich versichere, dass ich diese Arbeit selbstständig verfasst habe und keine anderen als die angegebenen Quellen und Hilfsmittel benutzt habe.

Heidelberg, March 2022

María Isabel Dias Astros